

Study on the role of hyaluronan synthase 3 in the pathogenesis of atherosclerosis

Inaugural dissertation

for the attainment of the title of doctor
in the Faculty of Mathematics and Natural Sciences
at the Heinrich Heine University Düsseldorf

presented by

Susanne Friederike Homann

from Filderstadt

Düsseldorf, April 2017

from the Institute for Pharmacology and Clinical Pharmacology
at the Heinrich Heine University Düsseldorf

Published by permission of the
Faculty of Mathematics and Natural Sciences at
Heinrich Heine University Düsseldorf

Supervisor: Prof. Dr. rer. nat. Jens W. Fischer
Co-supervisor: Prof. Dr. rer. nat. Ulrich Rüther

Date of the oral examination: June 8th 2017

Contents

Contents	I
List of figures	IV
List of tables	VI
Abbreviations	VII
1. Introduction	1
1.1. Atherosclerosis	1
1.1.1. Pathogenesis	1
1.1.1.1. Cholesterol.....	2
1.1.1.2. Immune cells.....	3
1.1.1.2.1. Innate immunity	4
1.1.1.2.2. Adaptive immunity	5
1.1.1.3. Vascular smooth muscle cells (VSMCs).....	6
1.1.1.4. Extracellular matrix (ECM).....	7
1.2. Hyaluronan (HA)	8
1.2.1. Synthesis and degradation.....	8
1.2.2. Function and receptor-mediated effects.....	9
1.2.3. HA and inflammation	10
1.2.4. HA in atherosclerosis	10
1.3. Aim of the study	12
2. Materials and Methods	14
2.1. Animal experiments	14
2.1.1. Animals	14
2.1.2. Study design	16
2.1.3. Tissue preparation	16
2.2. Cell culture experiments	17
2.2.1. Isolation of T cells from spleen and lymph nodes	18
2.2.2. T cell activation using anti-CD3/-CD28 beads	19
2.2.3. Generation of bone marrow-derived dendritic cells (BM-DCs).....	19
2.2.3.1. Isolation and differentiation of BM-DCs	19
2.2.3.2. Stimulation of BM-DCs	20
2.3. Flow cytometry	21
2.3.1. Blood	26
2.3.1.1. Lymphocytes	26
2.3.1.2. T helper cells (Th1, Th2, Th17) and regulatory T cells (Treg)	26
2.3.1.3. Monocytes	27
2.3.2. Spleen	27
2.3.3. Lymph nodes.....	28

2.3.4.	Aorta and PVAT	28
2.3.5.	Isolated T lymphocytes and BM-DCs	29
2.3.5.1.	Purity of T lymphocytes and BM-DCs	29
2.3.5.2.	<i>In vitro</i> activation	29
2.3.5.2.1.	Activation status of T lymphocytes	29
2.3.5.2.2.	Activation status of BM-DCs	30
2.4.	Blood plasma analysis	30
2.4.1.	Multiplex analysis	30
2.4.2.	Plasma cholesterol levels	30
2.5.	Histology and immunohistochemistry	31
2.5.1.	Hematoxylin & eosin staining (H&E)	33
2.5.2.	Staining of macrophage- and SMC-like cells	33
2.5.3.	Determination of the atherosclerotic lesion area at the aortic root	34
2.5.4.	Oil Red O (ORO) staining of whole aortas	34
2.6.	Gene expression analysis	35
2.6.1.	RNA isolation	35
2.6.1.1.	Isolated T cells	35
2.6.2.	cDNA synthesis	35
2.6.3.	Quantitative polymerase chain reaction (qPCR)	35
2.7.	Statistical analyses	36
3.	Results	37
3.1.	Impact of Has3 on atherosclerotic lesion size and cellular composition	37
3.1.1.	Atherosclerotic plaque burden	37
3.1.2.	Analyzing plasma cholesterol	38
3.1.3.	Atherosclerotic lesions at the aortic root	39
3.1.4.	Atherosclerotic plaques and vessel remodeling at the brachiocephalic artery (BCA)	42
3.1.5.	Immune cells in advanced atherosclerotic lesions	43
3.1.6.	Aortic immune cells in early plaques	44
3.2.	Effect of <i>Has3</i>-deficiency on immune cell distributions and cytokines	47
3.2.1.	Circulating immune cells	47
3.2.2.	Plasma cytokines	49
3.2.3.	Circulating CD8a ⁺ T lymphocytes	51
3.2.4.	T lymphocytes in spleen and lymph nodes	53
3.2.5.	Immune cells in perivascular adipose tissue (PVAT)	56
3.3.	Role of <i>Has3</i> in the generation of effector and memory T lymphocytes	58
3.3.1.	<i>Has3</i> expression in T lymphocytes	58
3.3.2.	<i>In vitro</i> T cell activation	59
3.3.2.1.	Anti-CD3/-CD28 bead-mediated T cell stimulation	59
3.3.2.2.	Activation of BM-DCs	63
4.	Discussion	65
4.1.	Effect of <i>Has3</i>-deficiency on morphology and localization of atherosclerotic lesions	65

4.2. Origin of macrophage- and SMC-like cells in atherosclerotic plaques	66
4.3. Impact of Has3 on immune cells in the context of atherosclerosis	68
4.4. Role of Has3 in T cell-mediated immune responses	70
4.5. Limitations and prospect	75
5. Summary.....	77
6. Zusammenfassung	78
References	80
Appendix	90
Publications	101
Congress participation	102
Abstracts	102
Curriculum vitae	103
Acknowledgement.....	104
Eidesstattliche Erklärung	105

List of figures

Figure 1: Characteristic stages in atherosclerotic lesion development.	2
Figure 2: Illustration of the chemical structure of a disaccharide unit of HA.....	8
Figure 3: Has3 and macrophage elevation coincided at early times in the aorta.	13
Figure 4: Diagram of the generation of global <i>Has3</i> ^{-/-} mice.....	15
Figure 5: Experimental setup.	16
Figure 6: T cell isolation in three steps.	18
Figure 7: Experimental setup for the generation of BM-DCs.	19
Figure 8: <i>Has3</i> -deficiency reduced atherosclerotic plaque burden in <i>ApoE</i> ^{-/-} mice fed WD for 15 weeks.....	38
Figure 9: Lack of <i>Has3</i> significantly reduced HDL cholesterol levels in <i>ApoE</i> ^{-/-} -deficient mice after 15 weeks of WD.....	39
Figure 10: No alterations in atherosclerotic lesion size at the aortic root after 4, 7, and 15 weeks of WD.....	40
Figure 11: No alterations in the cellular composition of lesions at the aortic root after 4, 7, and 15 weeks of WD.	41
Figure 12: <i>Has3</i> -deficiency affected atherosclerotic remodeling at the BCA after 15 weeks of WD.	42
Figure 13: No alterations in the aortic immune cell composition after 15 weeks of WD.	44
Figure 14: <i>Has3</i> -deficiency significantly reduced leukocytes, especially macrophages and neutrophils, within early atherosclerotic lesions after 4 weeks of WD.	46
Figure 15: Significantly reduced number of circulating Th1 cells in <i>ApoE</i> ^{-/-} / <i>Has3</i> ^{-/-} mice after 4 weeks of WD.....	48
Figure 16: <i>Has3</i> -deficiency significantly affected serum cytokine levels after 7 and 15 weeks of WD.....	50
Figure 17: Delayed increase of circulating effector CD8a ⁺ T lymphocytes in <i>ApoE</i> ^{-/-} mice lacking <i>Has3</i>	52
Figure 18: In spleens of <i>ApoE</i> ^{-/-} / <i>Has3</i> ^{-/-} mice, the number of naïve CD4 ⁺ T lymphocytes was significantly reduced after 15 weeks of WD.....	54
Figure 19: After 15 weeks of WD feeding, <i>ApoE</i> ^{-/-} / <i>Has3</i> ^{-/-} mice had reduced numbers of naïve CD4 ⁺ and CD8a ⁺ T cells in lymph nodes.	55
Figure 20: <i>Has3</i> -deficiency reduced the number of macrophages in the thoracic PVAT after 15 weeks of WD.....	57
Figure 21: Isolated T cells from the spleen and axillary lymph nodes exhibited 97% purity.	58

Figure 22: Isolated splenic T cells from <i>ApoE</i> ^{-/-} mice expressed <i>Has2</i> and <i>Has3</i>	59
Figure 23: <i>Has3</i> -deficiency in T cells slightly impaired T cell expansion.	60
Figure 24: <i>Has3</i> -deficiency did not affect CD3-/CD28-induced stimulation of T cells.	62
Figure 25: LPS activated BM-DCs of <i>ApoE</i> ^{-/-} and <i>ApoE</i> ^{-/-} / <i>Has3</i> ^{-/-} mice equally. .	64
Figure 26: Possible mechanisms for <i>Has3</i> -dependent acceleration of atherosclerotic lesion development.	74
Figure 27: Gating strategy for the defection of monocytes, macrophages, and dendritic cells in the aortic wall after 4 weeks of WD feeding.	90
Figure 28: Gating scheme for the flow cytometric analyses of immune cells in the aorta and PVAT after 15 weeks of WD feeding.	91
Figure 29: Diagram for the analyses of circulating monocytes, B cells, and T cells.	92
Figure 30: Representative gating for the determination of CD62L ⁺ CD44 ⁻ naïve, CD62L ⁻ CD44 ⁺ effector, and CD62L ⁺ CD44 ⁺ memory T cells in the blood.	93
Figure 31: Scheme for the flow cytometric analysis of circulating Th1 and Th2 lymphocytes.	94
Figure 32: Gating strategy for the analysis of circulating Th17 and Treg cells. 95	
Figure 33: Diagram for the gating of naïve, effector, and memory T cells in axillary lymph nodes, spleen, and <i>in vitro</i> experiments.	96
Figure 34: Scheme for the gating of CD25-expressing T cells after stimulation with anti-CD3/-CD28 beads <i>in vitro</i>	97
Figure 35: Gating strategy for the determination of T cell purity after T cell isolation.	98
Figure 36: Representative gating to analyze the purity of the BM-DC culture on day 8 of cultivation.	99
Figure 37: Scheme for the flow cytometric analysis of the activation status of BM-DCs after LPS stimulation <i>in vitro</i>	100

List of tables

Table 1: List of culture media.....	17
Table 2: Substances used for cell culture experiments.	17
Table 3: List of buffers used for flow cytometry.	21
Table 4: Antibody combinations for flow cytometric stainings.....	22
Table 5: Marker combinations for the identification of immune cells.....	25
Table 6: Buffers and solutions for histological stainings.	32
Table 7: Primary and secondary antibodies for immunohistochemistry.....	32
Table 8: Primers used for qPCR.....	36

Abbreviations

ANOVA	Analysis of variance
ApoE	Apolipoprotein E
BCA	Brachiocephalic artery
BM-DC	Bone marrow-derived dendritic cell
BSA	Bovine serum albumin
CANTOS	Canakinumab Anti-Inflammatory Thrombosis Outcomes Study
CCL	CC-chemokine ligand
CD	Cluster of differentiation (e.g. CD45)
cDNA	Complementary deoxyribonucleic acid
CHD	Coronary heart disease
CIRT	Cardiovascular Inflammation Reduction Trial
CO ₂	Carbon dioxide
CCR	C-C motif chemokine receptor
CVD	Cardiovascular diseases
CX3CR	C-X3-C motif chemokine receptor
DAB	3,3'-diaminobenzidine
DC	Dendritic cell
DPBS	Dulbecco's Phosphate Buffered Saline
ECM	Extracellular matrix
EDTA	Ethylenediaminetetraacetic acid
EEL	External elastic lamina
FCS	Fetal calf serum
FRET	Fluorescence resonance energy transfer
FSC	Forward Scatter
GAG	Glycosaminoglycan
G-CSF	Granulocyte-colony stimulating factor
GlcA	D-glucuronic acid
GlcNAc	N-acetyl-D-glucosamine
GM-CSF	Granulocyte-macrophage colony-stimulating factor
HA	Hyaluronan
HAS	Hyaluronan synthase
HBSS	Hank's Balanced Salt Solution
HDL	High-density lipoprotein
H&E	Hematoxylin and eosin (histological staining)
HEV	High endothelial venule
HMG-CoA	3-hydroxy-3-methyl-glutaryl-coenzyme A
HMW-HA	High molecular weight HA

HRP	Horseradish peroxidase
hsCRP	High sensitivity C-reactive protein
HUVEC	Human umbilical vein endothelial cell
HYAL	Hyaluronidase
IDL	Intermediate-density lipoprotein
IEL	Internal elastic lamina
IFN	Interferon
IL	Interleukin
IL-2R	Interleukin-2 receptor
iNOS	Inducible nitric-oxide synthase
KC	Keratinocyte-derived cytokine
KLF	Kruppel-like factor
LANUV	<i>Landesamt für Natur, Umwelt und Verbraucherschutz</i>
LDL	Low-density lipoprotein
LDLR	LDL-receptor
LMW-HA	Low molecular weight HA
LPS	Lipopolysaccharide
LYVE	Lymphatic vessel endothelial HA receptor
MCP	Monocyte chemoattractant protein
MIP	Macrophage inflammatory protein
MHC	Major histocompatibility complex
MMP	Matrix metalloproteinase
N/A	No data available
n.d.	Not detectable
NF- κ B	Nuclear factor kappa-light-chain-enhancer of activated B cells
ORO	Oil Red O
oxLDL	Modified (oxidized) LDL
PBS	Phosphate buffered saline
PFA	Paraformaldehyde
PCSK9	Proprotein convertase subtilisin kexin 9
PVAT	Perivascular adipose tissue
qPCR	Quantitative polymerase chain reaction
RANTES	Regulated on activation, normal T cell expressed and secreted
RHAMM	Receptor of HA-mediated motility
RNA	Ribonucleic acid
ROI	Region of interest
RT	Room temperature
SEM	Standard error mean
SSC	Side Scatter
SMA	Smooth muscle actin

SMC	Smooth muscle cell
STAT	Signal transducer and activator of transcription
TBX	T-box transcription factor
TCR	T cell receptor
TGF	Transforming growth factor
Th cell	T helper cell
TLR	Toll-like receptor
TNF	Tumor necrosis factor
Treg	Regulatory T lymphocyte
VCAM	Vascular adhesion molecule
VLDL	Very low-density lipoprotein
VSMC	Vascular smooth muscle cell
WD	Western-type diet
4-MU	4-methylumbelliferone

1. Introduction

1.1. Atherosclerosis

With over 17.5 million deaths per year worldwide, which is approximately one-third of all deaths, cardiovascular diseases (CVD) are the leading cause of mortality, although the death rates due to CVD decreased globally over the past three decades. The term CVD summarizes a group of disorders associated with the heart and the vasculature, such as coronary heart disease, cerebrovascular disease, cardiomyopathies, and others. In 2013, around 80% of cardiovascular deaths were caused by ischemic heart disease and stroke. With atherosclerosis as the common and main underlying pathological mechanism of ischemic heart disease and stroke, atherosclerosis is a major contributor to global mortality [1, 2]. Several risk factors are known to promote the development of atherosclerosis. These include aging and gender, behavioral risk factors, such as tobacco smoking or physical inactivity, and metabolic disorders, e.g. hypertension, obesity, and hypercholesterolemia [2]. Besides life style changes, the current therapy of option to lower the risk of cardiovascular events is the lowering of blood cholesterol levels by statin therapy [3, 4]. Due to the important impact of immune cells in the pathogenesis of atherosclerosis, anti-inflammatory therapies for atherosclerosis are currently under investigation. In order to find even further therapeutic options, it is of great interest to continue the examination of the pathology of atherosclerosis.

1.1.1. Pathogenesis

Atherosclerosis is a multifactorial disease. The development of the lesions is a process that starts at an early age and lasts for decades until lesions are formed that can cause clinical manifestations, such as myocardial infarction. Characteristic stages in atherosclerotic lesion development are illustrated in **Figure 1**. Atherosclerotic lesion development is initiated by endothelial dysfunction, resulting in leakiness, and thus enabling the accumulation of low-density lipoproteins (LDL). In the intima, LDL particles are susceptible to modification, e.g. oxidation. These deposited modified lipids (oxLDL) further stimulate the activation of endothelial cells and promote the production of pro-inflammatory factors. This induces the recruitment of leukocytes, which infiltrate into the intima to remove deposited oxLDL. Lipid uptake by phagocytic cells gives rise to foam cells, which are characteristic for early fatty streak lesions. Foam cells eventually undergo apoptosis and apoptotic bodies are then cleared by efferocytosis. However, in advanced lesions, clearance of apoptotic

cells is not efficient and finally apoptotic cells undergo secondary necrosis leading to the formation of a necrotic core where debris and cholesterol crystals accumulate. These processes further enhance the inflammatory responses and consequently the progression of lesion development. All these processes during atherosclerotic lesion formation result in characteristic narrowing of the blood vessel, which leads to disturbed blood flow and thus further enhances leukocyte attachment [5].

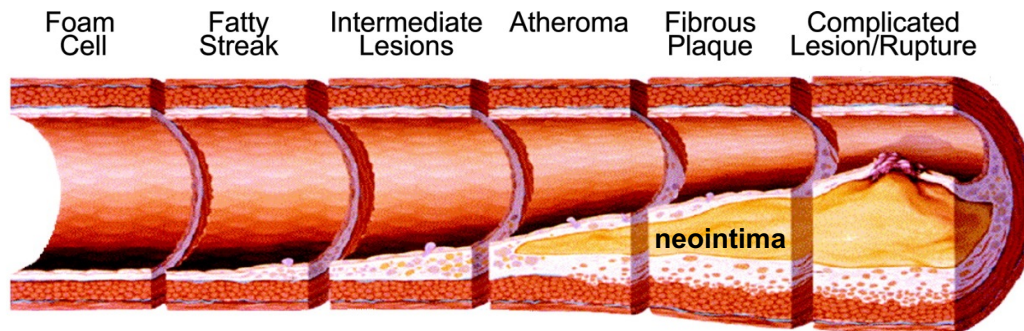


Figure 1: Characteristic stages in atherosclerotic lesion development.

The development of atherosclerosis begins early in life without being recognized. Age combined with other risk factors, e.g. smoking, can accelerate lesion progression. Usually, first symptoms occur when the vessel lumen is severely narrowed or totally occluded. Figure modified from Koenig *et al.* [6].

1.1.1.1. Cholesterol

As mentioned previously, cholesterol, and especially LDL cholesterol, is crucially involved in the initiation and progression of atherosclerotic plaques as it is a major risk factor triggering immune cell recruitment.

Cholesterol is either absorbed from the intestine or it can be synthesized in the liver. As cholesterol is lipophilic, its transport through the blood is mediated by lipoprotein particles, which consist of a hydrophilic core containing cholesterol and lipids surrounded by polar phospholipids. Depending on their density, triglyceride, and cholesterol content, lipoproteins are classified into chylomicrons, chylomicron remnants, very low-density lipoproteins (VLDL), intermediate-density lipoproteins (IDL), low-density lipoproteins (LDL), and high-density lipoproteins (HDL). LDL particles consist of approximately 50% of cholesterol and cholesteryl esters and thus, LDL particles are the major carrier of cholesterol in the blood. It is the function of LDL particles to distribute cholesterol into the periphery. Binding to the LDL-receptor (LDLR) mediates the internalization of LDL particles into cells and consequently, cholesterol becomes integrated into the cell membrane. In contrast to LDL, HDL

picks up cholesterol from extrahepatic tissues and the plasma and returns it to the liver for degradation and excretion [7].

Both human and murine studies have shown a positive correlation of total serum cholesterol levels and coronary heart disease (CHD) risk [8-10]. As approximately one-third of ischemic heart diseases is due to high cholesterol levels, a reduction of cholesterol levels by 10% would reduce CHD mortality by 20% [10]. Thus, lowering blood cholesterol levels is a good prevention strategy for atherosclerosis-mediated mortality. However, despite extensive cholesterol lowering in high risk patients, some patients still have a high remaining risk for CHD. Independently, in both the PROVE-IT [11] and the IMPROVE-IT trial [12] it was shown that in addition to lowering LDL levels the reduction of the high sensitivity C-reactive protein (hsCRP), which serves as marker for inflammation, efficiently reduces vascular events. Thus, these studies indicate that for an individual treatment it might be beneficial to categorize patients according to their residual cholesterol versus their residual inflammatory risk to optimize their treatment and efficiently reduce cardiovascular events.

Among lipid-lowering drugs, statins are the most potent ones for lowering serum cholesterol levels and thus count as first class therapeutics. They inhibit the enzyme 3-hydroxy-3-methyl-glutaryl-coenzyme A (HMG-CoA) reductase, which catalyzes a critical step in the synthesis of cholesterol in hepatocytes. Thereby, the endogenous biosynthesis of cholesterol is reduced. Furthermore, the expression of LDLRs in hepatocytes is induced by HMG-CoA reductase inhibition. Consequently, LDL particle uptake by hepatocytes is increased. Both mechanisms finally lead to a lowering in serum cholesterol levels [13]. Since 2015 a second class of very potent LDL lowering agents, the proprotein convertase subtilisin kexin 9 (PCSK9) inhibitors, is approved for therapy of high-risk patients that either exhibit high cholesterol levels despite statin therapy or do not tolerate statin therapy. PCSK9 inhibitors are monoclonal antibodies that bind and inactivate the PCSK9 protein, which induces LDLR internalization and degradation. Through its inhibition, LDLR surface expression increases and thereby leads to the reduction of circulating LDL levels [14].

Until now, the question whether solely the LDL lowering potency of statins is atheroprotective or if also the anti-inflammatory effects contribute to their success is not solved. Thus, further research and clinical assessment are required to assess the advantage of anti-inflammatory therapies on atherosclerotic events.

1.1.1.2. Immune cells

To evaluate the potential of anti-inflammatory therapies in atherosclerosis-driven diseases anti-inflammatory therapies are currently under investigation. At the

moment, low-dose methotrexate and Canakinumab are in Phase III clinical trials in the Cardiovascular Inflammation Reduction Trial (CIRT; <http://www.thecirt.org/>; as of 01/22/2017) and the Canakinumab Anti-Inflammatory Thrombosis Outcomes Study (CANTOS; <http://www.thecantos.org/>; as of 01/22/2017), respectively.

In atherosclerosis, all branches of the inflammatory cascade participate in development and progression, with macrophages and T lymphocytes as the most abundant immune cells.

1.1.1.2.1. Innate immunity

The innate immune system provides a non-specific, fast immune response to pathogens. Phagocytes, including macrophages, neutrophils, and dendritic cells (DCs), are a major component of the innate immunity and not only involved in the removal of foreign particles, but also in tissue homeostasis by removing dead cells. In the pathogenesis of atherosclerosis phagocytes, especially macrophages, play a key role.

An early step in atherosclerotic lesion development is the recruitment of monocytes from the circulation into the intima. Different subsets of monocytes have been described in humans and mice according to their CD14 or Ly6C expression, respectively [15, 16]. In mice, monocytes expressing low levels of Ly6C patrol on the endothelium, suggesting a role of endothelial cell surveillance [17]. Their role in atherogenesis is still unclear. In contrast, classical Ly6C^{high} monocytes exhibit a pro-inflammatory phenotype. Several studies showed that Ly6C^{high} monocytes infiltrated lesions and lesion-prone areas and became lesional macrophages [18, 19]. The entry of monocytes into the lesion relies on several chemokine receptors, such as C-C motif chemokine receptor (CCR) 2, C-X3-C motif chemokine receptor (CX3CR) 1, and CCR5. Genetic deletion of the chemokine receptors decreased atherosclerosis by reducing macrophage accumulation [20]. Also deficiency in monocyte chemoattractant protein (MCP)-1, the ligand of CCR2, diminished macrophage accumulation and thereby atherosclerotic plaque burden [21].

Once in the intima, monocytes differentiate into macrophages to implement phagocytic functions. The expression of receptors, such as toll-like receptors (TLRs), and pattern-recognition receptors, is upregulated to enable the engulfment of LDL particles [22, 23]. TLR4 seems to be crucially involved in LDL uptake and foam cell formation, as *Tlr4*-deficient mice have much fewer foam cells and less lipid accumulation than control animals [24]. Besides monocyte infiltration, there is also evidence showing that resident macrophages in the arterial wall contribute to the pool of lesional macrophages. These resident macrophages are supposed to have an anti-inflammatory M2-like macrophage phenotype and contribute to the clearance of apoptotic cells and thus mediate responses for the resolution of inflammation [25].

With these properties M2-like macrophages oppose the pro-inflammatory M1-like phenotype of macrophages that probably arise from infiltrating Ly6C^{high} monocytes [26]. In contrast to early lesion development that is mainly mediated by monocyte infiltration, macrophage proliferation was described to be the major cause of macrophage accumulation in later stages of atherosclerotic lesion development [27]. These findings indicate that there are several different sources of macrophages that contribute to early and late stage lesion development.

Besides macrophages, also DCs are able to take up lipids, become foam cells, and thus contribute to atherogenesis [28]. Apart from this, DCs as antigen-presenting cells display a major role in the crosstalk between innate and adaptive immunity by regulating T cell responses. DCs are involved in T cell recruitment, T cell activation, and proliferation [29, 30].

1.1.1.2.2. Adaptive immunity

The adaptive immune system is composed of B and T lymphocytes. In contrast to the innate immune system, the immune response induced by adaptive immunity is much slower. For their full activation they require a stimulus from other cells to become activated and expand. T lymphocytes depend on the presentation of antigens on major histocompatibility complex (MHC) I or MHC II. The antigen is then recognized by an antigen-specific T cell receptor (TCR). Further stimuli are required for the activation of T cells via co-stimulatory molecules, like cluster of differentiation (CD) 28. Upon activation, a naïve T cell alters its surface expression of several proteins, e.g. increases CD44 expression and loses CD62L, and becomes an activated effector T cell. In the process of T cell activation, a subpopulation of memory cells is produced that enables long-term immunity, a unique feature of the adaptive immune system [31].

In atherosclerotic lesions, T lymphocytes accumulate early during lesion development and are described to be the second most abundant immune cells after macrophages [32]. Two major subsets of T lymphocytes can be discriminated due to their surface expression of the glycoprotein CD4 and CD8, respectively. CD4-positive T cells constitute approximately two-thirds and CD8-expressing T cells one-third of T cells in atherosclerotic lesions [33].

Although immunodeficient mice have reduced lesion formation, and adoptive transfer of CD4⁺ T cells into immunodeficient mice accelerates lesion development, the impact of T cells on atherosclerotic lesion development is not just black and white [34, 35]. For CD4⁺ T cells four subsets have been found in the lesion so far: T helper (Th) 1, Th2, Th17, and regulatory T (Treg) cells. Th1 cells, which the most abundant Th cell type in lesions, aggravate atherosclerosis. This effect has been shown by several studies using different approaches. Interleukin (IL)-12 is the major cytokine

that promotes Th1 polarization by activating signal transducer and activator of transcription (STAT)-4 and T-box transcription factor (TBX) 21, the two lineage-defining transcription factors [36]. Mice deficient in IL-12 as well as Tbx21 showed reduced plaque development [37, 38]. In contrast, the administration of IL-12 accelerated atherosclerosis by increasing the Th1 population [39]. The archetypical cytokine that is synthesized by Th1 cells is interferon (IFN)- γ . IFN- γ has pro-atherogenic effects by promoting the activation of inflammatory macrophages. Further, IFN- γ reduces smooth muscle cell (SMC) proliferation and extracellular matrix (ECM) production and thereby crucially contributes to plaque destabilization [40].

Compared with Th1 cells, Treg cells depict distinct anti-atherogenic properties. The two cytokines IL-10 and transforming growth factor (TGF)- β mediate the immunoregulatory functions of Treg cells by suppressing the proliferation of effector T cells [41]. The role of Th2 and Th17 cells in atherosclerosis is still controversial. On the one hand, Th2 cells produce IL-5 and IL-33, which seem to account for the anti-atherogenic effects of Th2 cells. On the other hand, the secretion of IL-4 by Th2 cells enhances lesion development [42-44].

Recently, the role of CD8⁺ T cells has been examined by depleting the cells with CD8 antibodies. Atherosclerotic plaque burden was reduced in mice lacking CD8⁺ T cells. It was shown that T cells firstly induce a monocytosis under hypercholesterolemic conditions and thereby enhance the number of recruited monocytes [45]. Secondly, CD8⁺ T cells in the lesion produce perforin and granzyme B and mediate apoptosis of macrophages, SMCs, and endothelial cells [46].

1.1.1.3. Vascular smooth muscle cells (VSMCs)

In healthy vessels, differentiated, mature VSMCs are localized in the media surrounded by a basement membrane where they exhibit their contractile functions by regulating blood pressure. However, under pathological conditions, like vessel injury or atherosclerotic modifications, VSMCs can undergo a phenotypic switching from their contractile into a secretory phenotype. These phenotypically altered VSMCs show increased proliferation, migration, and secretion of ECM and cytokines [47]. Supposedly, ECM degradation in the media is an initial trigger in inducing VSMC phenotypic switching [48, 49]. The appearance of VSMCs, identified by the expression of conventional SMC markers, such as α -smooth muscle actin (α -SMA) or 22-kDa SMC lineage-restricted protein (SM22 α /tagln), has long been associated with atheroprotective functions of SMCs by contributing to lesion stability through the formation of the fibrous cap. Recent studies using *in vivo* SMC-lineage tracing models revealed that SMCs not only lose their contractile functions but also can

undergo phenotypic transition resulting in loss of their typical lineage markers. Furthermore, VSMCs can upregulate the expression of macrophage markers, gain phagocytic properties, and thus contribute to the pool of lesional foam cells [50-52]. This VSMC-to-macrophage transition in an atherosclerotic context seems to be crucially regulated by the stem cell factor kruppel-like factor 4 (KLF4) [53]. Analyses of these SMC-derived macrophages revealed that they had impaired phagocytic capacity compared to peritoneal macrophages [54]. Consequently, removal of debris, apoptotic cells, and oxLDL is diminished, which rather promotes lesion formation. These recent studies disclosed that the function of VSMCs in atherosclerosis can be both beneficial and detrimental depending on the origin, fate, and metabolic state of the SMC-like cell.

1.1.1.4. Extracellular matrix (ECM)

ECM is a complex network consisting of a variety of molecules, including proteoglycans, polysaccharides, collagens, elastins, fibronectins, and laminins. Secreted by cells, they provide important structural and mechanical features for tissues and single cells. Via receptor binding, ECM components mediate extracellular signaling and thereby affect cell-cell and cell-matrix interactions. Healthy vessels contain a diversity of ECM components which are mainly localized in basement membranes for the regulation of cellular integrity and in the endothelial glycocalyx, which is part of the vessel barrier [55]. However, during pathological disorders, ECM structures are disrupted. These alterations in ECM composition crucially contribute to atherogenesis. For example matrix metalloproteinases (MMPs) are key players in matrix remodeling as they mediate ECM degradation. Via degradation of ECM components ECM-bound growth factors or cytokines are released and by that induce changes in cellular behavior, such as proliferation. Besides ECM degrading enzymes, also the ECM components themselves influence the cell behavior. In vascular injury, SMCs and macrophages produce type VIII collagen. This collagen can induce SMC proliferation and migration [56, 57]. Other collagens, e.g. type I collagen, influence the monocyte-to-macrophage transition as well as the phagocytic activity [58, 59]. Another important contribution to atherosclerotic lesion development comes from the glycosaminoglycans (GAGs). Especially chondroitin sulfate proteoglycans in the arterial wall are markedly involved in binding LDL and thereby enhancing lipid accumulation [60, 61]. Among GAGs, hyaluronan (HA) is a unique polysaccharide, as it is not sulfated and not bound to a core protein. The role and impact of HA on atherosclerosis will be described in the following section.

1.2. Hyaluronan (HA)

1.2.1. Synthesis and degradation

As unbranched polysaccharide consisting of repeating disaccharide units of D-glucuronic acid (GlcA) and N-acetyl-D-glucosamine (GlcNAc) (**Figure 2**), HA belongs to the group of GAGs. Unlike the other GAGs, HA is not synthesized in the Golgi apparatus but at the plasma membrane by three transmembrane hyaluronan synthases (HAS1 through HAS3). These enzymes produce the HA chain by linking the two monomers via β -1,3- and β -1,4-glycosidic bonds in an alternating manner. The growing HA chain is directly extruded into the extracellular space. This allows a large degree of polymerization, leading to a broad size distribution, ranging from 10^5 to 10^7 Da. Furthermore, and in contrast to the other GAGs, HA chains are not covalently attached to core proteins [62].

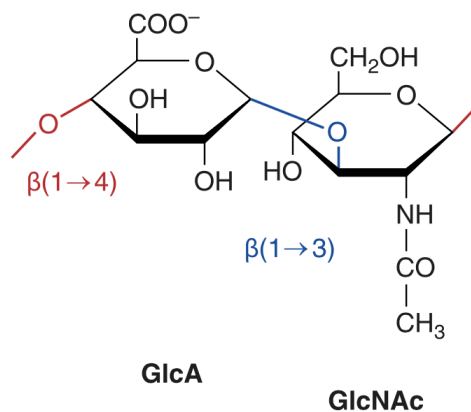


Figure 2: Illustration of the chemical structure of a disaccharide unit of HA.
Modified from Jiang *et al.* [62].

The amino acid sequences of the three HAS isoforms show a high degree of homology. All three enzymes are capable of producing HA chains independently. However, they differ in their enzymatic activity, their response to stimuli, enzyme stability, and localization in tissues and within the cell [63, 64]. Furthermore, recently it was shown by fluorescence resonance energy transfer (FRET) that HAS isoenzymes can form homo- and heterodimers [65]. These complexes are also supposed to influence the enzymatic activity. Their different biological functions are further underlined by the observations that *Has2*-deficient mice are embryonic lethal [66], while *Has1*- and *Has3*- deficient mice, respectively, are vital and fertile.

The degradation of HA is mediated by hyaluronidases (HYAL). They hydrolyze the β -1,4-glycosidic bonds between GlcNAc and GlcA and thus lead to the formation of HA fragments. Five genes encoding for HYAL1-4 and PH-20, plus one pseudogene

HYALP1 are identified thus far [67]. HYAL1 and HYAL2 are probably the two major HYALs involved in HA cleavage. HYAL2 is only capable of hydrolyzing high molecular weight HA (HMW-HA) into fragments of approximately 20kDa. In contrast to that HYAL1 is able to degrade HA to tetrasaccharides. Besides the enzymatic digestion of HA via HYALs, also reactive oxygen species are described to degrade HA, which probably is gaining in importance in tissue injury and inflammatory processes [62].

1.2.2. Function and receptor-mediated effects

HA is found in abundance in the skin, the vitreous body of the eye, synovial fluid, umbilical cord, and heart valves. As mentioned previously, HA exists as both HMW-HA and as HA fragments. But with respect to the size, the features and functions of HA change drastically. As HMW-HA, which is predominantly found in healthy tissue, HA is capable of storing huge amounts of water, it is involved in lubricating joints, and it has important impact on the cellular behavior by providing a matrix for cell adhesion and migration [68]. Further, HA displays anti-apoptotic effects on various cell types, such as SMCs or fibroblasts [69, 70]. However, under pathophysiological conditions, like tissue injury or inflammation, the sizes of HA polymers are more diverse with a dominance of low molecular weight HA (LMW-HA). LMW-HA displays properties that stimulate angiogenesis and immune cell responses, e.g. by inducing immune cell maturation [62].

To mediate this broad spectrum of functions, HA can interact with a variety of proteins and thus influence their function. Important HA binding proteins are e.g. CD44, receptor of HA-mediated motility (RHAMM), TLR, lymphatic vessel endothelial HA receptor 1 (LYVE1), versican, and many others. Via HA-receptor interactions, HA can trigger signaling pathways and by that influence proliferation, migration, adhesion, and inflammation [62].

One major HA receptor is the cell surface glycoprotein CD44, which is expressed in a large number of cell types. Multiple forms of the receptor due to alternative splicing and further glycosylation mediate the diverse roles of CD44 [71]. Important is that the affinity of the receptor to HA depends on posttranslational modifications and can be altered by physiological stimuli. In T cell responses, for example, it was shown that naïve T cells expressed low levels of the receptor, but are not able to bind HA, while T cell activation enables HA binding to CD44 [72-74].

1.2.3. HA and inflammation

The pro- and anti-inflammatory properties of HA are largely size dependent. Under inflammatory conditions HA strongly accumulates and is degraded into fragments. Thereby, a broad spectrum of effects of HA on different immune cells can be initiated. CD44 is an important receptor that mediates a large number of HA effects on leukocytes. HA-CD44 interaction is crucially involved in leukocyte rolling on endothelial cells, as well as firm adhesion and extravasation. It was shown that blocking of CD44 or lack of CD44 in diverse inflammatory diseases led to decreased leukocyte recruitment [71]. Besides CD44 as HA receptor, also TLR-HA binding seems to mediate inflammatory responses. HA fragments can bind to TLR2 and TLR4 and thereby trigger inflammatory responses. HA-mediated TLR signaling leads to the activation of nuclear factor kappa-light-chain-enhancer of activated B cells (NF- κ B), a critical factor in regulating inflammation. In macrophages, HA binding to TLR2/4 induces the expression of various inflammatory cytokines, e.g. MCP-1, regulated on activation, normal T cell expressed and secreted (RANTES), IL-12, or tumor necrosis factor (TNF)- α [75-77]. Also in DCs HA depicts regulatory functions. Termeer and colleagues demonstrated that HA fragments induced DC maturation and cytokine production via TLR4 [78, 79].

Not only the functions of cells of the innate immune system are regulated by HA, also cells of the adaptive immunity change their responses upon interaction with HA, e.g. T cells increase their surface levels of CD44 upon activation. In this way, primary T cell adhesion to endothelial HA is enabled and permits T cell extravasation [80]. In addition, HA-CD44 interaction at the immune synapse, the interface of DC-T cell interaction during T cell activation, has been reported to promote the formation and stability of this interaction and thereby optimize antigen presentation [81].

All these studies show that HA displays pivotal roles in mediating or regulating inflammation by directly interfering with cell surface receptors and thereby altering cell signaling.

1.2.4. HA in atherosclerosis

The presence of HA in non-primate intermediate and advanced atherosclerotic lesions has already been described in the 1990s [82]. Also in human lesions, Kolodgie *et al.* showed an intense staining of HA, especially at the luminal part of eroded plaques, suggesting a role of HA in plaque erosion [83]. HA was found to co-localize with lipids in atherosclerosis, indicating an impact of HA on lipid accumulation [82, 84]. Furthermore, Sakr and colleagues observed that HA synthesis in SMCs was elevated under hypercholesterolemic conditions [85]. These studies suggest an effect of HA already in early atherogenesis. Also *in vivo* studies where

Has2 was overexpressed in SMCs of *ApoE*^{-/-} mice demonstrated that HA promoted lesion formation [86]. Possible mechanisms that might explain HA-mediated atherogenesis in this model include an induction of SMC migration in a CD44-dependent manner [87]. SMC migration and proliferation assays *in vitro* further underlined the impact of HA on SMC behavior. Pharmacological inhibition of HA synthesis by 4-methylumbelliferone (4-MU) resulted in reduced migration and proliferation [88]. Moreover, it was shown that HA-rich matrices produced by SMCs had pro-inflammatory properties by serving as adhesive substrate for monocytes [89]. Thus, HA in atherosclerotic lesions does not only affect LDL retention and SMC phenotype, but also leukocytes. It was shown that HA promoted the uptake of oxLDL by macrophages by increasing the expression of the scavenger receptor CD36, which mediates LDL uptake in macrophages [90].

Many of the described effects of HA during atherogenesis depend on HA-CD44 interaction and the induction of CD44 signaling. Cuff and colleagues investigated the effect of *CD44*-deficiency in *ApoE*^{-/-} mice on the development of atherosclerotic lesions already in 2001. Lesions of *CD44*-deficient mice were up to 70% smaller than those in control mice. Lack of CD44 reduced the number of lesional macrophages probably by impaired recruitment of circulating immune cells [91]. Moreover, HA-CD44 signaling seems to be important in mediating SMC phenotypic switching by inducing the expression of vascular adhesion molecule (VCAM)-1. VCAM-1 expression in SMCs is associated with SMC phenotypic switching from a contractile into a synthetic phenotype [92]. Zhao *et al.* used bone marrow chimeras to assess the contribution of CD44 in both hematopoietic and non-hematopoietic cells on lesion formation. Indeed, they confirmed that CD44 on leukocytes, endothelial cells, and SMCs contributes to lesion formation by mediating leukocyte recruitment, leukocyte adhesion, and SMC migration, respectively [93].

Besides the inhibition of receptor-ligand interaction via *CD44*-deletion, also the impact of the pharmacological inhibition of HA synthesis by 4-MU on atherosclerotic lesion development was analyzed. However, contrary to expectations lesion formation was not impaired but accelerated upon 4-MU treatment. The reason for that was the destruction of the endothelial glycocalyx [94]. The glycocalyx on endothelial cells confines the interaction of platelets and leukocytes with endothelial cells and thus has protective functions. With HA as an important component, inhibition of HA synthesis increases leukocyte accumulation and thereby promotes lesion development.

Due to the pro-atherogenic effects of HA and the detrimental impact of long-term treatment with 4-MU on atherogenesis, it might be worth analyzing the role of the specific HAS isoenzymes in atherosclerotic lesion formation.

1.3. Aim of the study

As presented in section 1.2.4, HA is present at various stages during lesion development both in humans and mice. The influence of HA on a variety of effector cells in atherosclerosis, such as macrophages and SMCs, has been object of several investigations. These revealed that HA impacts apoptosis and adhesion of macrophages, and it can trigger SMC migration. Furthermore, it was demonstrated that HA co-localizes with lipoproteins and thus also affects LDL accumulation. However, the role of HAS3 in atherosclerosis has not been evaluated yet. Recently, the role of Has3 in a murine model of neointimal hyperplasia has been investigated. These data showed that Has3 promotes neointimal formation probably by enhancing both SMC migration and ECM deposition [95].

Furthermore, time lapse analyses of lesional macrophages and HA of *ApoE*^{-/-} mice have shown that an early macrophage accumulation in the lesion is accompanied by HA deposition (**Figure 3 A, B**; data not published). mRNA expression analyses of the three Has isoforms revealed that early HA staining coincided with an early upregulation of *Has3* expression. At an age of 22 weeks, *Has3* mRNA declined and *Has1* mRNA increased instead. The expression levels of *Has2* remained low over the time lapse (**Figure 3 C**; data not published).

Due to the impact of Has3 on neointimal hyperplasia and the observed early increase in Has3 mRNA expression in atherosclerosis, it was the aim of the present study to investigate the role of Has3 on atherogenesis. To address this question, *ApoE*-deficient mice with or without additional lack of *Has3* were fed a western-type diet (WD) to accelerate atherosclerotic lesion development. The potential influence of Has3 on inflammatory processes during lesion development and progression in lymphoid and non-lymphoid tissues as well as possible underlying mechanisms resulting in alterations in atherogenesis were examined.

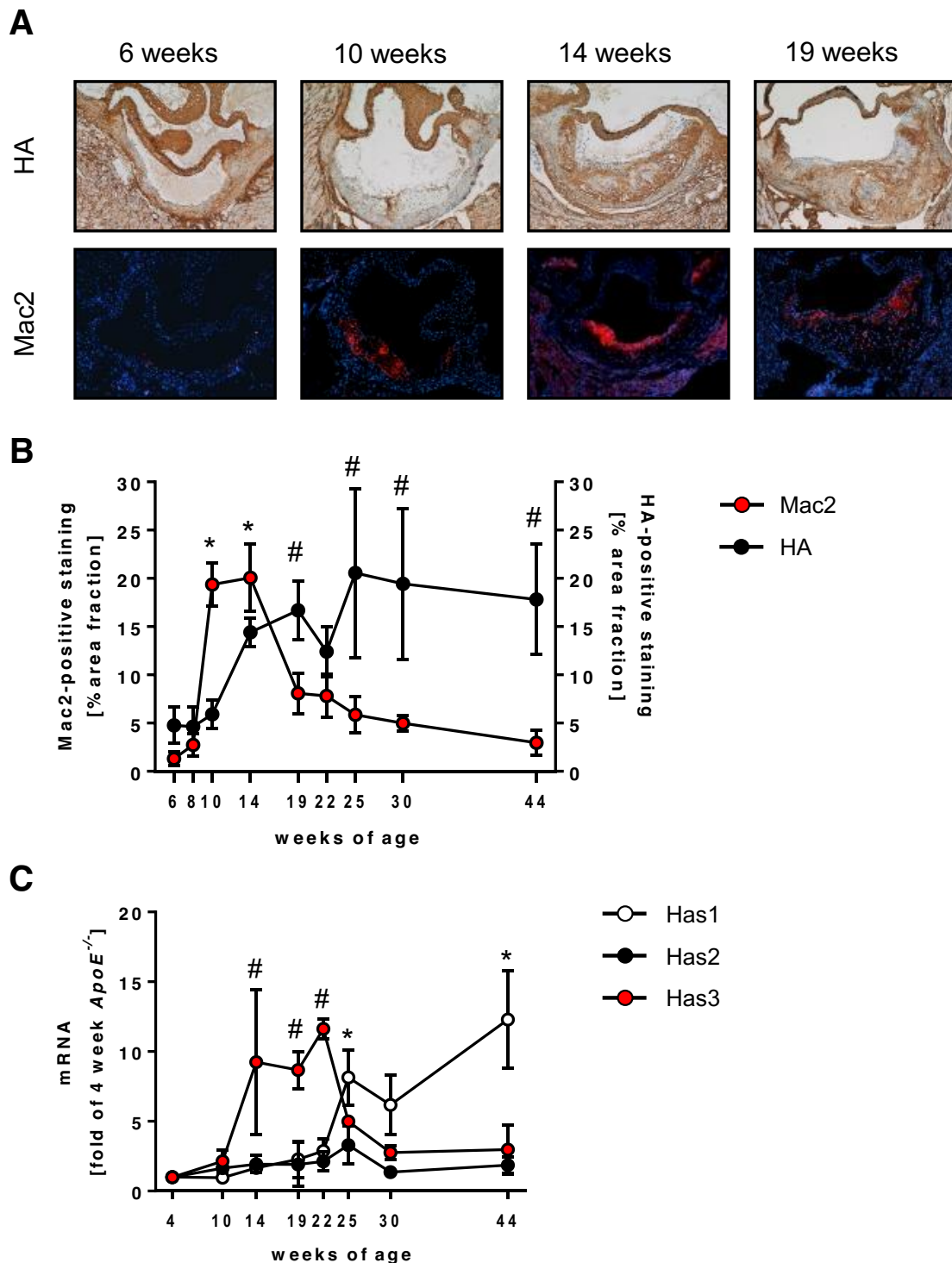


Figure 3: Has3 and macrophage elevation coincided at early times in the aorta. (A) In 6-, 10-, 14-, and 19-weeks-old *ApoE*^{-/-} mice HA and Mac2 content was assessed in histological sections of the aortic root. (B) Quantification of the area fraction of macrophages and HA in aortic root sections at different ages of *ApoE*^{-/-} mice; n=3-7; * p < 0.05 vs. Mac2 at 6 weeks of age; # p < 0.05 vs. HA at 6 weeks of age (two-way analysis of variance (ANOVA)). (C) RNA was extracted from aortas of *ApoE*^{-/-} mice and mRNA expression of *Has1*, *Has2*, and *Has3* was analyzed; n=3; * p < 0.05 vs. *Has1* at 4 weeks of age; # p < 0.05 vs. *Has3* at 4 weeks of age (two-way ANOVA). Values represent the means ± SEM; data not published; experiments and data were provided by Nadine Nagy.

2. Materials and Methods

2.1. Animal experiments

2.1.1. Animals

In this study, male mice double-deficient for *apolipoprotein E* (*ApoE*) and *hyaluronan synthase 3* (*Has3*) and respective control mice (*ApoE*^{-/-}) were used. To achieve double-deficient mice for *ApoE* and *Has3*, first *Has3*-deficient mice were generated by genOway (Lyon Cedex, France) and then crossbred with *ApoE*-deficient mice (Taconic; Hudson, NY, USA). In order to generate mice lacking the murine *Has3*, the strategy was to disrupt the gene function by replacing the start-codon in exon 2 by the human HAS3 cDNA. Thereby, the human cDNA cassette was flanked by a FRT-neomycin-FRT-loxP cassette at the 5' end and by a single loxP site at the 3' end, which was positioned within the downstream intron. First, mice expressing this construct were crossbred with mice constitutively expressing the Flp recombinase to delete the neomycin cassette flanked by FRT. In a second step, mice carrying the human HAS3 cDNA flanked by loxP sites were mated with deleter mice constitutively expressing the Cre recombinase to create constitutive knockout mice for the *Has3* gene in all cells (**Figure 4**) [95].

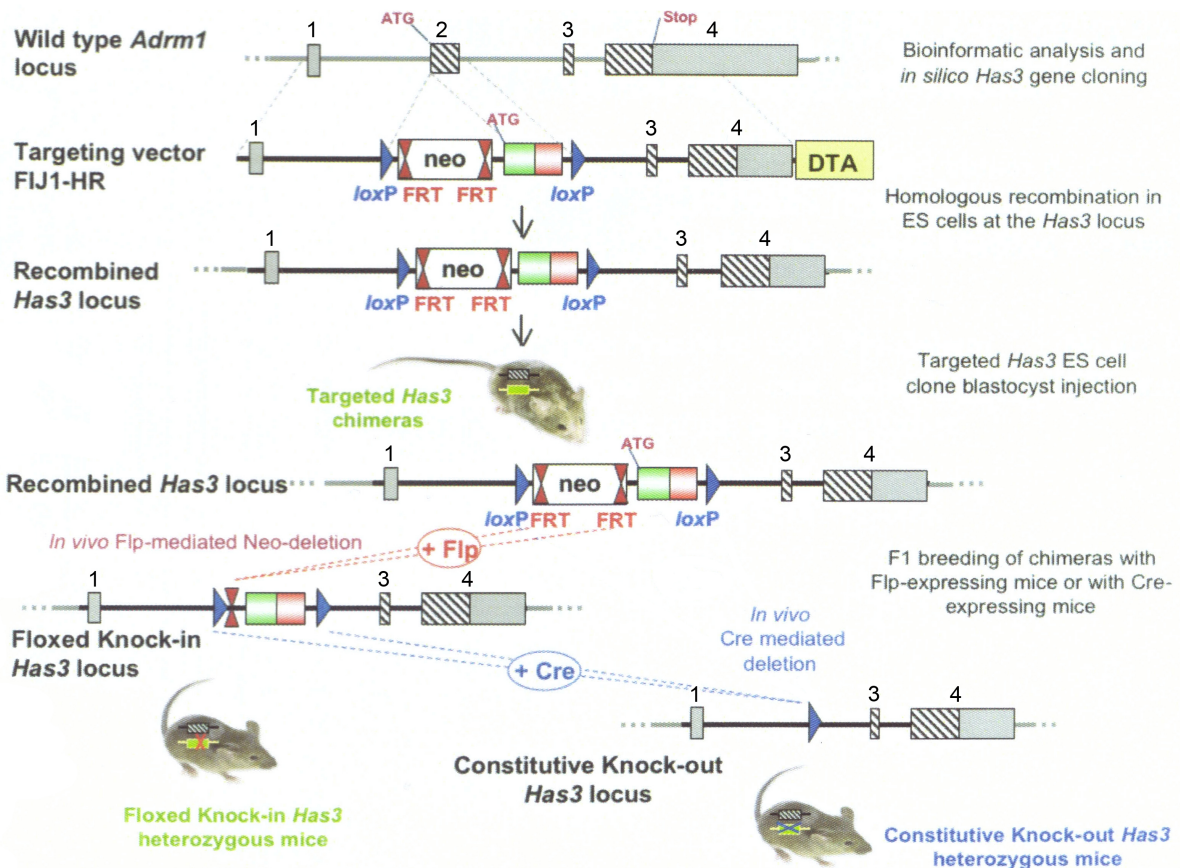


Figure 4: Diagram of the generation of global *Has3*^{-/-} mice.

This figure was modified from the original documentation received from genOway where the *Has3*^{-/-} mouse was generated as part of a commercial agreement with Prof. Fischer.

These generated *Has3*-deficient mice had a mixed background of 129v and C57BL/6J due to homologous recombination in embryonic stem cells of 129v, which were transferred into C57BL/6J blastocysts. To get a uniform genetic background, mice were backcrossed to C57BL/6J (Janvier Labs; Le Genest Saint Isle, France) using the speed congenics system for at least six generations. The genetic background was checked until 99% of congruence with C57BL/6J mice was achieved. Finally, *Has3*-deficient mice were crossbred with *ApoE*-deficient mice, which also have a C57BL/6J background, to get constitutive global *ApoE*^{-/-}/*Has3*^{-/-} mice.

Animal housing, breeding, and the experiments were performed in the animal facility of the Heinrich-Heine-University Düsseldorf. All animals had open access to food and pathogen-free drinking water and were kept at a regular 12-hour day/night rhythm. The authorizations for conducting animal experiments were granted by the “Landesamt für Natur, Umwelt und Verbraucherschutz (LANUV) Nordrhein-Westfalen, Bezirksregierung Düsseldorf” according to § 8 of the animal welfare act as amended on May 18th 2006 (Aktenzeichen 84-02.04.2013.A434).

2.1.2. Study design

Starting at 8 weeks of age, male *ApoE*^{-/-}/*Has3*^{-/-} mice and respective littermate *ApoE*^{-/-} control mice were fed a western-type diet (WD) containing 21% fat and 0.15% cholesterol (S8200-E010; Ssniff Spezialdiäten GmbH, Soest, Germany). After feeding the mice with WD for 4, 7, and 15 weeks, respectively, mice were sacrificed and organs were harvested for different analyses (Figure 5 green arrows).

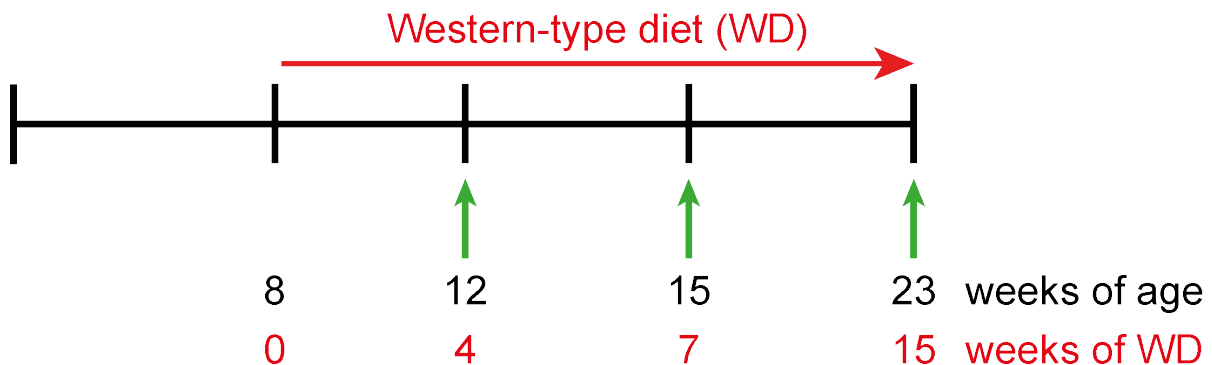


Figure 5: Experimental setup.

At the age of 8 weeks, male *ApoE*^{-/-}/*Has3*^{-/-} and *ApoE*^{-/-} mice were put on WD. After 4, 7, or 15 weeks of feeding (green arrows), mice were harvested.

2.1.3. Tissue preparation

After 4, 7, and 15 weeks of WD, *ApoE*^{-/-}/*Has3*^{-/-} mice and *ApoE*^{-/-} littermate controls were sacrificed either by inhalation of CO₂ or via intraperitoneal injection of ketamine/xylazine and subsequent perfusion with phosphate buffered saline (PBS) or paraformaldehyde (PFA).

Blood was collected via heart puncture of the right ventricle and anticoagulated either using ethylenediaminetetraacetic acid (EDTA; final concentration: 10mM) or heparin (final concentration: 50U/ml; ratiopharm GmbH, Ulm, Germany). Heparinized blood was used for flow cytometric stainings of intracellular cytokines produced by circulating immune cells. EDTA-anticoagulated blood samples were used for flow cytometric measurements of circulating immune cells and the generation of blood plasma. For the generation of blood plasma, whole blood was centrifuged for 15 minutes at 800 x g at 4°C. The supernatant was replaced into a new Eppendorf tube and centrifuged for 5 minutes at 15,700 x g at 4°C. Finally, the supernatant was carefully collected and stored at -80°C.

A variety of organs were harvested for different analyses. Samples that were harvested for histochemical and immunohistochemical analyses were fixed in Roti®-Histofix 4% (Carl Roth GmbH & Co KG, Karlsruhe, Germany). Organs that were taken for RNA preparations were collected under RNase free conditions and stored

at -80°C. Tissues for flow cytometric measurements were harvested, weighed, and directly processed as described in the section 2.3 Flow cytometry.

2.2. Cell culture experiments

All cells were cultured at 37°C and 5% CO₂.

In **Table 1** all culture media that were used for cell culture are listed. For heat-inactivation of fetal calf serum (FCS), serum was heated for 30 minutes at 56°C in a water bath. Freshly added substances, for example for cell differentiation or stimulation, are listed in **Table 2**.

Table 1: List of culture media.

Gibco® Life Technologies, Paisley, Great Britain.

Culture medium	Composition	Manufacturer
DC medium	RPMI Medium 1640 (1x) + GlutaMAX™-I 10% (V/V) heat-inactivated FCS 100 U/ml Penicillin 100 µg/ml Streptomycin 1 mM Sodium Pyruvate	Gibco® Life Technologies Gibco® Life Technologies Gibco® Life Technologies Gibco® Life Technologies Gibco® Life Technologies
RPMI, 10%	RPMI Medium 1640 (1x) + GlutaMAX™-I 10% (V/V) FCS 100 U/ml Penicillin 100 µg/ml Streptomycin	Gibco® Life Technologies Gibco® Life Technologies Gibco® Life Technologies Gibco® Life Technologies

Table 2: Substances used for cell culture experiments.

GM-CSF: granulocyte-macrophage colony-stimulating factor, IL: interleukin, LPS: lipopolysaccharide.

Substance	Final concentration	Manufacturer
Recombinant murine GM-CSF	10 ng/ml GM-CSF	PeproTech, Rocky Hill, NJ, USA
Murine IL-4, recombinant	2 ng/ml IL-4	Sigma-Aldrich, St. Louis, MO, USA
LPS	1 µg/ml LPS	Sigma-Aldrich, St. Louis, MO, USA

2.2.1. Isolation of T cells from spleen and lymph nodes

For T cell isolation, axillary lymph nodes and the spleen of *ApoE*^{-/-} and *ApoE*^{-/-}/*Has3*^{-/-} mice were harvested and directly processed. To gain a single cell suspension, lymph nodes were incubated for 15 minutes at 37°C under rotation in an enzymatic digestion mix (**Table 3**) and in parallel the spleen was dissociated in PEB buffer (**Table 3**) using the gentleMACS™ Dissociator (Miltenyi Biotec, Bergisch Gladbach, Germany). Afterwards, both tissue suspensions were combined by filtration through 40µm nylon filters (Greiner Bio-One, Frankfurt, Germany) and centrifuged at 500 x g for 10 minutes at 4°C. The cells were resuspended in PEB buffer and the cell number was determined using a Neubauer chamber. All following steps for T cell isolation were performed according to manufacturer instructions described for the Pan T cell isolation Kit II for murine cells (Miltenyi Biotec, Bergisch Gladbach, Germany) (**Figure 6**). Briefly, upon centrifugation at 300 x g for 10 minutes at 4°C, cells were resuspended in PEB and incubated for 5 minutes at 4°C with the Pan T Cell Biotin-Antibody Cocktail to label all cells but T lymphocytes (**Figure 6.1**). Next, PEB was added and another incubation step of 10 minutes at 4°C with Anti-Biotin MicroBeads followed to magnetically label the cells that were bound to the biotinylated antibodies (**Figure 6.2**). Thereupon, the cell suspension was applied onto an LS column (Miltenyi Biotec, Bergisch Gladbach, Germany) that was placed in a magnetic field (MACS Separator; Miltenyi Biotec, Bergisch Gladbach, Germany) to separate non-labeled T cells from magnetically labeled cells (**Figure 6.3**). The flow-through, which contained the non-labeled T cells, was collected and the column was washed once with PEB. Again, the flow-through, which contained T cells, was collected. These collected T cells were centrifuged, resuspended in RPMI, 10% (**Table 1**), and either used for direct flow cytometric analyses, cultivation, or RNA extraction.

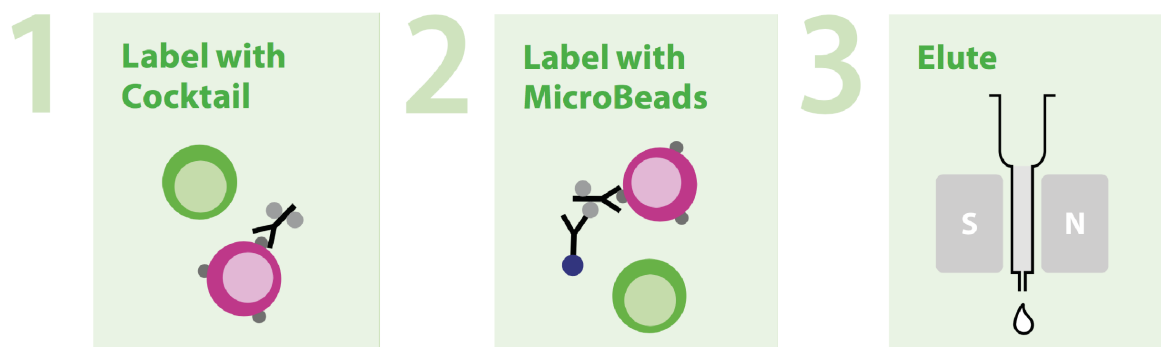


Figure 6: T cell isolation in three steps.

Modified from the product information provided by Miltenyi Biotec (Bergisch Gladbach Germany).

2.2.2. T cell activation using anti-CD3/-CD28 beads

Directly after T cell isolation, cells were cultured at a final density of 1×10^6 cells per ml and stimulated using the T Cell Activation/Expansion Kit for mouse T cells (Miltenyi Biotec, Bergisch Gladbach, Germany). The bead preparation and T cell activation was performed as described in the manufacturer's protocol. These particles are able to mimic T cell activation by antigen-presenting cells.

First, anti-biotin MACSiBead Particles were loaded with biotinylated CD3 ϵ and CD28 antibodies by an incubation for 2 hours at 4°C under rotation. After washing the loaded anti-biotin particles with RPMI, 10% medium (**Table 1**) once and a centrifugation step for 5 minutes at 300 x g at 4°C, the beads were ready to use for T cell stimulation. The beads were applied in a bead-to-cell ratio of 1:1 so that 1×10^6 beads were added to 1×10^6 T cells. As a negative control, no beads were added to the T cells. Both stimulated and unstimulated T cells were cultivated for 24 hours and 48 hours and then harvested for flow cytometric measurements.

2.2.3. Generation of bone marrow-derived dendritic cells (BM-DCs)

Figure 7 shows a timeline of DC cultivation and subsequent experiments as well as performed analyses.

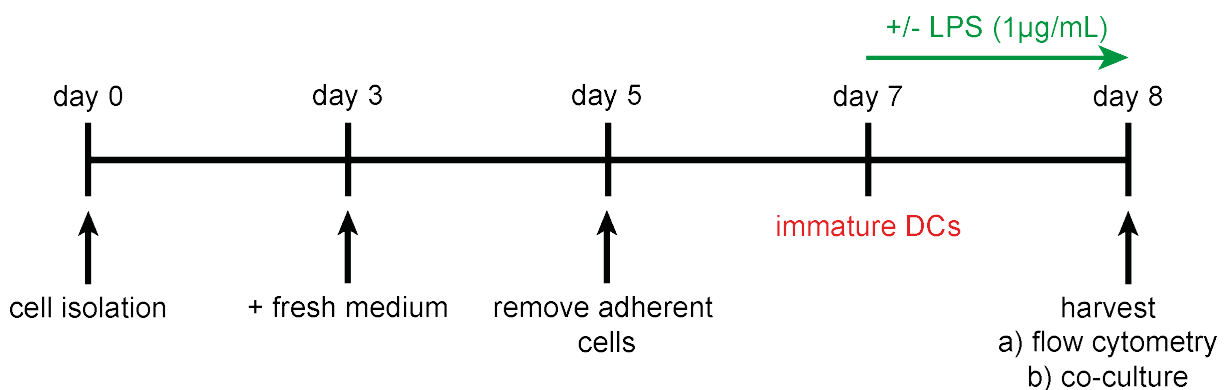


Figure 7: Experimental setup for the generation of BM-DCs.

Bone marrow cells were isolated on day 0 and cultivated for 7 days to obtain immature DCs. Those were treated with or without LPS to activate cells. LPS: lipopolysaccharide.

2.2.3.1. Isolation and differentiation of BM-DCs

Murine bone marrow-derived dendritic cells (BM-DCs) were isolated from 8 to 12 week-old female mice of the genotypes $ApoE^{-/-}$ and $ApoE^{-/-}/Has3^{-/-}$. For cell isolation, we refer to the protocol previously described by Madaan and colleagues [96], while minor changes were added to the protocol.

Mice were euthanized with CO₂ and the external areas were disinfected with 70% ethanol to reduce the risk of contamination with fur. All following steps were performed with disinfected or sterile forceps, scissors, and scalpels. First, the skin and the muscles were carefully removed on the leg bones to expose femur, tibia, and fibula. To gain the bone marrow, the joints of femur and tibia were cut off, the bones were rinsed with sterile DC medium (**Table 1**) using a syringe with a 26G needle, and the flow through containing the bone marrow cells was collected. To disrupt any cell clusters, the suspension was vigorously pipetted up and down and then filtered through a 100µm nylon filter (Greiner Bio-One, Frankfurt, Germany). After centrifugation at 300 x g for 5 minutes at room temperature (RT), the cell pellet was resuspended in DC medium (**Table 1**) and the cell yield was determined by counting viable cells using a Neubauer chamber. Finally, 10x10⁶ cells were cultivated in a 100mm petri dish at a final concentration of 1x10⁶ cells per ml medium. To induce cell differentiation of undifferentiated stem cells into the DC lineage, 10ng/mL recombinant murine granulocyte-macrophage colony-stimulating factor (GM-CSF; **Table 2**) and 2ng/mL murine interleukin-4 (IL-4; **Table 2**) were added freshly to the medium. After 3 days of cultivation, fresh DC medium and cytokines were added to the culture, and cells were cultivated for another 2 days under standard culture conditions. Then, non-adherent and loosely-adherent cells were collected, centrifuged for 5 minutes at RT at 300 x g, and cultivated in a new petri dish with fresh medium and cytokines for another 2 days. Adherent cells comprised of macrophages on the old petri dish were discarded. On day 7, immature DCs were ready to harvest to be used for further experiments.

2.2.3.2. Stimulation of BM-DCs

Immature DCs were harvested on day 7 by collecting the supernatant and adherent cells. Adherent cells were removed by incubation with cold PBS for 10 minutes at 4°C and then carefully scraped off the plate. After centrifugation at 300 x g for 5 minutes at RT, the pellet was resuspended in DC medium, and cells were counted. Cells were sowed at a final concentration of 1x10⁶ cells per ml medium and the medium was supplemented with GM-CSF and IL-4. To stimulate and activate DCs, 1µg/ml lipopolysaccharide (LPS; **Table 2**) was added to the medium. As control, DCs were cultivated without LPS stimulation. After 24 hours, stimulated and non-stimulated cells were harvested as indicated above and then cells were analyzed by flow cytometry.

2.3. Flow cytometry

For flow cytometric analyses of immune cells, a broad spectrum of lymphoid, non-lymphoid tissues, and isolated cells were harvested and directly processed to get a single cell suspension. To disrupt tissue structures and receive conditions for optimal epitope stainings different buffers were used. All buffers required for tissue preparation are listed in **Table 3**.

Table 3: List of buffers used for flow cytometry.

Sigma-Aldrich, St. Louis, MO, USA; Gibco® Life Technologies, Paisley, Great Britain; Worthington Biochemical Corporation, Lakewood, NJ, USA; Roche Diagnostics GmbH, Mannheim, Germany; Carl Roth GmbH & Co KG, Karlsruhe, Germany.

Buffer	Composition	Manufacturer
Lysis buffer	155 mM NH ₄ Cl 10 mM KHCO ₃ 0.1 mM EDTA	
PEB buffer	2 mM EDTA 0.5 % (M/V) BSA In DPBS	Sigma-Aldrich Gibco® Life Technologies
Hank's Balanced Salt Solution (HBSS)	1.26 mM CaCl ₂ 0.49 mM MgCl ₂ 0.41 mM MgSO ₄ 5.3 mM KCl 0.44 mM KH ₂ PO ₄ 4.17 mM NaHCO ₃ 137.39 mM NaCl 0.34 mM Na ₂ HPO ₄ 5.55 mM Glucose	
Enzymatic digestion mix	600 U/mL Collagenase II 60 U/mL DNase I In HBSS	Worthington Biochemical Corporation Roche Diagnostics GmbH
Fixation Solution	0.1% (V/V) Roti®-Histofix 4% In DPBS	Carl Roth GmbH & Co KG Gibco® Life Technologies

RPMI, 10%	RPMI Medium 1640 (1x) + GlutaMAX™-I 10% (V/V) FCS 100 U/ml Penicillin 100 µg/ml Streptomycin	Gibco® Life Technologies Gibco® Life Technologies Gibco® Life Technologies Gibco® Life Technologies
RPMI, 0%	RPMI Medium 1640 (1x) + GlutaMAX™-I 100 U/ml Penicillin 100 µg/ml Streptomycin	Gibco® Life Technologies Gibco® Life Technologies Gibco® Life Technologies

To identify immune cells within the single cell suspension, antibodies were used in different combinations. A list of antibody combinations, clone, and manufacturer is depicted in **Table 4**. Gating schemes for each staining are displayed in the Appendix.

Table 4: Antibody combinations for flow cytometric stainings.

PVAT: perivascular adipose tissue, Th: T helper cell, DC: dendritic cell.

BioLegend, San Diego, CA, USA; BD Biosciences, San Jose, CA, USA; eBioscience, San Diego, CA, USA; molecular probes® life technologies™, Eugene, OR, USA; Invitrogen, Waltham, MA, USA.

Immune cell Tissue	Antibody	Clone	Manufacturer
Monocytes Blood	Ly6C – AlexaFluor®488 CD11b – PE CD115 – APC	HKL1.4 M1/70 AFS98	BioLegend BD Biosciences eBioscience
Macrophages Aorta, PVAT	F4/80 – AlexaFluor®488 CD45 – PE CD11b – PacificBlue™ Live/Dead®-Aqua	BM8 30-F11 M1/70	BioLegend BioLegend BioLegend molecular probes® life technologies™
Granulocytes Aorta	Ly6C – AlexaFluor®488 CD45 – PE CD11b – PE/Dazzle™ 594 F4/80 – AlexaFluor®647 CD11c – APC/Cy7 Ly6G – PacificBlue™ Live/Dead®-Aqua	HKL1.4 30-F11 M1/70 BM8 N418 1A8	BioLegend BioLegend BioLegend BioLegend BioLegend BioLegend molecular probes® life technologies™

B and T lymphocytes Blood, aorta, PVAT	CD4 – FITC CD45 – PE CD8a – AlexaFluor®647 CD3 – APC/Cy7 CD19 – PacificBlue™ Live/Dead®-Aqua	RM4-5 30-F11 53-6.7 17A2 6D5	Invitrogen BioLegend BioLegend BioLegend BioLegend molecular probes® life technologies™
T cell activation Blood, spleen, lymph nodes	CD4 – FITC CD45 – PE CD44 – PE/Cy7 CD8a – AlexaFluor®647 CD3 – APC/Cy7 CD62L – PacificBlue™ Live/Dead®-Aqua	RM4-5 30-F11 IM7 53-6.7 17A2 MEL-14	Invitrogen BioLegend BioLegend BioLegend BioLegend BioLegend molecular probes®, life technologies™
T cell activation <i>In vitro</i> activation	CD4 – FITC CD25 – PE CD44 – PE/Cy7 CD8a – AlexaFluor®647 CD45 – AlexaFluor®700 CD3 – APC/Cy7 CD62L – PacificBlue™ Live/Dead®-Aqua	RM4-5 3C7 IM7 53-6.7 30-F11 17A2 MEL-14	Invitrogen BioLegend BioLegend BioLegend BioLegend BioLegend BioLegend molecular probes® life technologies™
Th1 and Th2 Blood	CD4 – FITC T-bet – PE IL-4 – PE/Dazzle™ 594 IFN-γ – PE/Cy7 IL-5 – APC CD3 – AlexaFluor®700 Gata3 – BrilliantViolet 421™ Live/Dead®-Aqua	RM4-5 4B10 11B11 XMG1.2 TRFK5 17A2 16E10A23	Invitrogen BioLegend BioLegend BioLegend BioLegend BioLegend BioLegend molecular probes® life technologies™

Th17 and Treg Blood	CD4 – FITC IL-17A – PE FoxP3 – PE/Cy7 ROR γ T – APC CD3 – AlexaFluor®700 Live/Dead®-Aqua	RM4-5 eBio17B7 FJK-16s B2D 17A2	Invitrogen eBioscience eBioscience eBioscience BioLegend molecular probes® life technologies™
DC activation <i>In vitro</i> activation	MHC II – FITC CD45 – PE CD86 – PE/Cy7 CD11c – APC CD3 – APC/Cy7 CD11b – PacificBlue™ Live/Dead®-Aqua	M5/114.15.2 30-F11 GL-1 N418 17A2 M1/70	eBioscience BioLegend BioLegend BioLegend BioLegend BioLegend molecular probes® life technologies™
Purity BM-DCs, isolated T cells	F4/80 – AlexaFluor®488 CD11b – PE CD11c – PE/Cy7 CD19 – APC CD45 – AlexaFluor®700 CD3 – APC/Cy7 Ly6G – PacificBlue™ Live/Dead®-Aqua	BM8 M1/70 N418 6D5 30-F11 17A2 1A8	BioLegend BioLegend BioLegend BioLegend BioLegend BioLegend BioLegend molecular probes® life technologies™

Each immune cell can be identified by a pattern of surface epitopes alone or in combination with intracellular proteins. In **Table 5** the used combinations of surface and intracellular markers are shown.

Table 5: Marker combinations for the identification of immune cells.

Immune cell	Marker combination for identification
Dendritic cell (DC)	CD45 ⁺ CD11b ⁺ CD11c ⁺
Unstimulated DC	CD45 ⁺ CD11b ⁺ CD11c ⁺ MHCII ⁺
Stimulated DC	CD45 ⁺ CD11b ⁺ CD11c ⁺ MHCII ⁺⁺ CD86 ⁺
Neutrophil	CD45 ⁺ CD11b ⁺ Ly6G ⁺
Monocyte	CD45 ⁺ CD11b ⁺ CD115 ⁺ Ly6C ^{low / int / high}
Macrophage	CD45 ⁺ CD11b ⁺ F4/80 ⁺
B lymphocyte	CD45 ⁺ CD19 ⁺
T lymphocyte	CD45 ⁺ CD3 ⁺
CD4 ⁺ T lymphocyte	CD45 ⁺ CD3 ⁺ CD4 ⁺
Th1 cell	CD45 ⁺ CD3 ⁺ CD4 ⁺ T-bet ⁺ IFN- γ ⁺
Th2 cell	CD45 ⁺ CD3 ⁺ CD4 ⁺ Gata3 ⁺ IL-5 ⁺
	CD45 ⁺ CD3 ⁺ CD4 ⁺ Gata3 ⁺ IL-4 ⁺
Th17 cell	CD45 ⁺ CD3 ⁺ CD4 ⁺ ROR γ T ⁺ IL-17A ⁺
Treg	CD45 ⁺ CD3 ⁺ CD4 ⁺ FoxP3 ⁺
CD8 ⁺ T lymphocyte	CD45 ⁺ CD3 ⁺ CD8 ⁺
Naïve T lymphocyte	CD45 ⁺ CD3 ⁺ CD62L ⁺ CD44 ⁻
Effector T lymphocyte	CD45 ⁺ CD3 ⁺ CD62L ⁻ CD44 ⁺
Central memory T lymphocyte	CD45 ⁺ CD3 ⁺ CD62L ⁺ CD44 ⁺

In general, all antibodies as well as the Live/Dead®-Fixable Aqua Dead Cell Stain Kit (Live/Dead®-Aqua; molecular probes® life technologies™, Eugene, OR, USA) were used in a dilution of 1:25. As different staining protocols were required for optimal surface and intracellular stainings no general staining protocol is described here. The respective protocols are described in the corresponding sections below.

To determine absolute cell numbers in the tissue, Flow-Count™ Fluorospheres (Beckman Coulter Inc., Krefeld, Germany) were used according to the manufacturer's instructions.

Just before measuring, 200µl Coulter® Isoton II Diluent (Isoton; Beckman Coulter Inc., Krefeld, Germany) were added to each sample. Then, all samples were measured on the Gallios™ flow cytometer (Beckman Coulter Inc., Krefeld, Germany) and analyzed using Kaluza® Flow Analysis Software (Beckman Coulter Inc., Krefeld, Germany).

2.3.1. Blood

After 4, 7, and 15 weeks of WD feeding, blood was collected in a final experiment by cardiac puncture and anticoagulated with EDTA or heparin for flow cytometric measurements.

2.3.1.1. Lymphocytes

For flow cytometric analysis of circulating B and T lymphocytes, EDTA-anticoagulated blood samples were incubated for 7 minutes at 4°C with hypotonic lysis buffer (**Table 3**) to lyse erythrocytes. Afterwards, cells were centrifuged for 10 minutes with 300 x g at 4°C, the supernatant was removed, and the cell pellet was resuspended in PEB buffer (**Table 3**). Then, the cells were incubated with purified anti-mouse CD16/32 (Clone 93; BioLegend, San Diego, California, USA) for 10 minutes at 4°C to inhibit unspecific binding of the antibodies. Finally, the samples were stained with antibodies to discriminate T and B lymphocytes, and to identify T cells of different activation (**Table 4**). Cell numbers are depicted as cells per μl blood or as percentage.

2.3.1.2. T helper cells (Th1, Th2, Th17) and regulatory T cells (Treg)

Activated CD4⁺ T lymphocytes can display different effector functions and thus they can be further differentiated into Th1, Th2, Th17, and Treg cells. These cells are defined by a combination of transcription factors and cytokines. To stain intracellular cytokines and transcription factors a specialized protocol with fixation and permeabilization steps is required. The used protocol was modified from the “Intracellular Flow Cytometry Staining Protocol: For the Detection of Intracellular Cytokines and Other Intracellular Targets” provided by BioLegend (San Diego, CA, USA).

Blood was collected via heart puncture and anticoagulated with heparin (final concentration: 50U/ml; ratiopharm GmbH, Ulm, Germany). Heparinized blood was mixed in a 1:1 ratio with RPMI, 0% medium (**Table 3**) and plated in a 6-well plate. Then whole blood samples were stimulated for 4 hours at 37°C and 5% CO₂ with a Cell Stimulation Cocktail containing protein transport inhibitors (eBioscience, San Diego, CA, USA) to induce cytokine production and at the same retaining cytokines in the vacuoles by protein transport inhibition. After stimulation, all cells were carefully removed from the 6-well plate and erythrocytes were lysed for 7 minutes at RT using lysis buffer (**Table 3**). Next, cells were centrifuged for 10 minutes with 800 x g at 4°C, washed with PEB buffer once, and resuspended in PEB buffer for the following surface staining. First, the cells were incubated with purified anti-mouse

CD16/32 (Clone 93, BioLegend, San Diego, California, USA) for 10 minutes at 4°C, then Live/Dead®-Aqua as well as anti-CD4 and anti-CD3 antibodies were added and incubated for 30 minutes at 4°C in the dark. Upon surface marker staining, cells were washed with PEB, fixed with FoxP3 Fix/Perm buffer (BioLegend, San Diego, CA, USA) for 20 minutes at RT in the dark, and permeabilized with FoxP3 Perm (BioLegend, San Diego, CA, USA) for 15 minutes at RT in the dark. After centrifugation, cells were resuspended in FoxP3 Perm buffer and stained for 20 minutes at RT in the dark for intracellular cytokines and transcription factors to investigate Th1, Th2, Th17, and Treg cells (**Table 4**). Finally, stained cells were washed once with FoxP3 Perm buffer, centrifuged, and resuspended in PEB. Then, cells were measured on the Gallios™ flow cytometer.

2.3.1.3. Monocytes

The analysis of circulating monocytes was performed according to the protocol described by Breslin and colleagues [97] using CD115 for the identification of monocytes. At first, EDTA-anticoagulated blood samples were incubated with purified anti-mouse CD16/32 for 10 minutes, followed by antibody staining for 15 minutes at 4°C. Afterwards, red erythrocytes were removed by incubation with lysis buffer for 7 minutes and immediate centrifugation for 10 minutes with 800 x g at 4°C. In the next step, the cells were fixed for 20 minutes at RT by resuspending the cells in fixation solution (**Table 3**). After a last centrifugation for removing the paraformaldehyde, cells were resuspended in PEB and measured using the Gallios™ flow cytometer. Quantification is indicated as cell numbers per µl blood.

2.3.2. Spleen

To obtain single cell suspensions of spleens, they were placed in gentleMACS C Tubes (Miltenyi Biotec, Bergisch Gladbach, Germany) containing PEB buffer and mechanically dissociated by using the gentleMACS dissociator (Miltenyi Biotec, Bergisch Gladbach, Germany). Afterwards, tissue debris was removed by a filtration step through a 70µm nylon filter (Greiner Bio-One, Frankfurt, Germany). Samples were centrifuged with 300 x g at 4°C for 10 minutes and thereafter, erythrocytes were lysed for 7 minutes using the lysis buffer (**Table 3**). To remove the lysis buffer, the samples were centrifuged again and then resuspended in RPMI, 10% (**Table 3**) and incubated for 30 minutes at 37°C to allow the cells to recover from dissociation and the hypotonic buffer. After another centrifugation step, single cells were finally resuspended in PEB buffer for optimal staining conditions. First, unspecific binding was prohibited by pre-incubation with purified anti-mouse CD16/32 (Clone 93;

BioLegend, San Diego, California, USA) for 10 minutes at 4°C. An incubation of 30 minutes at 4°C with Live/Dead®-Aqua followed to allow the exclusion of dead cells. Finally, antibodies against surface antigens were added to the cells for 15 minutes according to combinations for splenic staining listed in **Table 4**. Naïve, effector, and memory T cells are shown as cell numbers per mg tissue.

2.3.3. Lymph nodes

The proper axillary and the accessory axillary lymph nodes [98] (in the following termed as axillary lymph nodes) from the right-hand and the left-hand side were harvested and used for flow cytometric measurements. Per animal the four lymph nodes were pooled and in a first step digested using an enzymatic digestion mix (**Table 3**) for 15 minutes at 37°C on the MaxRotator (Miltenyi Biotec, Bergisch Gladbach, Germany). Digested lymph nodes were then mashed through a 70µm nylon filter (Greiner Bio-One, Frankfurt, Germany) and centrifuged for 10 minutes at 4°C and 300 x g to remove the digestion mix. Then, the cell pellet was resuspended in RPMI, 10% (**Table 3**) for an incubation at 37°C for 30 minutes. Another centrifugation step followed to remove the medium and then cells were resuspended in PEB buffer. The staining was performed as previously described for splenic cells (section 2.3.2 Spleen) starting with an incubation with purified anti-mouse CD16/32 (Clone 93; BioLegend, San Diego, California, USA), followed by a Live/Dead®-Aqua stain, and finally the antibodies were added. Stained samples were measured on the Gallios™ flow cytometer. The cell numbers per mg tissue are displayed.

2.3.4. Aorta and PVAT

The preparation of a single cell suspension of the aorta and PVAT was performed according to the protocol of Butcher *et al.* [99] with minor changes. Briefly, before removing the aortas they were flushed with DPBS (Gibco® Life Technologies, Paisley, Great Britain) supplemented with heparin (final concentration: 20U/ml; ratiopharm GmbH, Ulm, Germany) via the left ventricle to remove the blood. Next, aortas were carefully excised from the curvature till the femoral bifurcation, the surrounding adipose tissue was carefully removed, and PVAT was retained for following digestion. The aortic tissues were cut into small pieces and digested separately in an collagenase containing enzymatic digestion mix (**Table 3**) for 1 hour at 37°C on a MaxRotator (Miltenyi Biotec, Bergisch Gladbach, Germany) for optimal digestion. Digested samples were vortexed twice for 5 seconds to mechanically disrupt remaining pieces of tissue and then directly mashed through a 70µm nylon filter (Greiner Bio-One, Frankfurt, Germany). The samples were centrifuged at

300 x g for 10 minutes at 4°C to remove the enzymatic digestion buffer and the pellet was resuspended in RPMI, 10% medium (**Table 3**) and incubated for 30 minutes at 37°C to recover the cells after the harsh digestion. Upon another centrifugation step, the cells were resuspended in PEB buffer, incubated with purified anti-mouse CD16/32 for 10 minutes, stained with Live/Dead®-Aqua for 30 minutes, and finally stained with several antibody combinations for 15 minutes to analyze macrophages, monocytes, neutrophils, dendritic cells, and lymphocytes (**Table 4**). For all aortas and PVAT, the percentage of erythrocytes determined by TER119 staining was measured. When the percentage of TER119⁺ staining was greater than 30% the sample was excluded from the analysis. In the quantification graphs, the cell numbers per total tissue are shown.

2.3.5. Isolated T lymphocytes and BM-DCs

2.3.5.1. Purity of T lymphocytes and BM-DCs

Directly after T cell isolation, T lymphocytes were processed to analyze purity by flow cytometry. The purity of BM-DCs was assessed at day 8 just after differentiation and stimulation. Cultivated BM-DCs were harvested by incubation with cold DPBS for 10 minutes at 4°C, followed by scraping.

Both T cells and BM-DCs were centrifuged at 800 x g for 10 minutes at 4°C and resuspended in PEB buffer (**Table 3**). Next, they were incubated with purified anti-mouse CD16/32 for 10 minutes to inhibit unspecific antibody binding, then Live/Dead®-Aqua staining for 30 minutes followed, and for another 15 minutes cells were stained with a combination of different antibodies (**Table 4**). Detected cell types are depicted as percentage of living cells.

2.3.5.2. *In vitro* activation

2.3.5.2.1. Activation status of T lymphocytes

The activation status of isolated T lymphocytes was investigated before and after *in vitro* stimulation. Initially, the distinction of naïve, effector, and central memory T cells (**Table 5**) was analyzed directly after T cell isolation. Secondly, these analyses were performed after 24 and 48 hours of T cell stimulation with anti-CD3/-CD28 beads (section 2.2.2).

If required, cells were harvested from a multi-well plate and collected in an Eppendorf tube. Thereupon, cells were centrifuged at 800 x g for 10 minutes at 4°C, washed once with PEB buffer (**Table 3**), and centrifuged again. The resulting cell pellet was resuspended in PEB buffer and single cells were incubated consecutively with

purified anti-mouse CD16/32, Live/Dead®-Aqua, and antibodies. To measure the samples, 200µl Coulter® Isoton II Diluent were added. In the graphs, the percentage distribution of naïve, effector, and central memory T cells is depicted.

2.3.5.2.2. Activation status of BM-DCs

At day 8 of the BM-DC culture, the activation status of BM-DCs was examined by analyzing the co-expression of CD86 and MHC II using flow cytometry. Previously stimulated BM-DCs with LPS and unstimulated control cells were harvested after an incubation with cold DPBS for 10 minutes at 4°C. Then, cells were centrifuged at 800 x g for 10 minutes at 4°C and the cell pellet containing the BM-DCs was resuspended in PEB buffer (**Table 3**) for the following staining with Live/Dead®-Aqua and antibodies (**Table 4**). The results are depicted as percentage of CD11b⁺CD11c⁺ DCs.

2.4. Blood plasma analysis

2.4.1. Multiplex analysis

Circulating cytokines and chemokines were analyzed in murine plasma using multiplex analyses to examine a broad variety of different cytokines within one sample. The Bio-Plex Pro™ Mouse Cytokine 23-plex Assay (BioRad, Hercules, CA, USA) was used according to the provided instructions with plasma samples diluted 1:4 to measure the 23 cytokines eotaxin, granulocyte-colony stimulating factor (G-CSF), GM-CSF, IFN-γ, IL-1α, IL-1β, IL-2, IL-3, IL-4, IL-5, IL-6, IL-9, IL-10, IL-12(p40), IL-12(p70), IL-13, IL-17A, keratinocyte-derived cytokine (KC/CXCL1), MCP-1/CCL2, macrophage inflammatory protein (MIP)-1α, MIP-1β, RANTES/CCL5, and TNF-α. The measurement was performed with a Bio-Plex® 200 System (BioRad, Hercules, CA, USA) and the calculation of the concentrations were done with the Bio-Plex Manager Software™ (BioRad, Hercules, CA, USA). Absolute concentrations of the cytokines are shown as pg/ml. Dr. Sonja Hartwig and Dr. Stefan Lehr performed the measurement at the German Diabetes Center Düsseldorf.

2.4.2. Plasma cholesterol levels

The analyses of LDL/VLDL cholesterol, and HDL cholesterol were performed as specified by the manufacturer using the HDL and LDL/VLDL Qualification Colorimetric/Fluorometric Kit (BioVision Inc., Milpitas, CA, USA). All concentrations are shown as mg/dl. Irmhild Rüter carried out the measurement.

2.5. Histology and immunohistochemistry

The heart and the brachiocephalic artery (BCA) were harvested and fixed for 24 hours at 4°C in Roti®-Histofix 4% (Carl Roth GmbH & Co KG, Karlsruhe, Germany). Subsequently, they were dehydrated and embedded in paraffin. Using the rotary microtome RM 2255 (Leica Microsystems, Wetzlar, Germany), embedded hearts were sliced into tissue sections of a thickness of 5µm and BCAs into 10µm sections. As soon as the valves of the aortic root appeared, two consecutive sections were positioned on each slide. For each staining one slide with two sections was used. For the BCA, three consecutive sections were placed on one microscope slide.

Before staining, all tissue sections were fixed for 1 hour at 60°C on the slide. Afterwards, slices were deparaffinized by means of a decreasing ethanol series. For the aortic root sections, the dewaxing contained three consecutive incubation steps with Roticlear® (Carl Roth GmbH & Co KG, Karlsruhe, Germany) for 15 minutes each, followed by a 2 minute incubation in 100%, 95%, and 75% ethanol, respectively. Finally, heart sections were washed three times for 5 minutes each in PBS. BCA sections were deparaffinized by incubation for 5 minutes in each reagent: 2x xylene, 2x 100% ethanol, 2x 95% ethanol, 1x 70% ethanol, and 2x deionized water.

Buffers and solutions that were used for histochemical and immunohistochemical stainings are depicted in **Table 6**, including their composition and manufacturer.

Table 6: Buffers and solutions for histological stainings.

PBS: phosphate buffered saline, FCS: fetal calf serum, BSA: bovine serum albumin. Gibco® Life Technologies, Paisley, Great Britain; Sigma-Aldrich, St. Louis, MO, USA; Fluka, Buchs, Swiss; Waldeck GmbH & Co. KG, Münster, Germany.

Buffer/Solution	Composition	Manufacturer
PBS	137 mM NaCl 2.7 mM KCl 1.5 mM KH ₂ PO ₄ 8.3 mM Na ₂ HPO ₄ pH 7.4	
Blocking buffer	20 mM Tris-HCl 137 mM NaCl 10% (V/V) FCS 1% (M/V) BSA	Gibco® Life Technologies Sigma-Aldrich
3% H ₂ O ₂	3% (V/V) H ₂ O ₂ in PBS	
Oil-Red-O staining solution	35ml of 0.5% (M/V) Oil-Red-O stock solution (in methanol) 10ml 1 M NaOH	Sigma-Aldrich

In **Table 7** all primary and secondary antibodies required for immunohistochemical stainings to detect macrophage- and smooth muscle cell (SMC)-like cells are listed.

Table 7: Primary and secondary antibodies for immunohistochemistry.

HRP: horseradish peroxidase.

Antibody	Dilution	Manufacturer
Anti-Mouse/Human Mac-2 (Galectin-3)	1:1000 in 1% BSA in PBS	Cedarlane, Burlington, Canada
Goat anti-Rat IgG2A Secondary Antibody [HRP]	1:1500 in PBS	Novus Biologicals, Abingdon, Great Britain
Anti-alpha smooth muscle Actin antibody	1:300 in 1% BSA in PBS	Abcam, Cambridge, Great Britain
Goat anti-rabbit IgG-HRP	1:400 in PBS	Santa Cruz Biotechnology, Dallas, TX, USA

2.5.1. Hematoxylin & eosin staining (H&E)

After dewaxing and washing with water, BCA sections were stained. First, tissue sections were incubated for 15 seconds with hematoxylin, followed by a washing step with tap water, thereafter a bluing reagent (Richard-Allan Scientific, San Diego, CA, USA) was used for 1 minute, and then the sections were rinsed for 2 minutes with tap water. This process stains all basophilic structures, such as the nuclei, in a blue color. In a next step, slides were incubated for 5 minutes with 70% ethanol. The staining of acidophilic structures using eosin followed. Finally, the tissue sections were dehydrated again by three incubations in 100% ethanol, and two xylene steps for 5 minutes each. Then, slides were covered with coverslips using a xylene-based mounting medium.

The Zeiss Axioskop 2 microscope (Carl Zeiss Microscopy GmbH, Jena, Germany) with an attached AxioCam MRc (Carl Zeiss Microscopy GmbH, Jena, Germany) was used to take pictures of H&E stained BCA sections using the 10x air objective. Image-Pro Plus 7.0 Software (Media Cybernetics, Rockville, MD, USA) was used to measure lesion area and the area bounded by the external elastic lamina (EEL) and the internal elastic lamina (IEL).

2.5.2. Staining of macrophage- and SMC-like cells

To investigate the cellular composition of atherosclerotic lesions at the aortic root, immunohistochemical stainings for Mac-2 (Galactin-3) and α -smooth muscle actin were performed. For this purpose, dewaxed and rehydrated tissue sections were treated for 1 hour at RT with blocking buffer (**Table 6**) to prevent unspecific binding of the antibodies. Afterwards, sections were incubated with either anti-mouse/human Mac-2 or anti-alpha smooth muscle actin antibody (**Table 7**) as primary antibodies over night at 4°C in a humid chamber to avoid dehydration of the sections by evaporation. One section on each slide was used as negative control and was not incubated with primary antibody but only with buffer. The next day, all sections were washed three times with PBS, followed by a treatment with 3% H₂O₂ (**Table 6**) to inactivate endogenous peroxidases. Sections were washed again with PBS and then incubated for 1 hour at RT with the secondary antibodies goat anti-rat IgG2a and goat anti-rabbit IgG (**Table 7**), respectively. Both secondary antibodies were conjugated with horseradish peroxidase (HRP), which enables the detection of bound antibodies by its reaction with 3,3'-diaminobenzidine (DAB; Zytomed, Berlin, Germany). Nuclei were counterstained with hemalum solution (Merck KGaA, Darmstadt, Germany) and finally, stained tissue sections were dehydrated again and cover slips were mounted with Roti®-Mount (Carl Roth GmbH & Co KG, Karlsruhe, Germany) on microscope slides.

Pictures were taken using an AxioImager.A2 microscope with AxioCam and AxioVS40V 4.8.2.0 Software (Carl Zeiss Microscopy GmbH, Jena, Germany). To quantify the stainings, pictures were exported into tiff-files and analyzed using the ImageJ 1.45s Software (National Institutes of health, USA) and the additional color deconvolution plugin (http://imagej.net/Colour_Deconvolution; as of 11/27/2016) to split the image into the three colors green, blue, and red. Only the red channel was used to analyze the DAB staining. First, a threshold was determined in the red channel, which discriminated specific staining signal from background signals. Defined once, the threshold was applied to all pictures of one staining. In a next step, the atherosclerotic lesions within the aortic root were defined as region of interest (ROI). Lastly, the threshold was used to measure the area fraction of positive signal within the ROI. The quantification of immunohistochemical stainings is depicted as area fraction. Stainings and analyses of aortic roots from mice fed WD for 15 weeks were accomplished by Lena Kiene.

2.5.3. Determination of the atherosclerotic lesion area at the aortic root

Three aortic root sections with a distance of 50µm were taken to determine atherosclerotic lesion area within the aortic root. For this purpose, the area of lesions located in all three aortic valves was measured using the AxioVision Software (Carl Zeiss Microscopy GmbH, Jena, Germany). Lesion area is figured as percentage of aortic root area. To gauge aortic root area, the internal elastic lamina was defined as the outer border of the root. As three sections per aortic root were analyzed, the average per animal was used for depiction. Analysis of animals receiving WD for 15 weeks was done by Lena Kiene.

2.5.4. Oil Red O (ORO) staining of whole aortas

To assess atherosclerotic plaque burden, lipid depositions within the aortic wall can be visualized by ORO stainings. Therefore, the aorta was perfused via the left heart chamber with heparin-containing (final concentration: 20U/ml; ratiopharm GmbH, Ulm, Germany) DPBS to remove the blood. Then, the whole aorta was removed from the heart to the iliac bifurcation. Excised aortas were fixed for 24 hours at 4°C in Roti®-Histofix 4% (Carl Roth GmbH & Co KG, Karlsruhe, Germany). After fixation, the surrounding adipose tissue was carefully removed. Cleaned aortas were then washed for 5 minutes in 78% methanol and stained for 90 minutes in Oil-Red-O staining solution (**Table 6**). Finally, aortas were washed in 78% methanol for 5 minutes again, to remove non-attached staining solution. For analyzing lipid

deposition, aortas were opened longitudinally. Using a camera (Canon Power Shot G6, Canon inc., Tokyo, Japan) placed on a stereomicroscope (Stemi 2000C, Carl Zeiss AG, Oberkochen, Germany) pictures were taken of stained aortas. Red staining was finally quantified using the ImageJ 1.45s Software (National Institutes of health, USA). Lena Kiene did the whole procedure, including quantification.

2.6. Gene expression analysis

2.6.1. RNA isolation

2.6.1.1. Isolated T cells

Isolated T lymphocytes from *ApoE*^{-/-} mice were resuspended in 0.5ml peqGOLD TriFast™ (PEQLAB, Biotechnologie GmbH, Erlangen, Germany) and incubated for 5 minutes at RT to lyse the cells. The following RNA preparation using the RNeasy Microarray Tissue Mini Kit (QIAGEN, Hilden, Germany) was conducted according to the manufacturer's protocol.

2.6.2. cDNA synthesis

RNA isolated from T cells was transcribed into cDNA using the QuantiTect Reverse Transcription Kit (QIAGEN, Hilden Germany) according to the manufacturer's information. After cDNA synthesis, the samples were diluted by the addition of 100µL of water.

2.6.3. Quantitative polymerase chain reaction (qPCR)

The primer sequences that were used for qPCR are listed in **Table 8**. mRNA sequences of the target genes provided by NCBI Gene were taken to design primers by the use of the Primer3Plus Software (<http://primer3plus.com/cgi-bin/dev/primer3plus.cgi>; as of 11/26/2016). To canvass specificity of the designed sequences they were blasted using NCBI primer blast.

Table 8: Primers used for qPCR.

Gene	Forward primer (5' → 3')	Reverse primer (5' → 3')
<i>Has1</i>	TATGCTACCAAGTATACCTCG	TCTCGGAAGTAAGATTTGGAC
<i>Has2</i>	CAAAAATGGGGTGGAAAGAG	ACAGATGAGGCAGGGTCAAG
<i>Has3</i>	CTCAGTGGACTACATCCAGG	GACATCTCCTCCAACACCTC
<i>Rn 18S</i>	GCAATTATTCCCCATGAACG	GGCCTCACTAAACCATCCAA

The qPCR was performed in a 96-well-plate using the Platinum® SYBR® Green qPCR SuperMix-UDG (Applied Biosystems, Foster City, CA, USA) containing a polymerase, SYBR® Green, dNTPs, and buffer. The samples were investigated for the genes listed in **Table 8**. Samples were analyzed in doublets each. 2.5µl of transcribed first-strand cDNA and 0.625µM of the respective forward and reverse primers were utilized per well in a total volume of 20µl.

For the qPCR the StepOnePlus™ Real-Time PCR System (Applied Biosystems, Foster City, CA, USA) was used. Data were analyzed with the StepOne™ Software Version 2.2.2 (Applied Biosystems, Foster City, CA, USA). Dissociation curves were analyzed to control for specificity of the amplification product and then data were evaluated by the calculation of the $2^{-\Delta\Delta C_t}$ values with the housekeeping gene 18S (*Rn 18S*) as reference gene.

2.7. Statistical analyses

Statistical evaluation was accomplished using the GraphPad Prism Software Version 7.0 (GraphPad Software, La Jolla, CA, USA). All data are presented as mean ± standard error mean (SEM) calculated from n independently performed experiments. Statistical outliers that were computed by means of the Grubb's test ($\alpha=0.05$) were excluded from the analysis. For all data sets a Gaussian distribution was assumed.

When comparing two experimental setups, data sets were analyzed using the unpaired, two-tailed student's t-test. If the f-test, which compares variances between two groups, was significant, the nonparametric, unpaired, two-tailed Mann-Whitney test was performed.

To analyze two or more independent data sets over time, e.g. immune cell changes during 15 weeks of WD feeding, the two-way ANOVA was taken for statistical calculations.

Probabilities of $p < 0.05$ were considered statistically significant.

3. Results

Time lapse analyses of *Has* mRNA expression and macrophage accumulation in murine atherosclerotic lesions revealed that early macrophage accumulation coincided with increased *Has3* expression (**Figure 3**). To investigate the role of *Has3* in atherogenesis and atheroprogession, *ApoE*-deficient mice were used as a well-established mouse model of accelerated atherosclerosis. In order to analyze if *Has3* influences the development of atherosclerosis, male *ApoE*^{-/-} mice were compared to *ApoE*^{-/-}/*Has3*^{-/-} mice. All mice were fed a cholesterol- and fat-rich WD, starting at 8 weeks of age. Atherosclerotic lesion development and concomitant changes in lymphoid and non-lymphoid tissues were assessed at different stages of lesion development (**Figure 5**).

3.1. Impact of *Has3* on atherosclerotic lesion size and cellular composition

3.1.1. Atherosclerotic plaque burden

In order to investigate if *Has3* is having an impact on atherosclerotic plaque burden in *ApoE*^{-/-} mice, atherosclerotic plaque burden was analyzed after 15 weeks of WD. Therefore, aortas from *ApoE*^{-/-} and *ApoE*^{-/-}/*Has3*^{-/-} mice were excised from the aortic arch to the aortic bifurcation. To quantify atherosclerotic plaques, Oil Red O (ORO) staining, which is a widely used histological technique to assess atherosclerosis in mice, was performed. ORO effectively stains lipids, such as triglycerides or cholesterol esters that accumulate in the lesions and thereby enable the evaluation of atherosclerotic plaque burden. Finally, the plaque burden was quantified in *en face* prepared whole aortas.

As illustrated in **Figure 8**, lipid accumulation in the aorta was significantly reduced in mice lacking *Has3* compared to *ApoE*^{-/-} control mice.

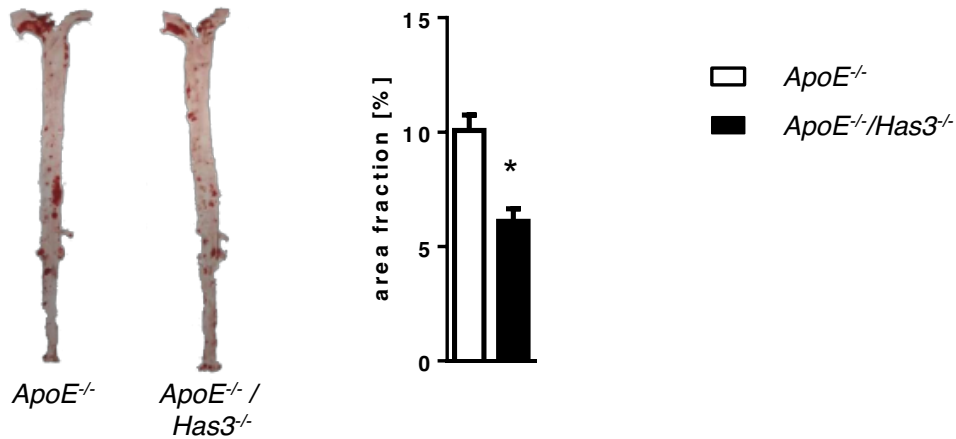


Figure 8: *Has3*-deficiency reduced atherosclerotic plaque burden in *ApoE^{-/-}* mice fed WD for 15 weeks.

Aortas from *ApoE^{-/-}* and *ApoE^{-/-} / Has3^{-/-}* mice were stained with ORO and the aortic plaque score was determined. Representative images of *en face* and ORO stained aortas are depicted. Experiments and analyses were conducted by Lena Kiene. Data are presented as mean \pm SEM; n=7; *p < 0.05.

3.1.2. Analyzing plasma cholesterol

Several epidemiological studies showed a positive correlation between serum cholesterol levels, especially LDL cholesterol levels, and the incidence of death induced by cardiovascular heart disease [100-102]. Hence, to examine whether reduced atherosclerotic plaque burden in *Has3*-deficient mice is caused by reduced serum cholesterol, cholesterol levels were measured in *ApoE^{-/-}* and *ApoE^{-/-} / Has3^{-/-}* mice after 15 weeks of WD feeding. Interestingly, while LDL/VLDL cholesterol was not different between both analyzed genotypes (**Figure 9 A**), HDL cholesterol levels were significantly reduced in *ApoE^{-/-} / Has3^{-/-}* mice despite reduced atherosclerotic plaque burden (**Figure 9 B**).

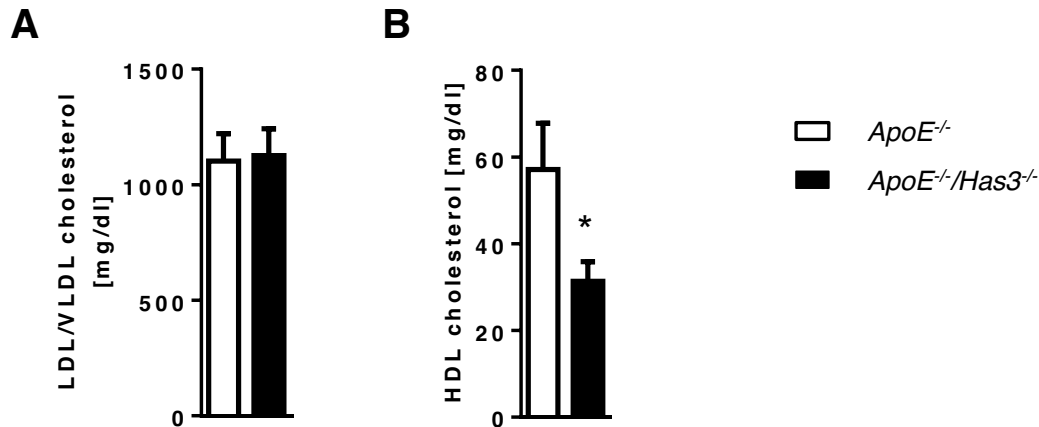


Figure 9: Lack of Has3 significantly reduced HDL cholesterol levels in *ApoE*^{-/-}-deficient mice after 15 weeks of WD.

After 15 weeks of WD, LDL/VLDL cholesterol (A) and HDL cholesterol (B) were determined in blood plasma samples of male *ApoE*^{-/-}/*Has3*^{-/-} and respective *ApoE*^{-/-} control mice. Data are shown as mean \pm SEM; n=9; * p < 0.05.

3.1.3. Atherosclerotic lesions at the aortic root

As *Has3*-deficiency did not affect LDL/VLDL cholesterol levels, it should be investigated if *Has3*-deficiency may affect the cellular composition of atherosclerotic plaques. Therefore, paraffin-embedded aortic root sections were analyzed using immunohistochemistry. As HA is known to influence both immune cells and SMCs, two different markers were used: Mac2 and α -SMA. Mac2 is a commonly used marker in atherosclerosis research to detect macrophage-like cells. But, as the origin of Mac2 expressing cells can be both of SMCs and the myeloid lineage, this staining does not allow conclusions about their origin. However, it provides information about the inflammatory processes. In contrast, α -SMA is detected in SMC-like cells [50, 103, 104]. Similar to macrophage-like cells, also SMC-like cells can be of different origins. In detail, Caplice and colleagues showed that more than 10% of cells expressing SMC markers, like α -SMA, are not of SMC origin but of hematopoietic lineage [104].

At the aortic root, atherosclerotic lesion size and cellular composition of *ApoE*^{-/-} and *ApoE*^{-/-}/*Has3*^{-/-} mice were examined after 4, 7, and 15 weeks of WD feeding. The immunohistochemical analyses of the lesions did not reveal differences in the plaque area between *ApoE*^{-/-} and *ApoE*^{-/-}/*Has3*^{-/-} mice at any of the investigated time points (Figure 10).

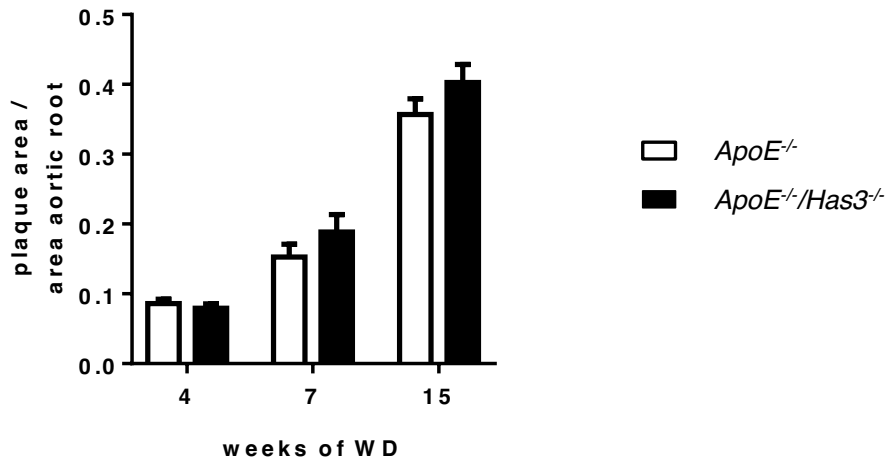


Figure 10: No alterations in atherosclerotic lesion size at the aortic root after 4, 7, and 15 weeks of WD.

Aortic roots of *ApoE*^{-/-} and *ApoE*^{-/-}/*Has3*^{-/-} mice were histologically analyzed after 4, 7, and 15 weeks of WD feeding. The quantification of normalized plaque area per aortic root area is shown. Histological stainings and analyses of mice that were fed WD for 15 weeks were performed by Lena Kiene. Data are presented as mean ± SEM; n=6-10.

Moreover, neither the area fraction of macrophage-like cells detected by Mac2 staining (**Figure 11 A**) nor the fraction of α-SMA positive cells (**Figure 11 B**) was different between the analyzed groups after 4, 7, and 15 weeks of WD, respectively, suggesting that *Has3*-deficiency did not affect the amount of the cells at the aortic root. In addition, the localization of positively stained areas is similar between *ApoE*^{-/-} and *ApoE*^{-/-}/*Has3*^{-/-} mice. However, the question if *Has3* may affect the origin of macrophage-like and SMC-like cells cannot be answered with this animal model.

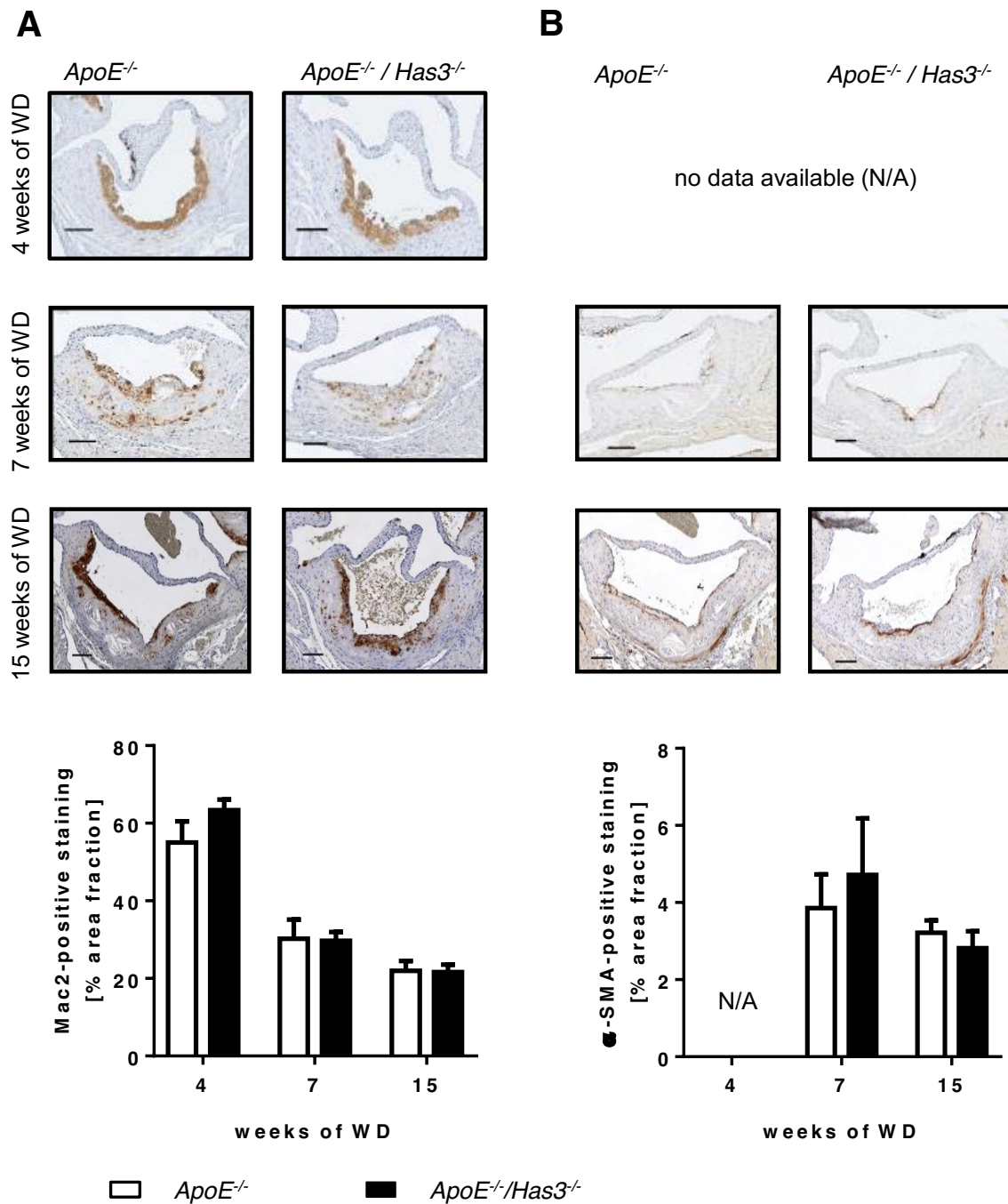


Figure 11: No alterations in the cellular composition of lesions at the aortic root after 4, 7, and 15 weeks of WD.

After 4, 7, and 15 weeks of WD feeding, paraffin-embedded aortic roots of *ApoE*^{-/-} and *ApoE*^{-/-}/*Has3*^{-/-} mice were immunohistologically stained and analyzed. Representative images and respective quantification of (A) Mac2- and (B) α-SMA-stained cells within the aortic root are displayed. All pictures were taken with a 100-fold magnification. Lena Kiene did the histological stainings and analyses of the aortic roots after 15 weeks of WD feeding. Scale bar: 100μm; data are presented as mean ± SEM; n=6-10; N/A: no data available.

3.1.4. Atherosclerotic plaques and vessel remodeling at the brachiocephalic artery (BCA)

Blood flow patterns crucially influence the localization and progression of atherosclerotic lesion development [105, 106]. Consequently, plaques develop faster at distinct locations, such as the aortic root. At other positions, atherosclerotic plaque development requires more time, such as at the BCA [107]. To investigate if *Has3*-deficiency affects atherosclerotic plaques at other positions with another flow pattern, plaque burden within the BCA was analyzed. Furthermore, as human lesions usually do not develop at the aortic root, plaques within the BCA more closely mimic human lesions [108].

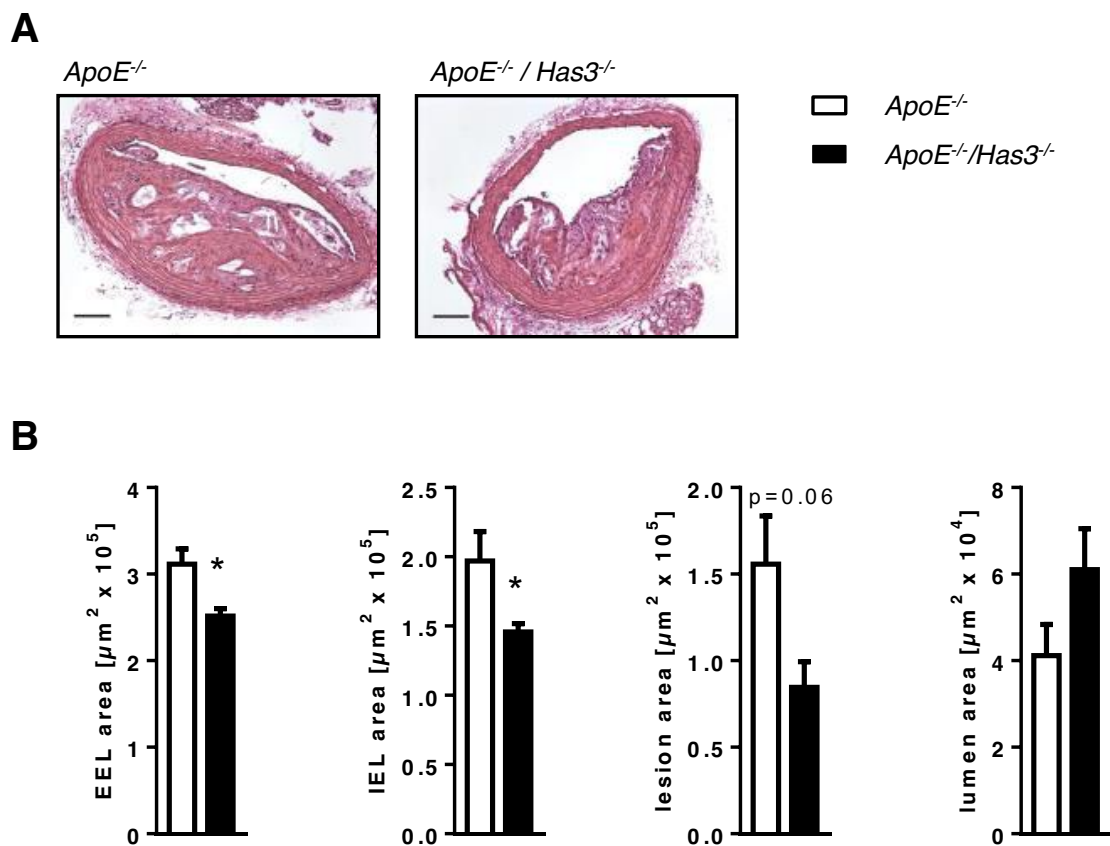


Figure 12: *Has3*-deficiency affected atherosclerotic remodeling at the BCA after 15 weeks of WD.

(A) Representative images of an H&E stained BCA section from *ApoE*^{-/-} and *ApoE*^{-/-}/*Has3*^{-/-} mice, respectively. (B) Quantification of the area within the external elastic lamina (EEL) and the internal elastic lamina (IEL) as well as the lesion area and the lumen area are shown. Scale bar: 100 μm ; data are shown as mean \pm SEM; $n=3/4$; * $p < 0.05$.

After 15 weeks of WD, BCAs were isolated from *ApoE*^{-/-} and *ApoE*^{-/-}/*Has3*^{-/-} mice, paraffin-embedded, cut, and two sections per animal (distance 300 μm) H&E stained and analyzed. To determine outward remodeling, the areas embraced by the external

elastic lamina (EEL) and the internal elastic lamina (IEL), respectively, were measured. Both the area surrounded by the EEL and by the IEL (**Figure 12 A**) was significantly reduced in *ApoE^{-/-}/Has3^{-/-}* mice compared to *ApoE^{-/-}* control mice. Additionally, the lesion area and lumen area were analyzed to assess lesion coverage. The atherosclerotic lesion area tended to be decreased ($p=0.06$) in *ApoE^{-/-}/Has3^{-/-}* mice compared to respective *ApoE^{-/-}* control mice (**Figure 12 A**). In contrast, analysis of the lumen area showed no differences between the analyzed genotypes.

3.1.5. Immune cells in advanced atherosclerotic lesions

Atherosclerosis is in a large part driven by inflammatory processes and thus immune cells substantially contribute to plaque development and progression. Besides macrophages, which are the most abundant immune cells within the lesion, a broad variety of different immune cells are found within the lesions and exhibit both pro- and anti-atherogenic properties. To get detailed information about the role of Has3 in mediating inflammatory processes in atherosclerosis, immune cells within the aortic wall were analyzed using flow cytometry.

After 15 weeks of WD, immune cells within the aortic wall were analyzed in *ApoE^{-/-}/Has3^{-/-}* and *ApoE^{-/-}* mice. As cells belonging to the innate immune system, CD11b⁺F4/80⁺ macrophages, CD11b⁺Ly6G⁺ neutrophils, and CD11b⁺CD11c⁺ dendritic cells (DCs), which exhibit phagocytic and proteolytic functions, were identified. Cell numbers of these analyzed immune cells were not different between *ApoE^{-/-}/Has3^{-/-}* and *ApoE^{-/-}* mice (**Figure 13 A-C**). Furthermore, also the number of lymphocytes was determined in the aortic wall. Neither the total cell number of B and T cells (**Figure 13 D**) nor CD4⁺ and CD8a⁺ T cell subsets (**Figure 13 E**) were different in *Has3*-deficient mice.

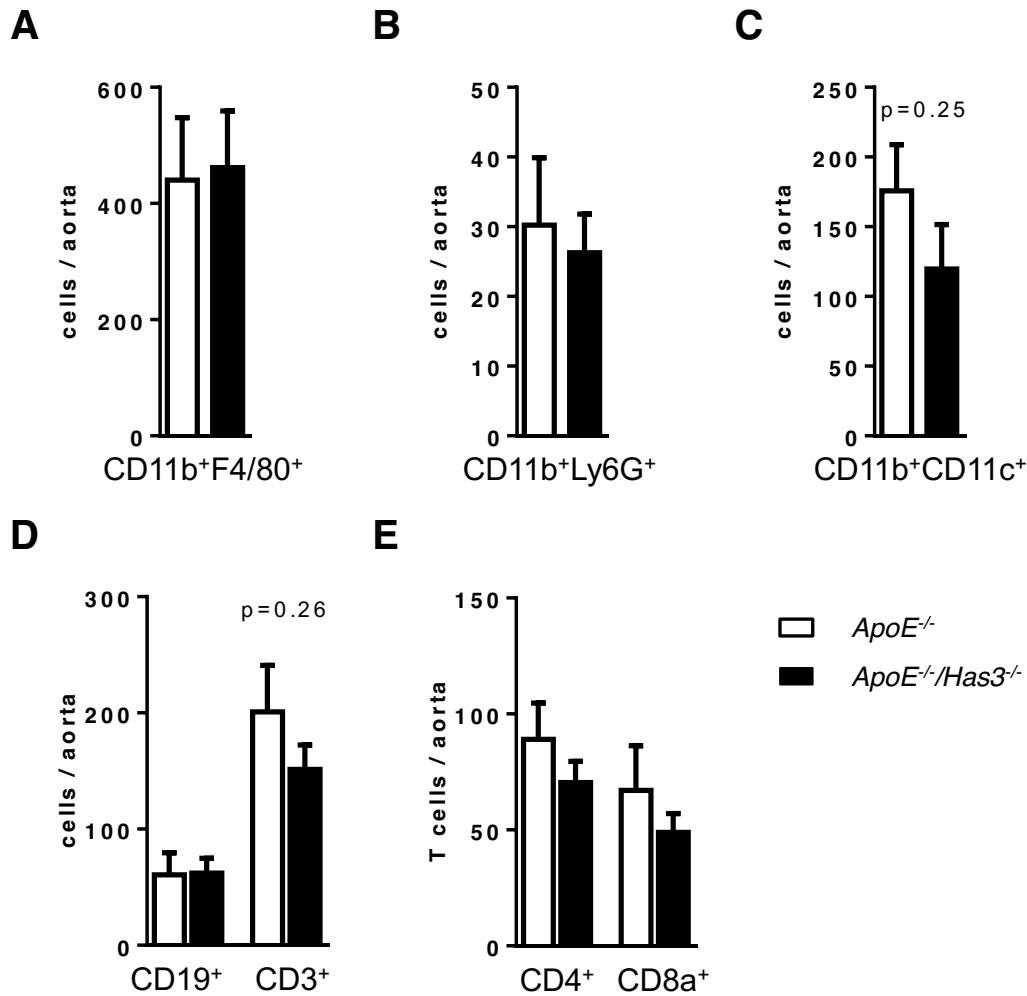


Figure 13: No alterations in the aortic immune cell composition after 15 weeks of WD.

After 15 weeks of WD feeding, *ApoE*^{-/-/Has3}^{-/-} mice and respective littermate controls were sacrificed, the whole aorta isolated and immune cell subsets analyzed within the aortic wall using flow cytometry. Respective quantification of CD11b⁺F4/80⁺ macrophages (**A**; n=6/9), CD11b⁺Ly6G⁺ neutrophils (**B**; n=6/10), CD11b⁺CD11c⁺ dendritic cells (**C**; n=6/10), CD19⁺ B cells and CD3⁺ T cells (**D**; n=8/9), and CD4⁺ as well as CD8a⁺ T lymphocytes (**E**; n=8/10) are illustrated. Values represent the means ± SEM.

3.1.6. Aortic immune cells in early plaques

In order to better understand the underlying mechanisms causing the observed reduction in plaque burden due to lack of Has3, the immune cell composition of the aortic wall was assessed in early atherosclerotic lesions. Thus, aortas were harvested after 4 weeks of WD and processed for flow cytometric analyses. At this point of time, the total number of CD45⁺ leukocytes as well as the relative proportion of CD45⁺ cells on the total number of living cells (**Figure 14 A**) was significantly lower

in *ApoE^{-/-}/Has3^{-/-}* mice than in age- and treatment-matched control mice. Leukocytes were further differentiated into CD45⁺SSC^{low} lymphocytes (**Figure 14 B**) and CD11b-expressing cells. Especially the number of CD11b⁺ cells was decreased in mice lacking Has3 (**Figure 14 C**), which explains the strong reduction of CD45⁺ cells. Circulating monocytes are recruited early into atherosclerosis-prone regions where they can differentiate into macrophages and thus contribute to foam cell formation [19]. Accordingly, CD11b⁺Ly6C⁺ monocytes were analyzed by flow cytometry to assess whether monocyte recruitment is altered by *Has3*-deficiency in early lesion development. A slight but not significant reduction of monocytes was observed in *ApoE^{-/-}/Has3^{-/-}* mice (**Figure 14 D**). Interestingly, the amount of CD11b⁺F4/80⁺ macrophages was significantly reduced in the aortic wall of *ApoE^{-/-}/Has3^{-/-}* mice compared to age- and treatment-matched control mice (**Figure 14 E**). Analysis of further CD11b⁺ cells revealed that besides the number of macrophages, also that of neutrophils was significantly lower in *ApoE^{-/-}/Has3^{-/-}* mice (**Figure 14 F**). These findings suggest that Has3 promotes immune cell accumulation at a very early stage of lesion formation and consequently influences lesion formation.

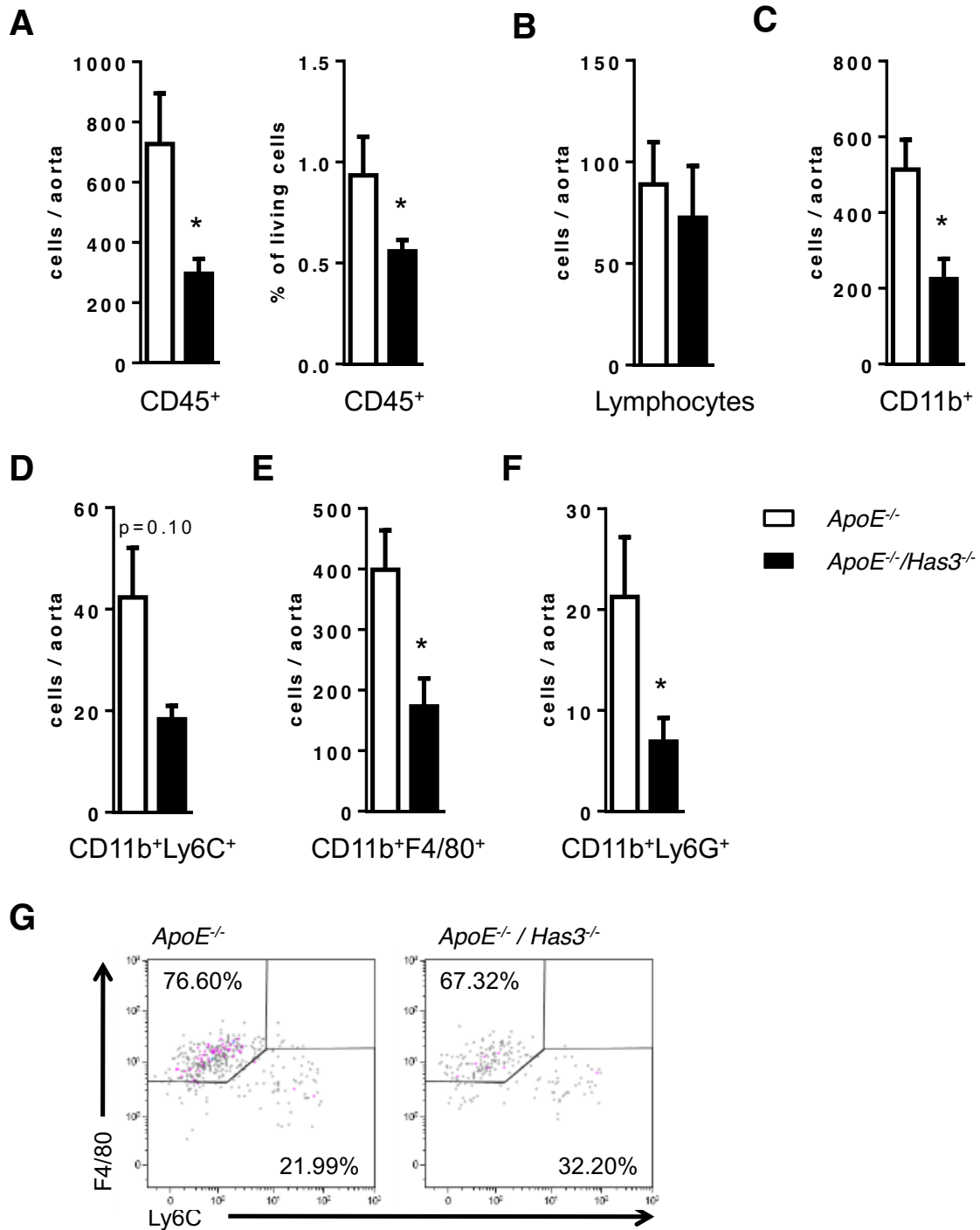


Figure 14: *Has3*-deficiency significantly reduced leukocytes, especially macrophages and neutrophils, within early atherosclerotic lesions after 4 weeks of WD.

Flow cytometric measurements were performed on atherosclerotic plaques of *ApoE*^{-/-} mice with and without *Has3* after 4 weeks of WD feeding. Immune cells were detected by surface CD45 expression (**A**) and then further discriminated into CD45⁺SSC^{low} lymphocytes (**B**) and CD11b⁺ granulocytes. Lastly, CD11b⁺ cells were subdivided into CD11b⁺Ly6C⁺ monocytes (**D**), CD11b⁺F4/80⁺ macrophages (**E**), and CD11b⁺Ly6G⁺ neutrophils (**F**). (**G**) Representative plots of the flow cytometric analyses are depicted. Data are represented as mean ± SEM; n=7; **p* < 0.05.

3.2. Effect of *Has3*-deficiency on immune cell distributions and cytokines

3.2.1. Circulating immune cells

Due to the observed reduction of lesional macrophages in early stages of atherosclerosis, the question arose whether circulating immune cells might be altered and thereby contribute to alterations in aortic immune cell composition. For this purpose, circulating immune cells were analyzed in blood samples collected via heart puncture in *ApoE*^{-/-} and *ApoE*^{-/-}/*Has3*^{-/-} mice that received WD for 4 weeks. The number of CD11b⁺CD115⁺ monocytes, and the three monocyte subsets termed classical (Ly6C^{high}), intermediate (Ly6C^{int}), and non-classical (Ly6C^{low}) monocytes (**Figure 15 A**), as well as neutrophils (data not shown) were not different between control animals and mice lacking *Has3*. Also, the number of lymphocytes (**Figure 15 B**), as well as that of CD4⁺ and CD8a⁺ T cell subsets (**Figure 15 C**) was not changed.

However, as different subtypes of CD4⁺ T cells exist, further analysis of the subgroups allows a more detailed conclusion about changes within the immune cell population. Upon activation, naïve CD4⁺ T cells differentiate into T helper (Th) cells, which have opposing roles in the development of atherosclerosis depending on their synthesized cytokines; these include Th1, Th2, Th17, and regulatory T cells (Treg). For these different effector cells diverse functions in mediating atherosclerotic lesion development are described. Th1 cells are the most abundant CD4⁺ T cells found in atherosclerotic lesions. The key cytokine produced by Th1 cells is interferon (IFN)- γ . In this way, Th1 cell responses are detrimental to the development of atherosclerosis by activating macrophages and inhibiting the proliferation of SMCs [37, 109, 110]. In contrast, Treg cells clearly show atheroprotective functions [111]. Whether Th2 and Th17 cells have pro- or anti-atherogenic properties is still controversial, as both pro- and anti-atherogenic roles have been postulated in murine models of atherosclerosis [112, 113]. Hence, circulating CD4⁺ T cells were analyzed by flow cytometry according to their Th cell phenotype. Analyses revealed that Th1 cell numbers were strongly diminished in *ApoE*^{-/-}/*Has3*^{-/-} mice to only one-third the amount detected in *ApoE*^{-/-} mice (**Figure 15 D, E**). In contrast, the number of Th2, Th17, and Treg cells per μ l blood was not different between both genotypes.

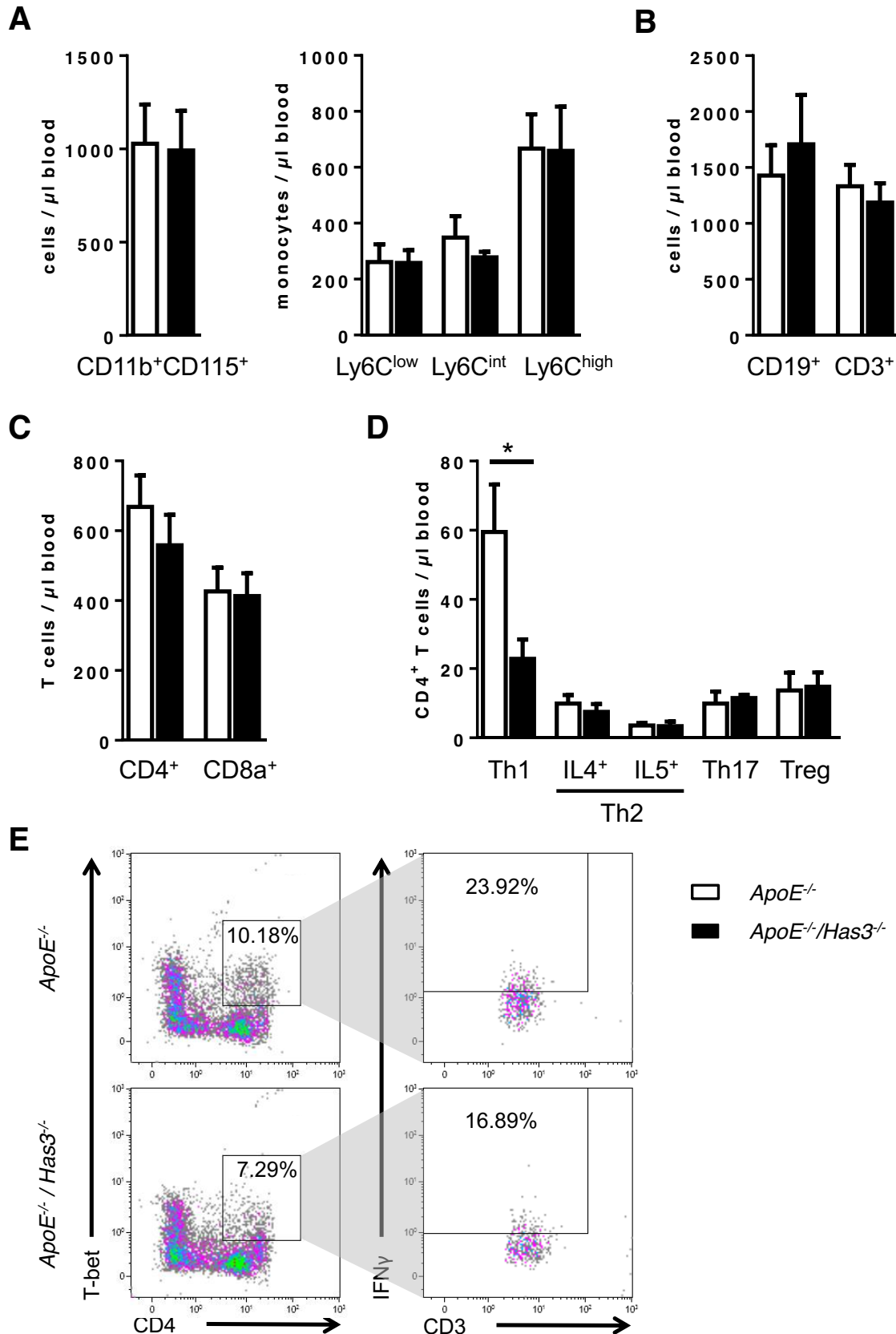


Figure 15: Significantly reduced number of circulating Th1 cells in *ApoE*^{-/-}/*Has3*^{-/-} mice after 4 weeks of WD.

After 4 weeks of WD, immune cells in the blood were investigated by flow cytometry. (A) Numbers of CD11b⁺CD115⁺ monocytes and the three monocyte subsets, which

express Ly6C differently, are depicted. **(B)** Lymphocytes were differentiated into CD19⁺ B cells and CD3⁺ T cells. Circulating CD4⁺ and CD8a⁺ T lymphocytes are shown in **(C)**. **(D)** Staining of intracellular molecules enabled the differentiation of CD4⁺ T cells into T-bet⁺IFN γ ⁺ Th1 cells, Gata3⁺IL4⁺ and Gata3⁺IL5⁺ Th2 cells, ROR γ T⁺IL17A⁺ Th17 cells, and FoxP3⁺ Treg cells. **(E)** Display of the plots for the determination of Th1 cells by flow cytometric analysis. Data are shown as mean \pm SEM; n=5-7; *p < 0.05.

3.2.2. Plasma cytokines

Because of the observed reduction of circulating Th1 cells in mice lacking Has3 in early atherosclerosis, the question if *Has3*-deficiency may also affect cytokine profiles within *ApoE*-deficient mice was examined in a further step. A broad spectrum of cytokines has been under investigation in atherosclerosis research and they depict both pro- and anti-atherogenic properties. Accordingly, 23 circulating cytokines were analyzed in murine plasma samples by using a multiplex-immunoassay. Plasma samples of *ApoE*^{-/-} and *ApoE*^{-/-}/*Has3*^{-/-} mice were taken and analyzed after both 7 and 15 weeks of WD.

In mice that received WD for 7 weeks, significant alterations in the three pro-atherogenic cytokines IL-12(p70), RANTES, and MIP-1 α were observed (**Figure 16 A**). While circulating IL-12(p70) and RANTES levels were reduced in *ApoE*^{-/-}/*Has3*^{-/-} mice, the MIP-1 α concentration was increased in these mice.

After 15 weeks of WD, the concentration of IL-12(p40), the 40kD subunit of the heterodimer IL-12(p70), but not of IL-12(p70) itself was significantly lower in mice lacking Has3 than in *ApoE*^{-/-} control mice (**Figure 16 B**). Furthermore, the concentration of IL-13 was reduced to approximately 25% in *ApoE*^{-/-}/*Has3*^{-/-} compared to respective *ApoE*^{-/-} control mice (**Figure 16 B**). Likewise, MCP-1 levels were considerably lower in *Has3*-deficient mice, and RANTES, which was significantly lower after 7 weeks of WD, also showed a tendency (p=0.06) towards reduced levels in *ApoE*^{-/-}/*Has3*^{-/-} mice after 15 weeks of WD (**Figure 16 B**).

Concerning IFN- γ , the effector cytokine produced by Th1 cells, no differences in the concentration after 7 weeks of WD was observed between both genotypes (**Figure 16 C**). However, after 15 weeks of WD, a trend towards reduced IFN- γ levels in *ApoE*^{-/-}/*Has3*^{-/-} mice could be seen (**Figure 16 D**).

Accordingly, these data indicate a crucial role of Has3 in regulating immune responses by altering different cytokines.

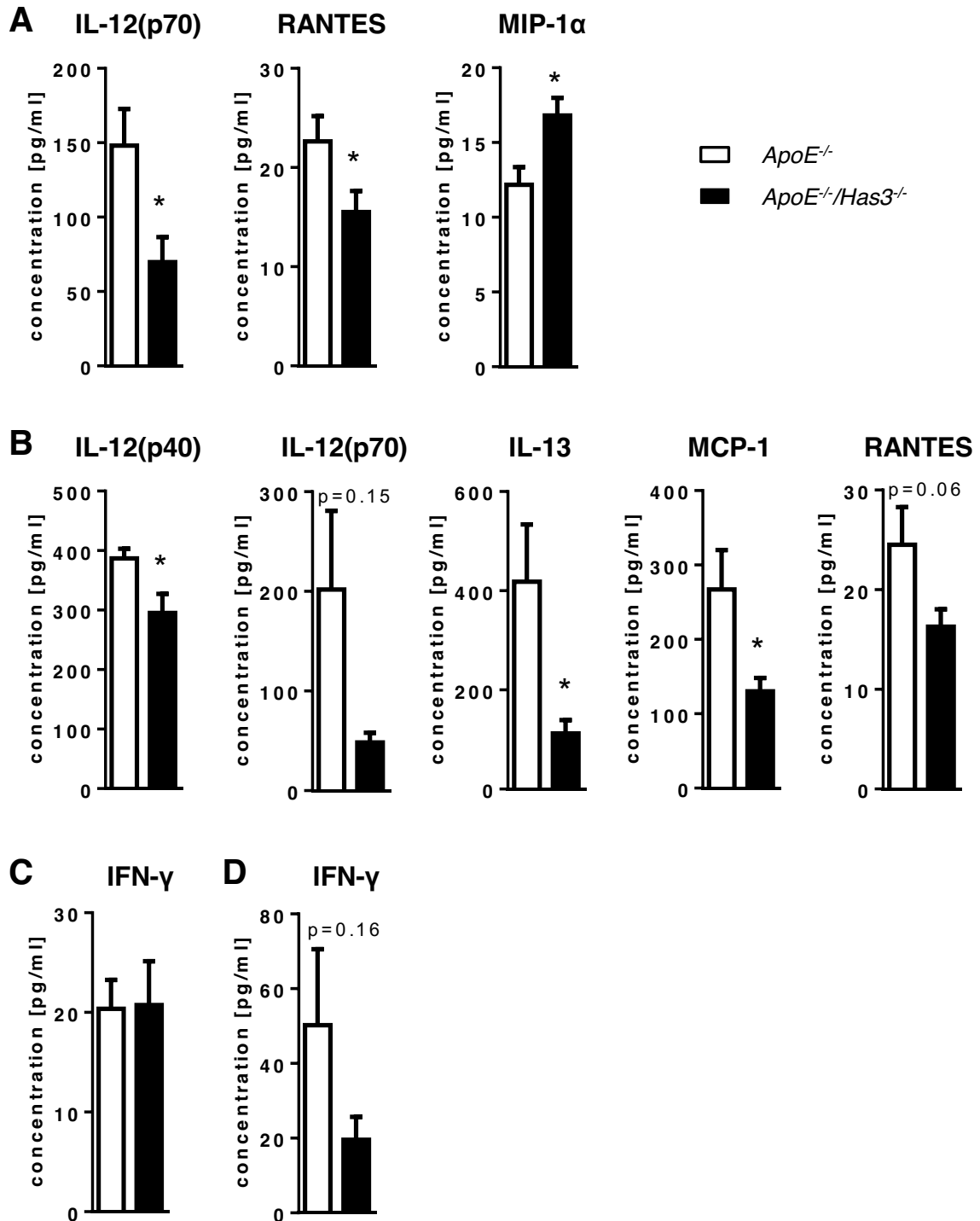


Figure 16: *Has3*-deficiency significantly affected serum cytokine levels after 7 and 15 weeks of WD.

Multiplex analysis of circulating cytokines of *ApoE*^{-/-} and *ApoE*^{-/-}/*Has3*^{-/-} mice receiving WD for 7 (**A**; IL12(p70): n=7/9; RANTES: n=9/10; MIP-1 α : n=7/9) or 15 (**B**; IL12(p40): n=8/11; IL-12(p70): n=4/5; IL-13: n=4/5; MCP-1: n=8/10; RANTES: n=8/9) weeks, respectively. In (**C**; n=6/7) levels of circulating IFN- γ after 7 weeks of WD are shown, and in (**D**; n=3/4) after 15 weeks of WD. Cytokine concentrations are depicted in pg/ml. Data are shown as mean \pm SEM; *p < 0.05.

3.2.3. Circulating CD8a⁺ T lymphocytes

On account of the alterations in several cytokines after 7 and 15 weeks, circulating immune cells were further examined by flow cytometry. While the number of monocytes (data not shown) and T lymphocytes (**Figure 17 A**) was not different between *ApoE*^{-/-}/*Has3*^{-/-} and control mice after 7 and 15 weeks of WD, further subtype analysis of CD8a⁺ T cells revealed significant differences between the genotypes. The fractions of CD44⁻CD62L⁺ naïve, CD44⁺CD62L⁻ effector, and CD44⁺CD62L⁺ central memory CD8a⁺ T cells were significantly altered by *Has3*-deficiency over time (**Figure 17 B**).

After 4 weeks of WD, approximately 60% of CD8a⁺ T cells were naïve, non-activated T cells revealing no differences between *ApoE*^{-/-} and *ApoE*^{-/-}/*Has3*^{-/-} mice. However, while the fraction of naïve CD8a⁺ T cells drastically declined from around 60% to approximately 40% from 4 to 7 weeks of WD in *ApoE*^{-/-} mice, this early decrease was absent in *ApoE*^{-/-}/*Has3*^{-/-} mice. In contrast, *ApoE*^{-/-}/*Has3*^{-/-} mice did show a delayed reduction of the naïve T cell fraction, which occurred between 7 and 15 weeks of WD feeding. Control mice showed a sustained decline in naïve T cells from 7 to 15 weeks of WD. (**Figure 17 B** left side).

The effect on the fraction of CD44⁺CD62L⁻ effector CD8a⁺ T cells opposed to that observed for CD44⁻CD62L⁺ naïve CD8a⁺ T cells. Effector T cells increased early in *ApoE*^{-/-} mice, while the rise was delayed in *ApoE*^{-/-}/*Has3*^{-/-} mice and resulted in a significantly decreased amount of effector T cells in *ApoE*^{-/-}/*Has3*^{-/-} mice after 7 and 15 weeks of WD (**Figure 17 B** middle).

The fraction of CD44⁺CD62L⁺ central memory CD8a⁺ T cells was approximately 20% in both *ApoE*^{-/-}/*Has3*^{-/-} and *ApoE*^{-/-} mice after 4 weeks of WD. Three weeks later still no difference was observable. However, after 15 weeks of WD, the fraction of central memory CD8a⁺ T cells declined significantly in *ApoE*^{-/-} mice, while there was no drop in *ApoE*^{-/-}/*Has3*^{-/-} mice leading to a significantly higher percentage of central memory CD8a⁺ T cells in *ApoE*^{-/-}/*Has3*^{-/-} mice compared to controls after 15 weeks of WD (**Figure 17 B** right-hand side).

All these changes in naïve, effector, and memory T cells with the delayed rise of CD44⁺CD62L⁻ effector T cells were only detectable for CD8a⁺ T cells but not for CD4⁺ T cells (data not shown).

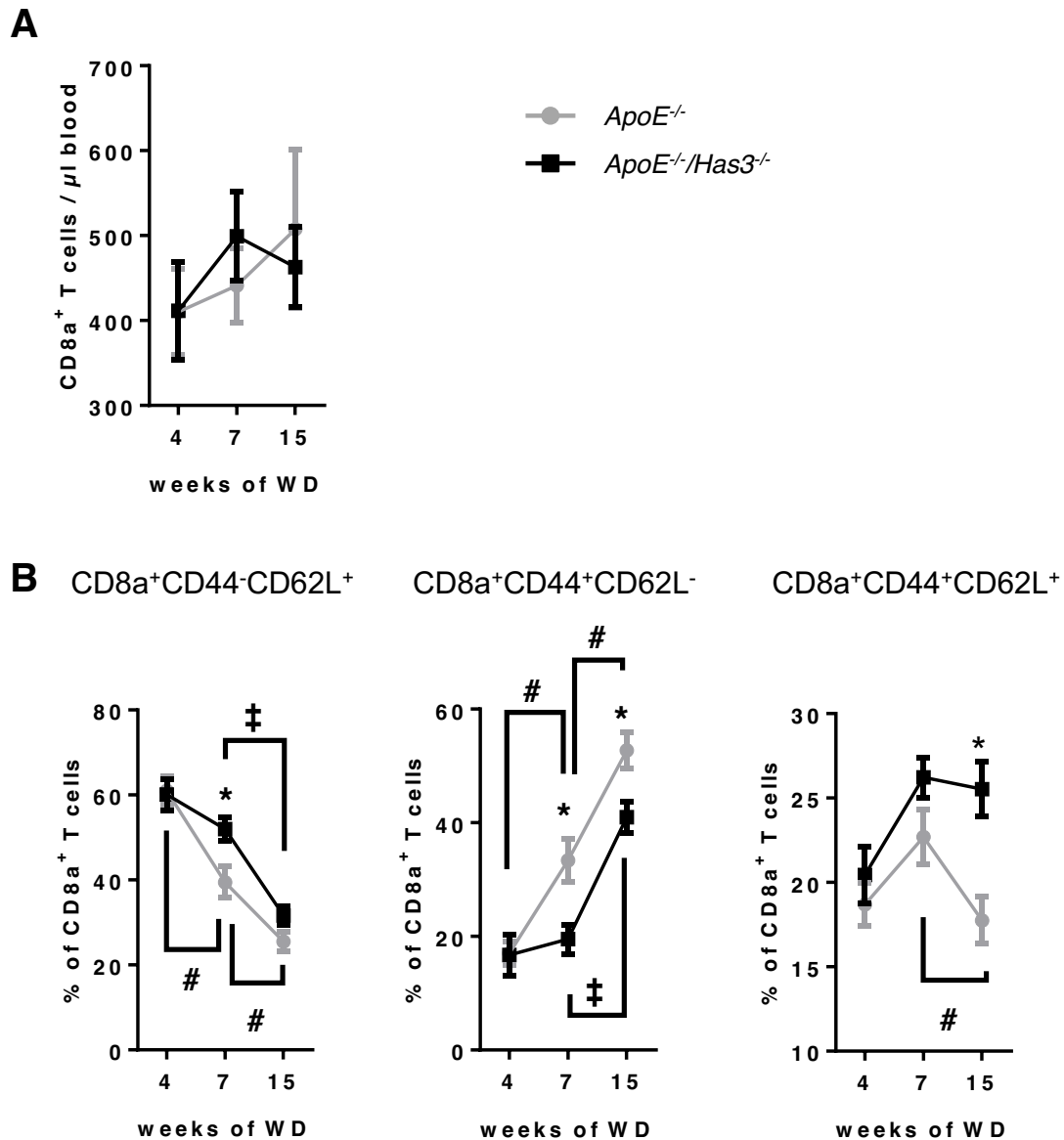


Figure 17: Delayed increase of circulating effector CD8a⁺ T lymphocytes in *ApoE*^{-/-} mice lacking *Has3*.

Blood was isolated from *ApoE*^{-/-} mice with and without *Has3*-deficiency after 4, 7, and 15 weeks of WD feeding and CD8a⁺ T cells were analyzed using flow cytometry. (A) Cell counts of CD8a⁺ T cells per µl blood are shown for all three points of time. (B) The relative proportion for CD44⁻CD62L⁺ naïve, CD44⁺CD62L⁻ effector, and CD44⁺CD62L⁺ central memory CD8a⁺ T cells is shown. Data are displayed as mean ± SEM; n=8-11; *ApoE*^{-/-} vs. *ApoE*^{-/-}/*Has3*^{-/-} *p < 0.05; *ApoE*^{-/-} vs. *ApoE*^{-/-} #p < 0.05; *ApoE*^{-/-}/*Has3*^{-/-} vs. *ApoE*^{-/-}/*Has3*^{-/-} ‡p < 0.05.

3.2.4. T lymphocytes in spleen and lymph nodes

Because priming of T cells occurs in secondary lymphoid tissues, such as lymph nodes and spleen [114, 115], lymphoid T cells were analyzed by flow cytometry to examine whether the alterations in circulating T cells are caused by changes in the ability to activate T lymphocytes in lymphoid organs.

Spleen and axillary lymph nodes were harvested from *ApoE^{-/-}/Has3^{-/-}* and control mice after 15 weeks of WD feeding. Neither the weight of the spleen (**Figure 18 A**) nor of the axillary lymph nodes (**Figure 19 A**) was different between *ApoE^{-/-}/Has3^{-/-}* and control mice. Interestingly, in *ApoE^{-/-}/Has3^{-/-}* mice a strong tendency of reduced cell numbers for CD3⁺ T lymphocytes was observed in both spleen (**Figure 18 B**) and lymph nodes (**Figure 19 B**). Further analyses of T cell subsets and activation status revealed significantly decreased naïve CD4⁺ T cell counts in the spleen (**Figure 18 D**) while no significant effects were observed for CD8a⁺ T cells (**Figure 18 E**). On the other hand, in the lymph nodes both naïve CD4⁺ (**Figure 19 D**) and naïve CD8a⁺ (**Figure 19 E**) T cell counts were significantly decreased in *ApoE^{-/-}/Has3^{-/-}* mice compared to *ApoE^{-/-}* mice.

These data suggest that naïve T lymphocytes might not be able to enter lymphoid tissues adequately resulting in reduced numbers of naïve T lymphocytes. Also, increased apoptosis or diminished proliferation within the lymphoid tissue might result in reduced numbers of naïve T cells. As a consequence, less CD8a⁺ effector T cells and less Th1 cells might be released into the circulation.

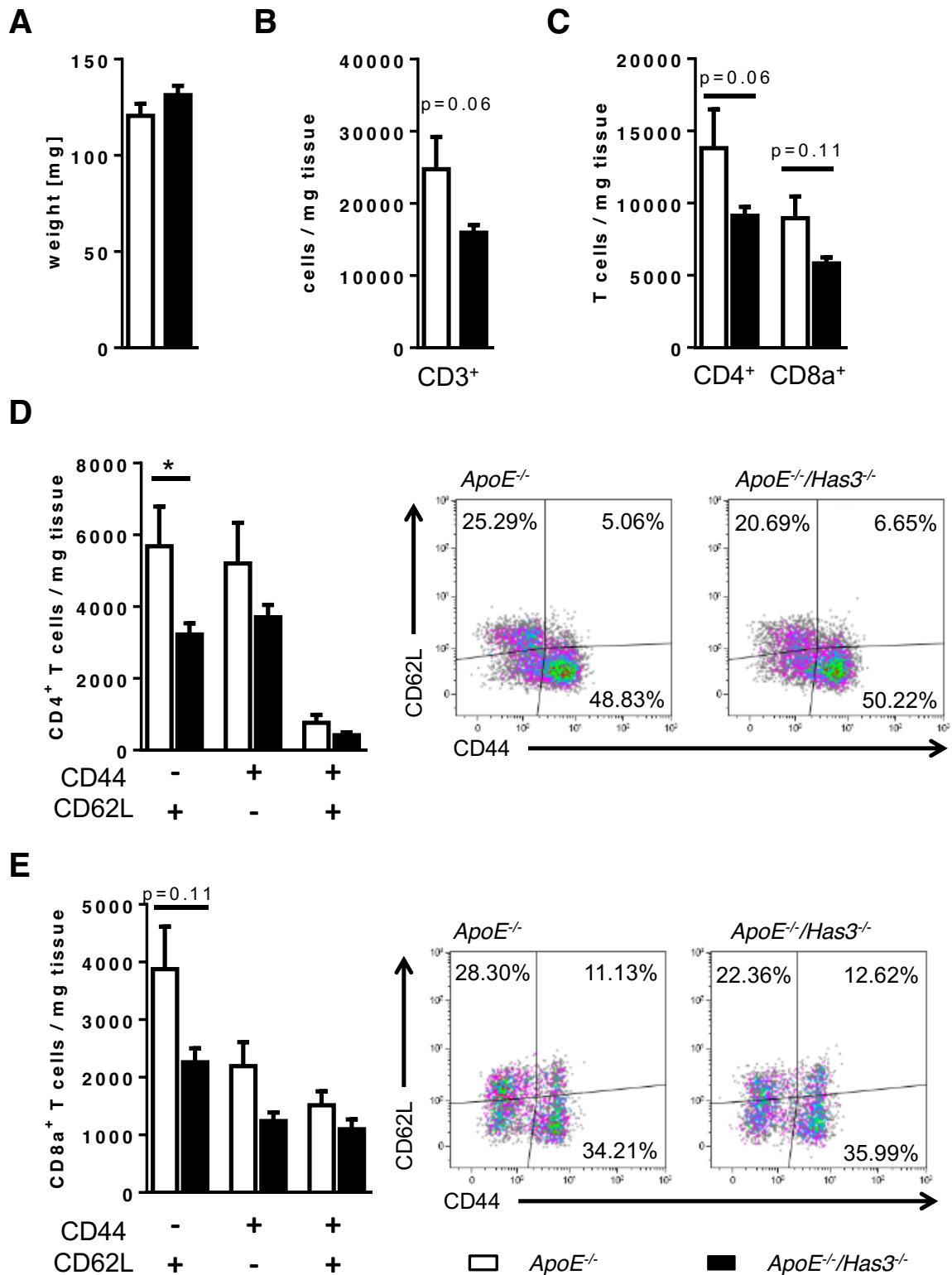


Figure 18: In spleens of *ApoE*^{-/-}/*Has3*^{-/-} mice, the number of naïve CD4⁺ T lymphocytes was significantly reduced after 15 weeks of WD.

Spleens were isolated from *ApoE*^{-/-}/*Has3*^{-/-} and control mice after 15 weeks of WD feeding. (A) After harvesting, the weight of spleens was measured. Using flow cytometry, T lymphocytes (B), as well as the cell number per mg tissue of CD4⁺ and CD8a⁺ T cells (C) were analyzed. Also, activation status of splenic CD4⁺ (D) and CD8a⁺ (E) T cells was determined. Representative plots for the activation status are shown in (D) and (E). Data are shown as mean ± SEM; n=6/8; *p < 0.05.

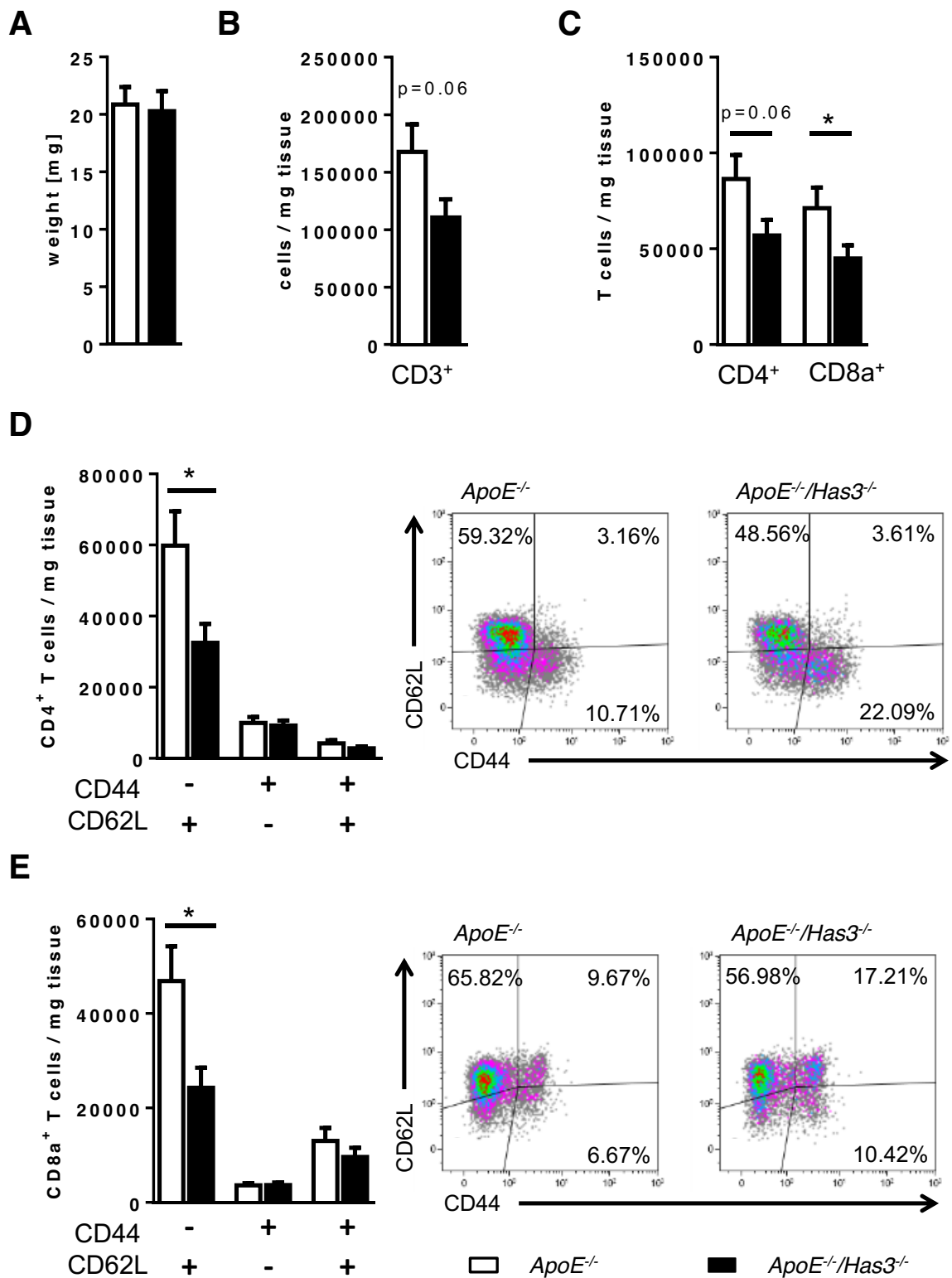


Figure 19: After 15 weeks of WD feeding, *ApoE*^{-/-/Has3}^{-/-} mice had reduced numbers of naïve CD4⁺ and CD8a⁺ T cells in lymph nodes.

Axillary lymph nodes were isolated, weighed, and analyzed using flow cytometry from *ApoE*^{-/-} mice with and without *Has3*-deficiency after 15 weeks of WD feeding. (A) The mean weight of isolated axillary lymph nodes is shown. Numbers of T lymphocytes (B) and CD4⁺ and CD8a⁺ T cell subsets (C) were analyzed. The cell numbers of naïve, effector, and central memory CD4⁺ (D) and CD8a⁺ (E) T cells with respective plots are also shown. Data are depicted as mean ± SEM; n=7/12; *p < 0.05.

3.2.5. Immune cells in perivascular adipose tissue (PVAT)

PVAT is importantly involved in various vascular functions, such as vessel relaxation, by the secretion of vasoactive molecules, like adipocyte-derived relaxing factor [116]. Moreover, PVAT harbors a broad number of resident inflammatory cells and adipocytes themselves produce cytokines to further recruit immune cells. Through these immunomodulatory functions, the perivascular tissue might also contribute to atherosclerotic lesion development. Several studies showed already that a) high-fat diet feeding in mice promoted the production of pro-inflammatory cytokines in the PVAT [117], and b) in humans an increased volume of thoracic PVAT was associated with a higher prevalence of cardiovascular diseases [118].

To investigate if *Has3*-deficiency is also having an effect on inflammatory processes in the PVAT and thereby might influence atherosclerotic lesion development, PVAT surrounding the thoracic aorta was harvested after 15 weeks of WD feeding. The weight of thoracic PVAT was not different between *ApoE*^{-/-} and *ApoE*^{-/-}/*Has3*^{-/-} mice (**Figure 20 A**). However, flow cytometric analyzes of accumulated immune cells within thoracic PVAT revealed significantly reduced numbers of leukocytes in the PVAT of *Has3*-deficient mice (**Figure 20 B**). Further examinations of different immune cell subsets showed that especially the numbers of CD11b⁺F4/80⁺ macrophages were reduced in *ApoE*^{-/-}/*Has3*^{-/-} mice compared to *ApoE*^{-/-} control mice (**Figure 20 C**). Additionally, the numbers of CD8a⁺ T cells tended to be lower ($p=0.09$) in *Has3*-deficient mice than in *ApoE*^{-/-} control mice (**Figure 20 E**).

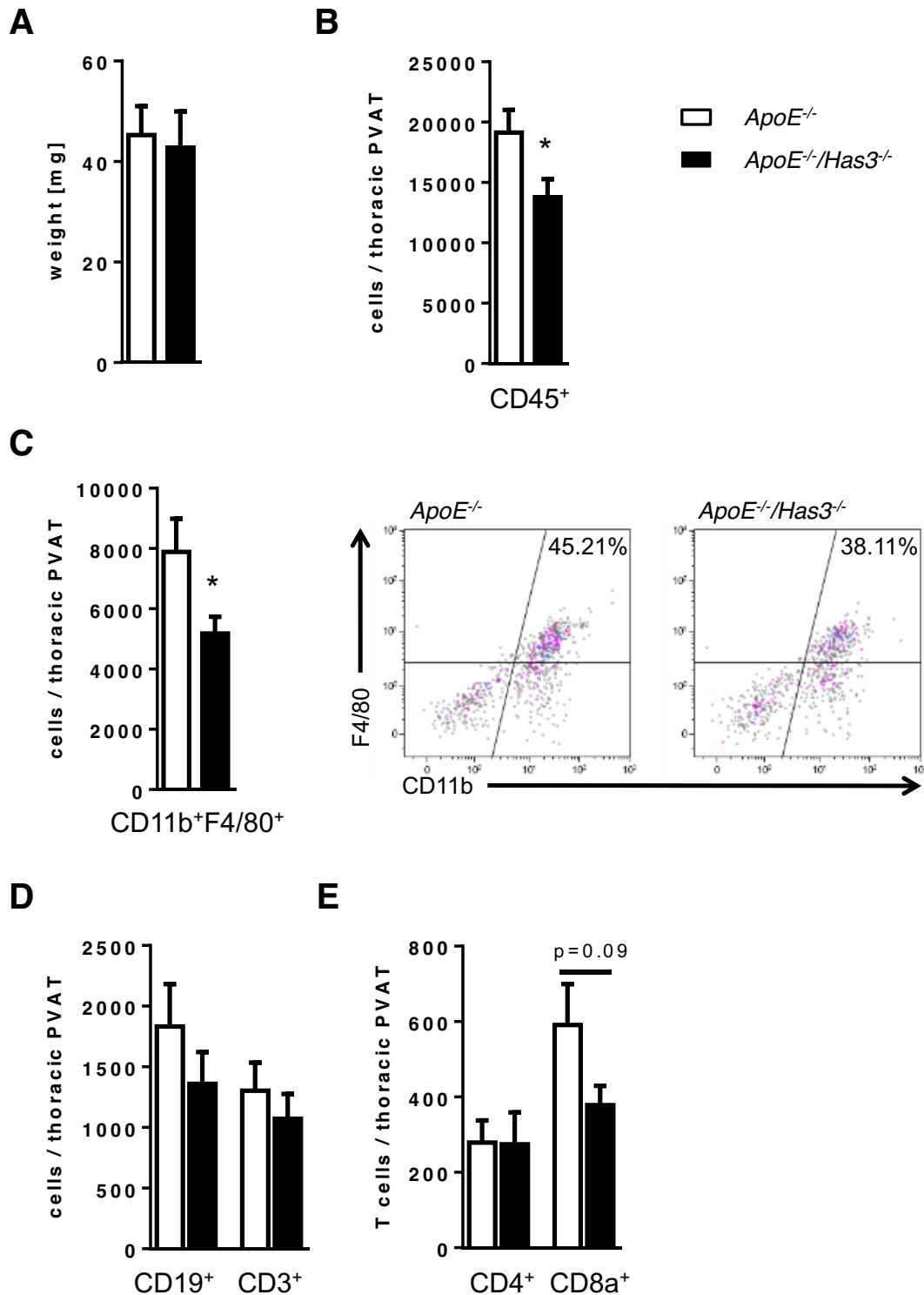


Figure 20: *Has3*-deficiency reduced the number of macrophages in the thoracic PVAT after 15 weeks of WD.

After 15 weeks of WD, PVAT surrounding the thoracic part of the aorta was used for flow cytometric analysis of immune cells. (A) Depiction of the weight of the mean thoracic PVAT of *ApoE*^{-/-} and *ApoE*^{-/-}/*Has3*^{-/-} mice. (B-E) Immune cells were analyzed by flow cytometry. CD45⁺ immune cells (B) were further discriminated into CD11b⁺F4/80⁺ macrophages (C), CD19⁺ B cells, CD3⁺ T cells (D), as well as CD4⁺ and CD8a⁺ T cell subsets (E). In (C) representative plots are shown for CD11b⁺F4/80⁺ macrophages. Data are shown as mean ± SEM; n=8/9; **p* < 0.05.

3.3. Role of Has3 in the generation of effector and memory T lymphocytes

3.3.1. Has3 expression in T lymphocytes

All analyzed points of time pointed to an effect of *Has3*-deficiency on T cell activation, T cell differentiation, and a shift in the cytokines, which regulate T cell function. However, these results did not give information about a putative influence of Has3 on the regulation of T cell activation. Therefore, the impact and role of Has3 in regulating T cell activation was assessed.

First of all, it was revealed if T cells themselves express Has isoforms and thus putatively influence their own activation via endogenous HA production.

To analyze *Has* mRNA expression in T cells, spleens were harvested from 12 weeks old *ApoE*^{-/-} mice to isolate T lymphocytes. First, the purity of the isolated T lymphocytes was tested using flow cytometry. Among the isolated living cell population, only a total of 2.85% was CD3-negative. All the rest, with an average percentage of 97.15% were CD3⁺ T cells (**Figure 21**). Thus, the isolated cells were termed a pure T cell population and the cells were used for further experiments addressing the questions of Has3 expression in T cells and the role of Has3 in T cell activation.

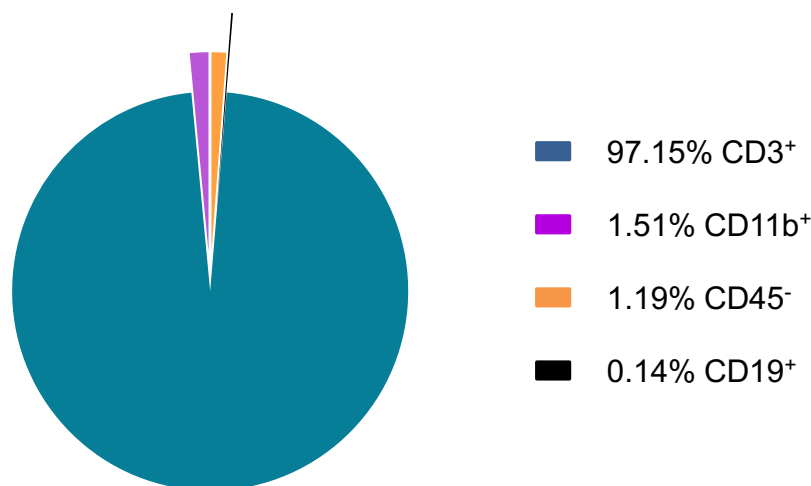


Figure 21: Isolated T cells from the spleen and axillary lymph nodes exhibited 97% purity.

T lymphocytes were isolated from the spleen of chow-fed *ApoE*^{-/-} mice. After isolation, the purity was analyzed by flow cytometry. The fraction of CD3⁺ (blue), CD11b⁺ (violet), CD45⁻ (orange), and CD19⁺ (black) cells of all living cells was calculated. Three independent experiments were performed and the average of all cell populations is shown.

Next, to analyze if the isolated T cells express the different Has isoforms, RNA was isolated from the T cells and analyzed using qPCR.

These data revealed that the *Has* isoforms 2 and 3 are expressed in murine splenic T lymphocytes of *ApoE*^{-/-} mice (**Figure 22**), while *Has1* could not be detected. Interestingly, only in two of four samples *Has2* was detected, while *Has3* was detected in every analyzed sample.

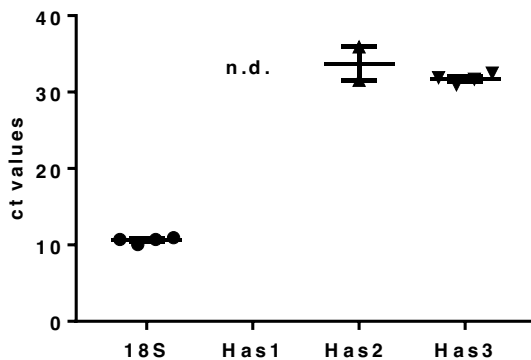


Figure 22: Isolated splenic T cells from *ApoE*^{-/-} mice expressed *Has2* and *Has3*. RNA was extracted from isolated splenic *ApoE*^{-/-} T lymphocytes and analyzed for transcript expression of the different *Has* isoforms. *Has1* mRNA was not detectable (n.d.) and only two out of our samples had detectable *Has2* mRNA expression. Data are presented as mean ± SEM; n=4.

3.3.2. *In vitro* T cell activation

3.3.2.1. Anti-CD3/-CD28 bead-mediated T cell stimulation

To examine whether *Has3* expressed by T lymphocytes impacts their activation, *in vitro* T cell cultures were established. T lymphocytes were isolated from spleens and axillary lymph nodes of *ApoE*^{-/-}/*Has3*^{-/-} and *ApoE*^{-/-} mice that received WD for 4 weeks. Then, the isolated T cells were cultivated and stimulated with anti-CD3/-CD28 beads. Anti-CD3 and anti-CD28 antibodies are sufficient to activate T cells as they mimic the stimulus of antigen-presenting cells. Stimulated T cells were cultivated for up to 48 hours. As control condition, T cells were cultivated without anti-CD3/-CD28 beads. At baseline, as well as after 24 and 48 hours of cultivation, cells were harvested and analyzed by flow cytometry.

First, the fraction of living cells was analyzed as fold of baseline (**Figure 23**). In the control condition, the amount of living cells drastically declined after 24 hours and 48 hours of cultivation. In contrast, the ratio of living cells in bead-stimulated conditions almost stayed the same (*Has3*-deficient T cells - red lines) or slightly increased

(Has3 expressing T cells - black lines). However, no significant differences were observed thus far in this time course.

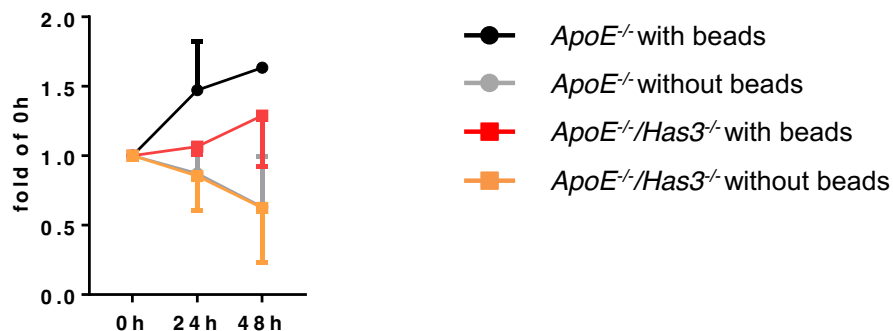


Figure 23: *Has3*-deficiency in T cells slightly impaired T cell expansion.

After 4 weeks of WD, T lymphocytes were isolated from *ApoE*^{-/-} and *ApoE*^{-/-}/*Has3*^{-/-} mice and stimulated for 24 and 48 hours. Living cells were analyzed by flow cytometry and depicted as fold of 0h. Data are shown as mean ± SEM; n=4/3.

Next, CD25 expression as an early marker for T cell activation was analyzed in the cell culture system. At baseline, around 95% of CD4⁺ T cells (**Figure 24 A**) and 99% of CD8a⁺ T lymphocytes (**Figure 24 B**) were CD25-negative. Upon stimulation with antibody-coated beads, already after 24 hours the fraction of CD25-negative T lymphocytes decreased drastically, while the percentage of CD25-positive T cells increased. In contrast to that, the CD25-negative and CD25-positive fractions in the unstimulated control wells did not change in CD4⁺ and CD8⁺ T cells (**Figure 24 A, B**). The cultivation for additional 24 hours did not change the fraction of CD25-expressing T cells. Also, lack of *Has3* did not influence the fraction of CD25-expressing T cells at any point of time.

In addition to CD25, also the markers CD44 and CD62L, which enable the characterization of naïve, effector, and memory T cells, were examined. Before stimulation, approximately 70% of CD4⁺ T cells were CD44-negative and CD62L-positive, indicating an unstimulated, naïve T cell phenotype. Upon stimulation, the fraction of naïve CD4⁺ T cells first declined, but increased again. In contrast, the amount of CD4⁺CD44⁺CD62L⁻ effector T cells almost stayed the same, while the amount of CD4⁺CD44⁺CD62L⁺ memory T cells increased from 2% at the time of stimulation up to 15% after 48 hours. Also here, *Has3*-deficiency did not affect the generation of effector and memory T cells (**Figure 24 C**).

In contrast to CD4⁺ T cells, bead-stimulation differently affected CD8a⁺ T cells. As already seen for the marker CD25, the overall activation and alterations in the different populations were weaker in CD8a⁺ compared to CD4⁺ T cells. The amount of naïve CD8a⁺ T cells increased from 70% at the time of stimulation up to 80% after

48 hours. For effector and memory T cells only minor changes were observed (**Figure 24 D**). Similar to CD4⁺ T cells, lack of Has3 did not influence T cell activation. These data suggest that Has3 expressed by T cells does not influence their general ability to become activated.

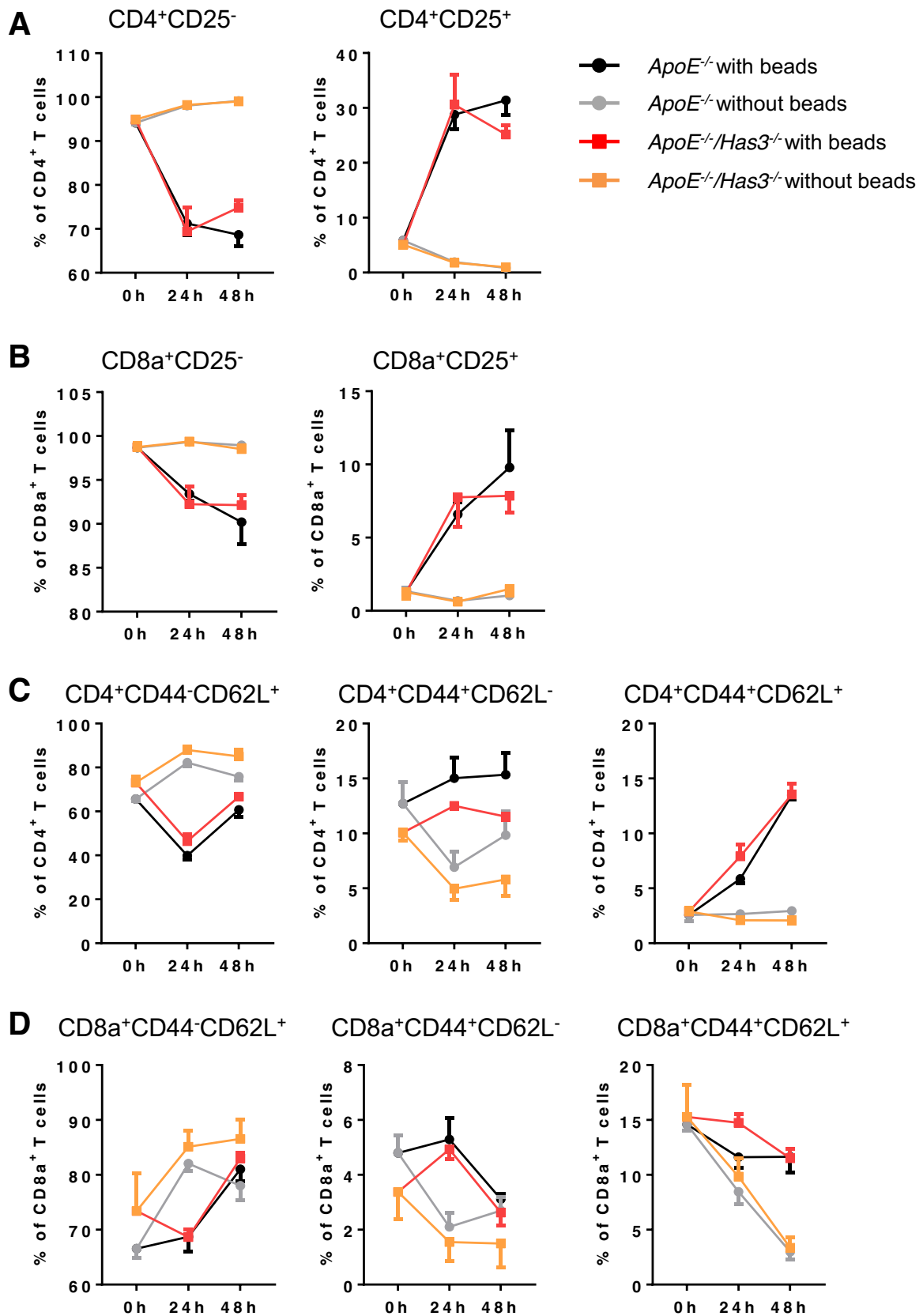


Figure 24: *Has3*-deficiency did not affect CD3-/CD28-induced stimulation of T cells.

After 4 weeks of WD, T lymphocytes were isolated from *ApoE*^{-/-} and *ApoE*^{-/-}/*Has3*^{-/-} mice and stimulated for 24 and 48 hours. Activation of CD4⁺ and CD8a⁺ T cells was assessed by flow cytometric measurements of the surface

antigens. As control condition, T cells were cultivated without anti-CD3/-CD28 beads for 24 and 48 hours, respectively (grey, orange). (**A, B**) Early T cell activation was assessed by the surface expression of CD25. (**C, D**) To discriminate naïve, effector, and memory T cells the surface markers CD44 and CD62L were stained. Data are shown as mean \pm SEM; n=4/3.

3.3.2.2. Activation of BM-DCs

In the process of T cell activation the interaction between T cells and antigen-presenting cells, such as DCs, is absolutely crucial. Interestingly, Bollyky and colleagues as well as Mummert and colleagues showed that human BM-DCs and murine BM-DCs expressed hyaluronan synthases with *HAS3* as the major isoform [81, 119]. Furthermore, the alterations in the cytokine profiles of *ApoE^{-/-}/Has3^{-/-}* mice suggest that the secretion of cytokines and the activation of antigen-presenting cells might be affected by *Has3*-deficiency, as DCs are major producers of the Th differentiating cytokine IL-12 [120, 121]. Consequently, the question arose whether endogenous *Has3*-expression in DCs might have a direct impact on DC maturation upon stimulation. To investigate this question, bone marrow cells from *ApoE^{-/-}* and *ApoE^{-/-}/Has3^{-/-}* mice were isolated to generate BM-DCs as illustrated in **Figure 7**. After 7 days in culture, BM-DCs were stimulated with LPS to activate DCs and to induce antigen presentation. In addition, the purity of the cell cultures as well the activation of BM-DCs with and without LPS stimulation was assessed using flow cytometry. The percentage of CD11c⁺ DCs of the living cells was approximately 60% in both LPS-stimulated and -unstimulated conditions, as well as for *ApoE^{-/-}* and *ApoE^{-/-}/Has3^{-/-}* cell cultures (**Figure 25 A**). Among the CD11c⁻ cells within the culture, the number of Ly6G⁺ neutrophils was similar in all analyzed conditions. In addition, F4/80⁺ macrophages were measured. In the culture condition without LPS, the fraction of F4/80⁺ macrophages was low with only 1 to 2%. Upon LPS stimulation, this population significantly increased up to 10% for *ApoE^{-/-}/Has3^{-/-}* and *ApoE^{-/-}* cells (**Figure 25 B**). Although the purity of the BM-DC culture was only around 60%, there were no substantial differences between cell populations of *ApoE^{-/-}/Has3^{-/-}* and *ApoE^{-/-}* mice. Therefore, the culture of BM-DCs was used for further experiments.

In a next step the activation of CD11c⁺ BM-DCs was assessed. For this purpose the surface expression of CD86 and the MHC II, which are known as typical maturation markers for DCs [122, 123], were analyzed by flow cytometry. Under unstimulated culture conditions, the fraction of non-activated MHC^{low}CD86⁻ BM-DCs was significantly higher compared to the LPS-stimulated condition. In contrast, approximately 80% of the BM-DCs were mature MHC^{high}CD86⁺ DCs in the LPS-treated culture compared to 40% in the unstimulated condition. Also here, additional *Has3*-deficiency did not influence BM-DC maturation (**Figure 25 C**).

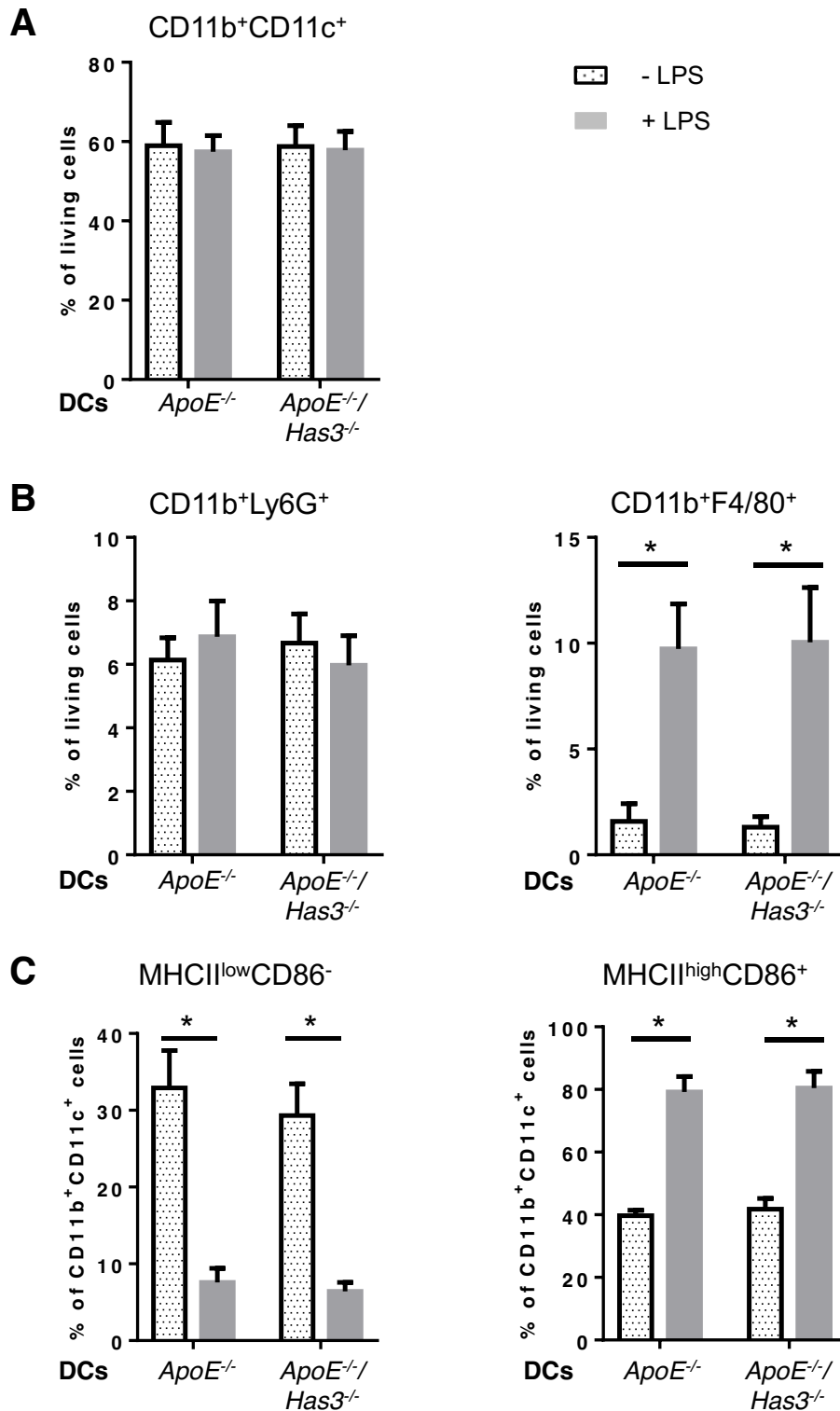


Figure 25: LPS activated BM-DCs of *ApoE*^{-/-} and *ApoE*^{-/-}/*Has3*^{-/-} mice equally. Dendritic cells were generated from bone marrow cells of *ApoE*^{-/-}/*Has3*^{-/-} and *ApoE*^{-/-} mice. On day 8 of cell culture, BM-DCs were harvested and analyzed by flow cytometry. The fractions of CD11b⁺CD11c⁺ DCs (A), CD11b⁺Ly6G⁺ neutrophils, and CD11b⁺F4/80⁺ macrophages (B) within the cell culture were determined. (C) The surface expression of CD86 and MHC II were examined to assess DC maturation. Data are shown as mean \pm SEM; n=4; *p < 0.05.

4. Discussion

4.1. Effect of *Has3*-deficiency on morphology and localization of atherosclerotic lesions

A number of pathologies have been associated with alterations in the metabolism of the ECM component HA. In healthy tissue, HA exists as large polymers that exhibit anti-inflammatory functions. However, during tissue injury or inflammatory conditions, increased HA degradation into chains of low molecular mass was observed, which may further exaggerate inflammatory processes [124]. The resulting HA plays a prominent role in mediating inflammatory responses by inducing cell maturation, migration, and adhesion. Also during atherosclerosis, a chronic inflammatory disease of the arteries, HA deposition is described throughout lesion development [83, 85]. In mouse models, increased HA synthesis by overexpressing *Has2* in VSMCs resulted in increased atherogenesis and SMC migration [86]. Also pharmacological inhibition of HA synthesis with 4-MU accelerated atherogenesis [94]. Interestingly, early macrophage accumulation coincided with HA accumulation that is probably driven by increased *Has3* expression. Thus, the aim of this study was to investigate the role of a global *Has3*-deficiency in *ApoE*-deficient mice on atherosclerotic lesion development.

Atherosclerotic lesion formation and inflammatory processes were significantly altered in male *ApoE-Has3*-double-deficient mice. After 15 weeks of WD feeding, *ApoE-Has3*-double-deficient mice exhibited significantly reduced ORO lipid staining in the aorta. Further morphological analyses of lesion size and plaque composition were performed in two vascular beds: the aortic root and the BCA. While differences in lesion size and outward remodeling were found in the BCA after 15 weeks of WD feeding, atherosclerotic lesion size at the aortic root was not affected by *Has3*-deficiency. One explanation for this observation could be that the lesions at the aortic root had already reached a maximum size as lesions at the aortic root develop relatively fast and thus minor differences might remain unseen. However, analyses of lesion size at the aortic root at earlier time points also did not indicate differences. Another reason for diverse lesion characteristics at the BCA and the aortic root could be the localization. It is well established that different flow patterns [105, 106] and disturbed flow at vascular branch points exacerbate atherogenesis. Not only are the flow patterns different between these locations, but also the origin of cells that build up the vessel are different, which is particularly evident in VSMCs.

Rigorous SMC lineage tracing has shown that VSMCs from the aortic root to the iliac bifurcation arise from four different sources: the secondary heart field, the neural crest, the somites, and the splanchnic mesoderm [125]. On top of that, it has been demonstrated that VSMCs from different locations respond differently to the same stimulus. While TGF- β 1 stimulation of VSMCs originated from the neural crest induced cell proliferation, the same stimulus inhibited growth in VSMCs from the mesoderm [126]. A similar phenomenon has been shown in human fibroblasts. TGF- β 1 stimulation of dermal fibroblasts induced proliferation, whereas TGF- β 1 reduced proliferation in oral fibroblasts. Additionally, Meran and colleagues showed that dermal fibroblasts generated higher levels of HA than oral fibroblasts indicating that HA may differentially influence growth responses to TGF- β 1 [127].

Taken together, it is possible that VSMCs of different origin respond differently to stimuli during atherogenesis in a Has3-dependent manner, resulting in altered lesion pathogenesis depending on their location.

4.2. Origin of macrophage- and SMC-like cells in atherosclerotic plaques

Besides lesion size, cellular composition of the lesion was also assessed at the aortic sinus. Histologically, the fraction of macrophage-like and SMC-like cells was investigated by staining for the markers Mac2 and α -SMA, respectively. Neither the area fraction nor the localization of Mac2 and α -SMA staining was different between *ApoE*^{-/-} mice with or without Has3 at three different stages of atherosclerotic lesion development suggesting similar lesion composition. However, *in vitro* studies and lineage tracing experiments of VSMCs have revealed that VSMCs can lose their typical SMC marker expression, such as α -SMA, in inflammatory environments like atherosclerosis and therefore are undetectable using traditional immunohistochemical markers. Interestingly, rigorous SMC lineage tracing has shown that they can express macrophage markers and contribute to foam cell formation [50, 52, 53]. Specifically, more than 80% of VSMC-derived cells within the lesion lack expression of VSMC markers and approximately 30% gained markers of hematopoietic lineage, like Mac2, a typical marker for macrophages [53, 128, 129]. Thus, relying on α -SMA staining may not be able to resolve the question of whether *Has3*-deficiency affects VSMC migration and monocyte/macrophage recruitment.

Importantly, several studies *in vitro* and *in vivo* have shown that HA affected SMC migration. To investigate the effect of HA on VSMCs migration, different methods were used which all yielded similar results. Specifically, VSMCs that were stimulated with HMW-HA showed a dose-dependent increase in migration [130]. Further, it was shown that aged VSMCs had an increased HA synthesis with an increased

expression of *HAS2* and *HAS3*. Comparing young and aged cells also showed that aged cells migrated faster than the young cells [131]. Consistent with these data, inhibition of HA synthesis *in vitro* using either 4-MU treatment [88] or by inhibiting HAS synthesis with siRNA [95, 132] showed the opposite effects with reduced migration of VSMCs. These data suggest that both exogenously added and endogenously synthesized HA induce VSMC migration *in vitro*. These data could partially explain the reduced neointima formation in a model of neointimal hyperplasia in *Has3*-deficient mice [95]. Transcriptome analysis of ligated carotid arteries from *Has3*-deficient mice and control mice strongly indicated a *Has3*-dependent regulation of VSMC migration pathways. Furthermore, significantly less HA was detected in the media of *Has3*-deficient mice while no compensatory expression of *Has1* and *Has2* was observed. This suggests that *Has3*-dependent HA accumulation may be an important trigger of SMC migration.

These previous studies strongly suggest that HA and HAS3 influence VSMC migration. Despite these observations there was no alteration in the amount and the localization of α -SMA-positive cells within atherosclerotic lesions at the aortic root in *ApoE*^{-/-}/*Has3*^{-/-} mice. Thus, either VSMC migration is not affected in mice with additional *ApoE*-deficiency or *Has3*-deficiency impacts phenotypic transition of lesional cells into α -SMA-expressing cells or VSMCs transition into macrophage-like cells. However, to definitely address whether *Has3* regulates SMC migration or phenotypic transitions *in vivo*, the use of rigorous SMC-lineage tracing is required and currently under investigation in collaboration with the University of Virginia.

While matrix synthesizing SMCs within plaques have beneficial effects by improving plaque stability, their dedifferentiation into macrophage-like cells may be detrimental [129]. Therefore, knowledge of the origin of SMC-like cells within the atherosclerotic lesion is of major importance when assessing the effect of novel therapeutics that may alter VSMC behavior. The factors that induce one state or the other are poorly understood and thus, it would be of great interest to investigate if *Has3*-deficiency affects not only SMC migration but also SMC dedifferentiation and SMC transition into macrophage-like cells.

Further evidence of a pivotal role of SMC-derived *Has3* in atherosclerosis is given by the observations that oxLDL and pro-inflammatory cytokines, such as IL-1 β , can induce expression of *Has3* in SMCs [133, 134]. IL-1 β is an important pro-inflammatory cytokine that is synthesized and secreted by many cell types including macrophages and DCs upon uptake of modified LDL via scavenger receptors [135]. Several groups have investigated the role of IL-1 β in atherosclerosis, including genetic deletion of IL-1 β , knockout of the IL-1 receptor, and administration of IL-1 β targeting antibodies, which have suggested a proatherogenic role of IL-1 β [136-139]. Currently, the CANTOS trial is investigating the effect of administering a monoclonal

anti-human IL-1 β antibody Canakinumab on cardiovascular outcomes (<http://www.thecantos.org/>; as of 01/22/2017). This trial is the first one to examine a targeted anti-inflammatory therapy on atherosclerosis-driven pathologies. Given the role of *Has3* in atherogenesis and the knowledge that *Has3* transcript expression is regulated by IL-1 β , it would be of particular interest to determine the effect of Canakinumab on HA and HAS3 synthesis in human atherosclerotic lesions. Additionally, SMC-specific deletion of *Has3* could further corroborate or disprove the hypothesis that IL-1 β -induced *Has3* expression by SMCs triggers lesional macrophage accumulation and thereby atherogenesis.

4.3. Impact of *Has3* on immune cells in the context of atherosclerosis

During inflammatory responses HA plays a critical role in multiple processes. An initial step in the inflammatory processes is the recruitment of immune cells to the site of inflammation. Thus, immune cell adhesion on endothelial cells under flow conditions and shear stress and their subsequent extravasation into the underlying tissue is required. HA-CD44 interactions appear to be critical for the primary adhesion of leukocytes on endothelial cells. It has been shown that pro-inflammatory cytokines, like IL-1 β , increase HA synthesis in human umbilical vein endothelial cells (HUVECs) by inducing *HAS2* expression. *HAS3* was expressed in HUVECs as well, but did not show cytokine dependent changes in transcript expression. Increased HA synthesis resulted in enhanced leukocyte adhesion. In contrast, inhibiting cytokine-induced *HAS2* expression by siRNA completely abolished leukocyte binding [140, 141].

In addition to leukocyte adhesion, HA-receptor interactions have been shown to induce leukocyte maturation and cytokine production [75, 77, 78].

Given the evidence that HA is involved in inflammatory responses at multiple levels and that *Has3* expression coincides with macrophage infiltration in *ApoE*^{-/-} mice, it has been hypothesized that *Has3*-deficiency might impact inflammatory processes during atherogenesis.

After 4 weeks of WD feeding, flow cytometric analyses of the aortic wall revealed that significantly fewer immune cells, especially macrophages, accumulated in the aortas of *Has3*-deficient mice. Currently, it is under debate whether monocyte recruitment or local proliferation is the major contributor to lesion development. However, it has been shown by monocyte-tracking, parabiosis, and macrophage turnover experiments that a) monocytes give rise to macrophages in atherosclerotic lesions [19], b) monocytes migrate to the lesions throughout lesion development [18], and c)

macrophage proliferation drives macrophage accumulation in advanced lesions over monocyte recruitment [27, 142]. Whether recruitment or proliferation is impaired by *Has3*-deficiency and thereby reduces macrophage accumulation in early lesions is not yet clarified. The number of monocytes in the aortic wall was slightly, but not significantly reduced in *ApoE^{-/-}/Has3^{-/-}* mice compared to *ApoE^{-/-}* mice. Thus, alterations in monocyte recruitment in early lesion development might be affected by *Has3*-deficiency and thereby contribute to the reduced numbers of macrophages.

Besides recruitment via endothelial HA-CD44 interaction, also monocyte/macrophage behavior might be altered in the lesion through lack of *Has3*. Previously, it was demonstrated *in vitro* that HA induced the expression of inflammatory cytokines like RANTES, MIP-1 α , IL-12, or MCP-1 in macrophages [75, 77, 143]. IL-12, RANTES, and MCP-1 cytokine levels were significantly lower in the plasma of *ApoE^{-/-}/Has3^{-/-}* mice in comparison with *ApoE^{-/-}* mice, indicating that *Has3* might regulate cytokine expression in macrophages under atherosclerotic conditions. Whether the cytokine levels are also reduced in atherosclerotic lesions is currently under investigation.

It is well established that there is not only one macrophage but there are several different pro- and anti-inflammatory macrophage phenotypes known, which are also present in atherosclerotic lesions. At the far ends of the scale of macrophage polarizations are the M1 and M2 macrophage phenotypes with M1 (classically activated) macrophages as pro-inflammatory cells and M2 (alternatively activated) macrophages exhibiting anti-inflammatory functions [144, 145]. M1 macrophages show a high expression of the inducible nitric-oxide synthase (iNOS). Interestingly, McKee and colleagues showed that HA fragments induced iNOS expression in a NF- κ B dependent mechanism [146]. This indicates that HA might induce the iNOS-expressing M1 macrophage phenotype under inflammatory conditions. Yet, it is not investigated whether *Has3*-deficiency affects macrophage polarization in atherosclerotic lesions. But favoring a macrophage phenotype away from M1 macrophages in mice lacking *Has3* might be a possible indication why atherosclerotic plaque burden is reduced after 15 weeks of WD feeding despite unchanged numbers of macrophages in advanced lesions. Additionally, M1 macrophages secrete higher levels of IL-12 [147, 148] and in *ApoE^{-/-}/Has3^{-/-}* mice markedly reduced circulating IL-12 levels were observed throughout lesion development (**Figure 16**) suggesting less M1 macrophages in *ApoE-Has3*-double-deficient mice. Thus, further investigation of macrophage polarization in mice lacking *Has3* might contribute to a better understanding of the role of *Has3*-mediated HA synthesis during atherogenesis and its impact on macrophages, which are the most abundant immune cells in atherosclerotic lesions and major drivers of atherosclerotic lesion development.

Besides lesional immune cells also immune cells within the thoracic PVAT were analyzed. After 15 weeks of WD feeding, fewer macrophages were detected in *ApoE^{-/-}/Has3^{-/-}* compared to *ApoE^{-/-}* mice. The PVAT has an important influence on atherosclerotic lesion development via the secretion of cytokines both by adipocytes and inflammatory cells [149-151]. Consequently, reduced numbers of immune cells in the PVAT might attenuate cytokine production of adipocytes and reduce the number of newly recruited immune cells both into the PVAT and adjacent atherosclerotic lesions. Furthermore, the activation of SMCs, which are located in the medial layer next to the PVAT, might be directly influenced by the cytokines produced in the PVAT.

4.4. Role of Has3 in T cell-mediated immune responses

Circulating leukocytes were also analyzed to get an impression of systemic alterations in inflammatory processes. Interestingly, *Has3*-deficiency had no effect on circulating monocyte subsets, but significantly altered T cell subsets at all investigated times. After 4 weeks of WD feeding, less Th1 cells were measured in *ApoE^{-/-}/Has3^{-/-}* mice compared to *ApoE^{-/-}* mice. After 7 and 15 weeks of WD, respectively, the fraction of CD8a⁺CD44⁺CD62L⁻ effector T cells was reduced in *ApoE^{-/-}/Has3^{-/-}* compared to age- and treatment-matched control mice. In addition, T cell subsets were analyzed in spleen and lymph nodes, as this is the place where T cell priming by antigen-presenting cells occurs. In lymphoid tissues of *Has3*-deficient mice less naïve T cells were observed, while the amount of central and effector memory T cells was unaffected. These results strongly indicate that *Has3* affects T cell immune responses. Alterations in naïve, but not effector and central memory T cell numbers in spleen and lymph nodes might point towards defects in either T cell recruitment to the lymphoid tissues or proliferation upon stimulation.

Lymphocytes that enter the lymphoid tissues have to pass through a specialized endothelial layer called high endothelial venules (HEVs). Their function is to enable the direct entry of circulating lymphocytes into lymph nodes. To accomplish this function, HEVs express various adhesion molecules on their surface, such as CD34 for interaction with CD62L, which is an important lymphocyte homing receptor to the lymph nodes. Further, it has been shown that HEVs express CD44 and LYVE-1, two HA receptors. However, it is not clarified yet, if and how leukocyte adhesion and migration through HEVs is dependent on HA-receptor interaction [152].

In this study (**Figure 22**) and previous studies by Mummert and colleagues [119], it was shown that T cells and DCs express HAS isoenzymes and thereby are able to produce HA. The functions of this endogenous HA synthesis by leukocytes is not understood. But maybe this endogenous HA synthesis is important for leukocyte

migration through HEVs and thus entry into lymph nodes. In this way, naïve *Has3*-deficient T cells may have an impaired ability to enter lymph nodes, resulting in reduced numbers of naïve T cells in lymph nodes and an increased fraction of circulating naïve T cells.

Secondly, proliferative expansion of T cells in secondary lymphoid tissues might be impaired due to lack of Has3 and thereby lead to reduced numbers of naïve T cells in lymphoid tissues. This hypothesis is supported by an observation of Mahaffey and Mummert. They showed that endogenous HA synthesis by T cells enhanced T cell proliferation in an IL-2 dependent manner [153]. IL-2 is the major cytokine enhancing T cell proliferation by binding to its IL-2 receptor (IL-2R). Upon stimulation, T cells transcribe IL-2 and begin to express the IL-2R α -chain (also known as CD25) on their surface [154, 155]. Stimulation of T cells with concurrent treatment of 4-MU abolished T cell proliferation. At the same time, T cell activation, measured by CD69 expression, was not affected by 4-MU treatment. Mahaffey *et al.* further demonstrated that IL-2 secretion was reduced by 4-MU treatment [153]. These results strongly indicate an important role of endogenous HA synthesis in T cell proliferation. However, our *in vitro* experiments using *Has3*-deficient T cells did not reveal significant effects of *Has3*-deficiency on the amount of cells after 24 and 48 hours of stimulation (**Figure 23**). Concerning the activation status of T cells with or without Has3, the results obtained upon bead-stimulation were similar to the observations of Mahaffey and colleagues. Lack of Has3 in T cells did not affect CD25 expression or the generation of CD44⁺CD62L⁻ effector and CD44⁺CD62L⁺ central memory T cells. Further experiments need to be performed to definitely determine if Has3 expression plays a role in T cell expansion in an autocrine manner.

Besides T cells expressing HAS enzymes to synthesize HA, it was described previously that DCs as important antigen-presenting cells also express *HAS3* [81, 119]. Mummert and colleagues demonstrated that blocking HA in DC-T cell co-cultures using a peptide reduced DC-mediated T cell proliferation [119]. Whether this effect was due to HA synthesis by DCs or T cells could not be answered conclusively. Instead of using a peptide that interferes with HA synthesized by either cell, the use of *Has3*-deficient cells might help to clarify this question.

In addition to a possible paracrine function of HA synthesized by DCs, HA might also directly affect DC function. In this study it was focused on the analysis of co-stimulatory molecules required in DC-mediated T cell activation due to the observed alterations in T cell functions in *Has3*-deficient mice. For this purpose, *ApoE*-deficient and *ApoE-Has3*-double deficient BM-DCs were cultivated and stimulated with LPS. Thereupon, the maturation of DCs was assessed by flow cytometric analysis of MHC II and CD86 surface expression [156]. These analyses did not indicate that *Has3*-deficiency impacted DC maturation. Whether *Has3*-deficiency in BM-DCs affects the cytokine secretion of DCs upon stimulation is currently under

investigation. Comparison of the plasma cytokine profiles of *ApoE*^{-/-} and *ApoE*^{-/-}/*Has3*^{-/-} mice strongly indicates an influence of *Has3*-deficiency on cytokine production due to the reduced levels of IL-12 in *ApoE*^{-/-}/*Has3*^{-/-} mice. As IL-12 is an important regulator of T cell differentiation into Th1 cells and DCs are the major antigen-presenting cells driving T cell responses, alterations in T cell populations and T cell regulating cytokines due to lack of *Has3* might suggest a role of *Has3*-mediated cytokine secretion in DCs. Thus, these results will help to understand the observed alterations in T cell differentiation, the cytokine profile, and on atherosclerotic lesion development.

The current data obtained by *in vivo* and *in vitro* experiments suggest that *Has3*-deficiency is not directly mediating T cell activation and effector/memory T cell generation. Whether T cell proliferation upon stimulation is affected by *Has3*-deficiency cannot be answered conclusively at this point. With regard to the alterations in circulating T cells and reduced numbers of naïve T cells in secondary lymphoid tissues, *Has3* appears to play an important role in T cell biology.

Besides the expected direct effect of *Has3*-deficiency on T cell expansion and activation, reduced numbers of naïve T cells in the lymphoid tissues, and reduced amounts of effector T cells in the circulation may be a secondary effect due to alterations in the number of Th1 cells. Bollyky and colleagues showed that Th1 cytokines but not Th2 cytokines induced the synthesis of HA by DCs. This enhanced HA synthesis promoted the interaction between DCs and T cells, which thereby affects T cell responses [81]. This study would suggest that lower numbers of Th1 cells in *Has3*-deficient mice would induce HA synthesis in DCs less efficiently and consequently T cell expansion is impaired. In this model, endogenous HA synthesis by T cells would not be a driving factor for T cell expansion. Further, Bollyky [81] and Mummert [119] showed that both DCs and T cells do not only express *Has3*. Maybe the direct effects of endogenously synthesized HA are due to the other HAS isoenzymes, which are equally affected by 4-MU treatment and thus might explain why no significant reduction of T cell expansion was detected in *Has3*-deficient T cells.

Besides the changes in circulating T cell subsets, the cytokine profile also indicated an important role of *Has3* on T cell immunity.

IL-12 plays a central role in the induction of IFN- γ producing Th1 cells [157, 158]. Besides its effects on CD4⁺ T cells, it was shown that IL-12 also augments the activation and priming of CD8-positive T cells by DCs by increasing the duration of interaction between T cell and DC [159]. Although these cytokines were only measured in the circulation and thus it is not clear which cell type secretes the cytokines, this might suggest that IL-12 secretion by DCs or macrophages is affected by lack of *Has3*. Previous studies have already shown that HA fragments induced

cytokine secretion, such as IL-12, by DCs and macrophages [75-79, 160]. Reduced levels of IL-12 might explain the lower numbers of Th1 cells in *ApoE^{-/-}/Has3^{-/-}* mice and might perhaps also affect T cell expansion [159]. The impact of IL-12 on atheroprotection was shown by several murine studies using knock-out models [38], vaccination [161], or daily administrations of IL-12 [39]. All these studies showed that IL-12 promotes atherosclerotic lesion development. Whether lesional IL-12 levels are altered in *ApoE^{-/-}/Has3^{-/-}* mice is currently under investigation. However, these systemic alterations strongly indicate a regulatory role of Has3 in IL-12 production.

RANTES also has an impact on T cells. On the one hand, RANTES mRNA is present in T cells and the protein secretion can be initiated by T cell receptor stimulation [162]. On the other hand, the chemokine also plays an important role in the recruitment of activated T cells and other immune cells to the site of inflammation [163]. Veillard *et al.* described a significant reduction of atherosclerotic lesions and lipid deposition in *ApoE^{-/-}* mice by blocking the interaction of RANTES with its receptor CCR5 [164]. Although most of the studies showing a correlation of RANTES and atherosclerosis described alterations in monocyte recruitment, the direct link between CCR5 on T cells and atherosclerosis was recently shown [163] by Li and colleagues who demonstrated that neutralization of RANTES reduced the infiltration of CD4⁺ T cells into atherosclerotic plaques.

MCP-1 is another cytokine that is crucially involved in atheroprotection. MCP-1 is best known for its role in monocyte recruitment [165], but also as a chemoattractant for CD4⁺ and CD8⁺ T cells [166, 167]. Apart from its function in immune cell recruitment it also affects T cell polarization. In the study by Gu *et al.* it was shown that MCP-1 is crucially involved in inducing Th2 cell responses [168]. In *MCP-1*-deficient mice extremely low concentrations of the Th2 cell cytokines IL-4, IL-5, and IL-10 were detected. Although circulating MCP-1 levels were lower in *ApoE^{-/-}/Has3^{-/-}* compared to *ApoE^{-/-}* mice, the concentrations of IL-5, and IL-10, which are the key cytokines secreted by Th2 cells, were not significantly decreased in mice lacking Has3.

Taken together, these alterations in circulating cytokines further support the hypothesis that Has3 has an important role in T cell responses. However, the question of whether both T cell polarization and T cell recruitment contribute equally to Has3-mediated effects on atherogenesis requires further investigation.

In summary, global knockout of *Has3* in *ApoE*-deficient mice fed a WD reduces the development of atherosclerotic lesions by affecting inflammatory processes. LDL/VLDL cholesterol levels were unaffected by *Has3*-deficiency. In addition to reduced macrophage accumulation in the plaques there were also systemic effects on polarization and activation of T lymphocytes, which probably contribute to the anti-

atherogenic effects of *Has3*-deficiency. Whether the T cell phenotype affects lesional macrophage accumulation or vice versa requires further investigation.

Taking all data together, one possible mechanism that could explain how *Has3* accelerates atherogenesis might be that IL-1 β and oxLDL induce *Has3* expression in SMCs and this newly synthesized HA drives the secretion of pro-inflammatory cytokines (e.g. IL-12). IL-12 further augments the differentiation of Th cells into the proatherogenic Th1 cell subset (**Figure 26 A**). Moreover, HA expression by DCs was described to be important for the interaction between DCs and T cells and the formation of the immune synapse. Thus, *Has3*-deficiency might also affect this DC-T cell interaction and consequently T cell proliferation and/or differentiation (**Figure 26 B**). Via a positive feedback loop, Th1 cells stimulate and enhance macrophage activation through the secretion of cytokines like IFN- γ and thus further promote the development of atherosclerotic lesions.

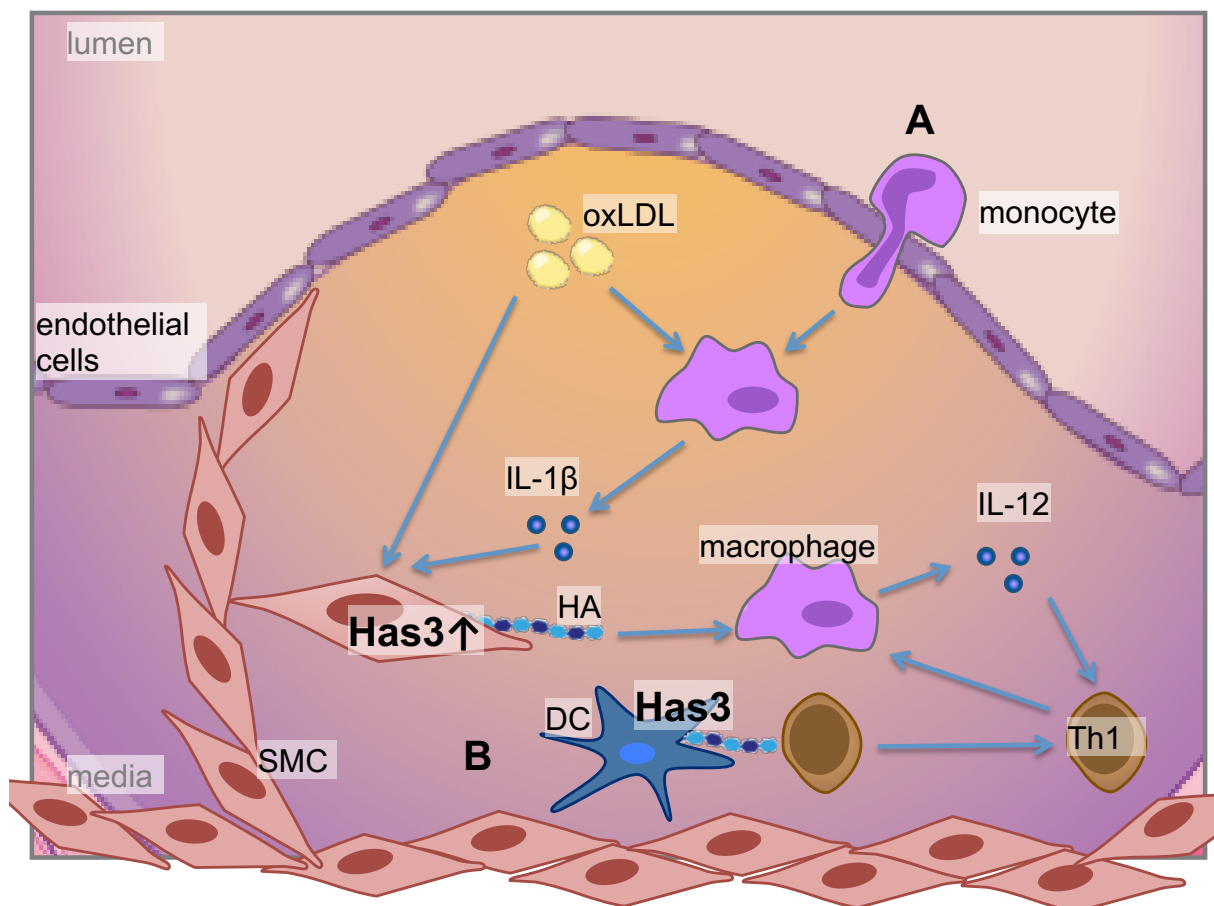


Figure 26: Possible mechanisms for *Has3*-dependent acceleration of atherosclerotic lesion development.

4.5. Limitations and prospect

In this study it was demonstrated for the first time that *Has3*-deficiency reduces the development of atherosclerotic lesions by modulating macrophage accumulation and T cell differentiation. At the same time, the localization and fraction of SMC-like cells in the luminal region of the lesion was not affected by *Has3*-deficiency, suggesting that *Has3*-deficiency does not impair plaque stability.

One limitation of the animal model might be that the mice were lacking *Has3* throughout embryonic development. No differences in the development of *ApoE*^{-/-}/*Has3*^{-/-} mice compared to littermate controls were observed. However, it cannot be ruled out that *Has3*-deficiency has any positive effects during the development of the vasculature that could promote the positive outcome in lesion development upon WD feeding. Further, it needs to be investigated whether *Has3*-deficiency slows down lesion development by interfering in processes early during lesion development or whether lack of *Has3* also has beneficial effects in advanced lesions. To reach clarification on these issues, it would require a model with an inducible knockout, which was induced once advanced lesions were developed. Such a model would also better mimic a possible treatment of humans, as therapeutic intervention is most often initiated just after the first symptoms, e.g. myocardial infarction, appeared.

Another point that might restrict the transferability of the results into the clinics might be the usage of a mouse model and murine cells for *in vivo* and *in vitro* experiments. Mice usually do not develop atherosclerotic lesions, probably due to a different cholesterol metabolism with much higher HDL cholesterol levels compared to humans [169, 170]. However, genetic manipulation enabled researchers to use mice to study atherosclerosis. Different models are available, among others the *ApoE*-deficient mouse that was used in the present study, which belongs to the most commonly used mouse model in atherosclerosis research [170]. Even so, there are still major differences in lesion development comparing humans and mice, including the localization of lesions or complications such as rupture that can occur [108, 171]. Thus, to exclude model-specific effects it might be worth examining the role of *Has3* on lesion development and progression in further models.

As a last point, it was not possible to conclusively clarify the mechanism that results in reduced atherosclerotic plaque burden in mice lacking *Has3*. Further experiments are required to evaluate whether alterations in the lesional immune cell composition affect the T cell phenotype or vice versa. In addition, a cell specific *Has3*-knockout in SMCs and immune cells, respectively, could identify the cell type that is responsible

for early HA accumulation in the lesion and thus give a more detailed understanding of the role of HA in atherosclerotic lesion development.

5. Summary

Cardiovascular diseases are the leading causes of death in the world. The cause of most of the cardiovascular morbidity and mortality is atherosclerosis, which leads to narrowing up to the complete occlusion of the vessel lumen. As chronic inflammatory disease, immune cells are a major contributor to the development and progression of atherosclerosis. Besides cellular components also secreted molecules and molecules of the extracellular matrix (ECM) have been shown to be involved in atheroprotection. Hyaluronan (HA), an unbranched polysaccharide, is found in both human and murine atherosclerotic lesions and is thought to affect the development of atherosclerotic lesions. HA synthesis is mediated by three HA synthase isoenzymes (HAS1, HAS2, HAS3). Especially Has3 expression was found to be increased in early lesion formation in mice and coincided with early macrophage infiltration. Therefore, the aim of the present study was to investigate the role of Has3 in a murine model of atherosclerosis. For this purpose, male *ApoE*^{-/-}/*Has3*^{-/-} and *ApoE*^{-/-} control mice were fed a fat- and cholesterol-rich western-type diet (WD) for 4, 7, or 15 weeks, respectively.

After 15 weeks of feeding mice with WD, ORO staining of *en face* prepared aortas revealed significantly reduced atherosclerotic plaque burden of *ApoE*^{-/-}/*Has3*^{-/-} compared to *ApoE*^{-/-} mice. In early atherosclerotic lesions, it was shown that less macrophages accumulated in the aortic wall of *ApoE*^{-/-}/*Has3*^{-/-} mice. Analyses of circulating immune cells using flow cytometry did not show alterations in total number of monocytes, B cells, and T lymphocytes. However, circulating T helper (Th) 1 cells as well as effector CD8a⁺ T cells were decreased in *ApoE*^{-/-}/*Has3*^{-/-} mice. Analyses of circulating cytokines revealed that IL-12, which plays a key role in mediating CD4⁺ T cell differentiation into the Th1 cell subset, were significantly reduced in *Has3*-deficient mice compared to control mice.

As both T lymphocytes and dendritic cells express HAS3, *in vitro* experiments were performed to assess the impact of Has3 on T cell activation and thereby gain further information on the role of HA in T cell responses. However, so far no direct function of Has3 could be attributed to T cell activation *in vitro*.

Although the mechanism remains unexplained, the results obtained *in vivo* suggest that reduced Th1 cell numbers and macrophage infiltration might mediate atheroprotection in *Has3*-deficient mice.

6. Zusammenfassung

Herz-Kreislaufkrankungen sind die häufigste Todesursache weltweit. Die Atherosklerose liegt den ischämischen Herz-Kreislaufkrankungen allen voran dem Myokardinfarkt zugrunde. Als chronisch-entzündliche Erkrankung sind diverse Immunzellen an der Entwicklung und Progression der atherosklerotischen Läsionen wesentlich beteiligt. Abgesehen von zellulären Bestandteilen finden sich jedoch auch sezernierte Moleküle und Bestandteile der extrazellulären Matrix in Plaques, welche die Entwicklung der Läsionen beeinflussen. Hyaluronsäure (HA), ein lineares Polysaccharid, wurde sowohl in humanen als auch murinen Läsionen detektiert. An der Synthese von HA sind drei HA-Synthase-Isoenzyme (HAS1, HAS2, HAS3) beteiligt. Im Mausmodell konnte gezeigt werden, dass insbesondere die *Has3* in der frühen Entstehung atherosklerotischer Läsionen von *ApoE*^{-/-}-Mäusen exprimiert wird und mit der frühen Makrophageninfiltration einhergeht.

Deshalb sollte in dieser Arbeit die Rolle der *Has3* in der Entwicklung atherosklerotischer Läsionen im Mausmodell untersucht werden. Männliche *ApoE*^{-/-}/*Has3*^{-/-}-Mäuse und *ApoE*^{-/-}-Kontrollmäuse wurden dazu für 4, 7 und 15 Wochen mit einer fett- und cholesterinreichen Diät (WD) gefüttert.

Nach 15 Wochen der WD-Fütterung wies die Aorta von *ApoE*^{-/-}/*Has3*^{-/-}-Mäusen signifikant weniger lipideingelagerte atherosklerotische Läsionen auf. Um die zugrunde liegenden Mechanismen zu erforschen, wurden Läsionen in einem früheren Entwicklungsstadium untersucht. Es konnte gezeigt werden, dass in frühen Plaques der Aorta weniger Makrophagen bei *ApoE*^{-/-}/*Has3*^{-/-}-Mäusen akkumulierten als in den Kontrolltieren. Mittels durchflusszytometrischer Messungen wurden zudem auch Immunzellen im Blut untersucht. Während die Zahl der Monozyten, B- und T-Lymphozyten nicht verändert war, fanden sich in *ApoE*^{-/-}/*Has3*^{-/-}-Mäusen weniger T-Helfer (Th) 1 Zellen, sowie weniger CD8a⁺ Effektor-T-Zellen. Zudem zeigten sich Veränderungen im Zytokin-Profil in *Has3*-defizienten Mäusen. So konnte signifikant weniger IL-12 in der Zirkulation der *ApoE*^{-/-}/*Has3*^{-/-}-Mäuse nachgewiesen werden. IL-12 spielt eine zentrale Rolle in der CD4⁺-T-Zell-Differenzierung zum Th1-Zelltypen.

Da sowohl T-Zellen als auch dendritische Zellen HAS3 exprimieren, sollte in *in vitro* Experimenten untersucht werden, welche Rolle HAS3 in der T-Zell-Aktivierung spielt. Bisher konnte jedoch kein direkter Zusammenhang zwischen *Has3*-Expression in T-Zellen und/oder dendritischen Zellen und der T-Zell-Aktivierung festgestellt werden.

Obwohl die *in vitro* Daten bisher die Veränderungen der T-Zellen *in vivo* nicht erklären können, deuten die erhobenen Daten darauf hin, dass die Veränderungen der T-Zell-Subtypen durch *Has3*-Defizienz einen wesentlichen Beitrag zur

Verringerung der Makrophagen-vermittelten Inflammation und damit der Progression atherosklerotischer Läsionen leisten.

References

1. Barquera, S., et al., *Global Overview of the Epidemiology of Atherosclerotic Cardiovascular Disease*. Arch Med Res, 2015. **46**(5): p. 328-38.
2. (WHO), W.H.O., *Global Atlas on cardiovascular disease prevention and control*. 2011.
3. Bibbins-Domingo, K., et al., *Statin Use for the Primary Prevention of Cardiovascular Disease in Adults US Preventive Services Task Force Recommendation Statement*. Jama-Journal of the American Medical Association, 2016. **316**(19): p. 1997-2007.
4. Gorelick, P.B., L.B. Goldstein, and B. Ovbiagele, *New guidelines to reduce risk of atherosclerotic cardiovascular disease: implications for stroke prevention in 2014*. Stroke, 2014. **45**(4): p. 945-7.
5. Weber, C. and H. Noels, *Atherosclerosis: current pathogenesis and therapeutic options*. Nat Med, 2011. **17**(11): p. 1410-22.
6. Koenig, W. and N. Khuseyinova, *Biomarkers of atherosclerotic plaque instability and rupture*. Arterioscler Thromb Vasc Biol, 2007. **27**(1): p. 15-26.
7. Grundy, S.M., *Cholesterol metabolism in man*. West J Med, 1978. **128**(1): p. 13-25.
8. Groot, P.H., et al., *Quantitative assessment of aortic atherosclerosis in APOE*3 Leiden transgenic mice and its relationship to serum cholesterol exposure*. Arterioscler Thromb Vasc Biol, 1996. **16**(8): p. 926-33.
9. Zhang, S.H., et al., *Spontaneous hypercholesterolemia and arterial lesions in mice lacking apolipoprotein E*. Science, 1992. **258**(5081): p. 468-71.
10. Jousilahti, P., et al., *Serum cholesterol distribution and coronary heart disease risk: observations and predictions among middle-aged population in eastern Finland*. Circulation, 1998. **97**(11): p. 1087-94.
11. Ridker, P.M., et al., *C-reactive protein levels and outcomes after statin therapy*. N Engl J Med, 2005. **352**(1): p. 20-8.
12. Bohula, E.A., et al., *Achievement of dual low-density lipoprotein cholesterol and high-sensitivity C-reactive protein targets more frequent with the addition of ezetimibe to simvastatin and associated with better outcomes in IMPROVE-IT*. Circulation, 2015. **132**(13): p. 1224-33.
13. Stancu, C. and A. Sima, *Statins: mechanism of action and effects*. J Cell Mol Med, 2001. **5**(4): p. 378-87.
14. Chaudhary, R., et al., *PCSK9 inhibitors: A new era of lipid lowering therapy*. World J Cardiol, 2017. **9**(2): p. 76-91.
15. Geissmann, F., S. Jung, and D.R. Littman, *Blood monocytes consist of two principal subsets with distinct migratory properties*. Immunity, 2003. **19**(1): p. 71-82.
16. Passlick, B., D. Flieger, and H.W. Ziegler-Heitbrock, *Identification and characterization of a novel monocyte subpopulation in human peripheral blood*. Blood, 1989. **74**(7): p. 2527-34.
17. Carlin, L.M., et al., *Nr4a1-dependent Ly6C(low) monocytes monitor endothelial cells and orchestrate their disposal*. Cell, 2013. **153**(2): p. 362-75.
18. Swirski, F.K., et al., *Monocyte accumulation in mouse atherogenesis is progressive and proportional to extent of disease*. Proc Natl Acad Sci U S A, 2006. **103**(27): p. 10340-5.

19. Swirski, F.K., et al., *Ly-6Chi monocytes dominate hypercholesterolemia-associated monocytosis and give rise to macrophages in atheromata*. J Clin Invest, 2007. **117**(1): p. 195-205.
20. Combadiere, C., et al., *Combined inhibition of CCL2, CX3CR1, and CCR5 abrogates Ly6C(hi) and Ly6C(lo) monocytosis and almost abolishes atherosclerosis in hypercholesterolemic mice*. Circulation, 2008. **117**(13): p. 1649-57.
21. Gosling, J., et al., *MCP-1 deficiency reduces susceptibility to atherosclerosis in mice that overexpress human apolipoprotein B*. J Clin Invest, 1999. **103**(6): p. 773-8.
22. Janeway, C.A., Jr. and R. Medzhitov, *Innate immune recognition*. Annu Rev Immunol, 2002. **20**: p. 197-216.
23. Peiser, L., S. Mukhopadhyay, and S. Gordon, *Scavenger receptors in innate immunity*. Curr Opin Immunol, 2002. **14**(1): p. 123-8.
24. Michelsen, K.S., et al., *Lack of Toll-like receptor 4 or myeloid differentiation factor 88 reduces atherosclerosis and alters plaque phenotype in mice deficient in apolipoprotein E*. Proc Natl Acad Sci U S A, 2004. **101**(29): p. 10679-84.
25. Zizzo, G., et al., *Efficient clearance of early apoptotic cells by human macrophages requires M2c polarization and MerTK induction*. J Immunol, 2012. **189**(7): p. 3508-20.
26. Ley, K., Y.I. Miller, and C.C. Hedrick, *Monocyte and macrophage dynamics during atherogenesis*. Arterioscler Thromb Vasc Biol, 2011. **31**(7): p. 1506-16.
27. Robbins, C.S., et al., *Local proliferation dominates lesional macrophage accumulation in atherosclerosis*. Nat Med, 2013. **19**(9): p. 1166-72.
28. Paulson, K.E., et al., *Resident intimal dendritic cells accumulate lipid and contribute to the initiation of atherosclerosis*. Circ Res, 2010. **106**(2): p. 383-90.
29. Choi, J.H., et al., *Identification of antigen-presenting dendritic cells in mouse aorta and cardiac valves*. J Exp Med, 2009. **206**(3): p. 497-505.
30. Han, J.W., et al., *Vessel wall-embedded dendritic cells induce T-cell autoreactivity and initiate vascular inflammation*. Circ Res, 2008. **102**(5): p. 546-53.
31. Pennock, N.D., et al., *T cell responses: naive to memory and everything in between*. Adv Physiol Educ, 2013. **37**(4): p. 273-83.
32. Hansson, G.K., *Immune mechanisms in atherosclerosis*. Arterioscler Thromb Vasc Biol, 2001. **21**(12): p. 1876-90.
33. Libby, P., et al., *Inflammation in atherosclerosis: from pathophysiology to practice*. J Am Coll Cardiol, 2009. **54**(23): p. 2129-38.
34. Song, L., C. Leung, and C. Schindler, *Lymphocytes are important in early atherosclerosis*. J Clin Invest, 2001. **108**(2): p. 251-9.
35. Zhou, X., et al., *Transfer of CD4(+) T cells aggravates atherosclerosis in immunodeficient apolipoprotein E knockout mice*. Circulation, 2000. **102**(24): p. 2919-22.
36. Szabo, S.J., et al., *A novel transcription factor, T-bet, directs Th1 lineage commitment*. Cell, 2000. **100**(6): p. 655-69.
37. Buono, C., et al., *T-bet deficiency reduces atherosclerosis and alters plaque antigen-specific immune responses*. Proc Natl Acad Sci U S A, 2005. **102**(5): p. 1596-601.

38. Davenport, P. and P.G. Tipping, *The role of interleukin-4 and interleukin-12 in the progression of atherosclerosis in apolipoprotein E-deficient mice*. *Am J Pathol*, 2003. **163**(3): p. 1117-25.
39. Lee, T.S., et al., *The role of interleukin 12 in the development of atherosclerosis in ApoE-deficient mice*. *Arterioscler Thromb Vasc Biol*, 1999. **19**(3): p. 734-42.
40. Lahoute, C., et al., *Adaptive immunity in atherosclerosis: mechanisms and future therapeutic targets*. *Nat Rev Cardiol*, 2011. **8**(6): p. 348-58.
41. Mallat, Z., H. Ait-Oufella, and A. Tedgui, *Regulatory T-cell immunity in atherosclerosis*. *Trends Cardiovasc Med*, 2007. **17**(4): p. 113-8.
42. Binder, C.J., et al., *IL-5 links adaptive and natural immunity specific for epitopes of oxidized LDL and protects from atherosclerosis*. *J Clin Invest*, 2004. **114**(3): p. 427-37.
43. Miller, A.M., et al., *IL-33 reduces the development of atherosclerosis*. *J Exp Med*, 2008. **205**(2): p. 339-46.
44. King, V.L., S.J. Szilvassy, and A. Daugherty, *Interleukin-4 deficiency decreases atherosclerotic lesion formation in a site-specific manner in female LDL receptor^{-/-} mice*. *Arterioscler Thromb Vasc Biol*, 2002. **22**(3): p. 456-61.
45. Cochain, C., et al., *CD8⁺ T Cells Regulate Monopoiesis and Circulating Ly6C-high Monocyte Levels in Atherosclerosis in Mice*. *Circ Res*, 2015. **117**(3): p. 244-53.
46. Kyaw, T., et al., *Cytotoxic and proinflammatory CD8⁺ T lymphocytes promote development of vulnerable atherosclerotic plaques in apoE-deficient mice*. *Circulation*, 2013. **127**(9): p. 1028-39.
47. Alexander, M.R. and G.K. Owens, *Epigenetic control of smooth muscle cell differentiation and phenotypic switching in vascular development and disease*. *Annu Rev Physiol*, 2012. **74**: p. 13-40.
48. Li, D.Y., et al., *Elastin is an essential determinant of arterial morphogenesis*. *Nature*, 1998. **393**(6682): p. 276-80.
49. Jiang, J.X., et al., *Phenotypic switching induced by damaged matrix is associated with DNA methyltransferase 3A (DNMT3A) activity and nuclear localization in smooth muscle cells (SMC)*. *PLoS One*, 2013. **8**(8): p. e69089.
50. Rong, J.X., et al., *Transdifferentiation of mouse aortic smooth muscle cells to a macrophage-like state after cholesterol loading*. *Proc Natl Acad Sci U S A*, 2003. **100**(23): p. 13531-6.
51. Allahverdian, S., et al., *Contribution of intimal smooth muscle cells to cholesterol accumulation and macrophage-like cells in human atherosclerosis*. *Circulation*, 2014. **129**(15): p. 1551-9.
52. Feil, S., et al., *Transdifferentiation of vascular smooth muscle cells to macrophage-like cells during atherogenesis*. *Circ Res*, 2014. **115**(7): p. 662-7.
53. Shankman, L.S., et al., *KLF4-dependent phenotypic modulation of smooth muscle cells has a key role in atherosclerotic plaque pathogenesis*. *Nat Med*, 2015. **21**(6): p. 628-37.
54. Vengrenyuk, Y., et al., *Cholesterol loading reprograms the microRNA-143/145-myocardin axis to convert aortic smooth muscle cells to a dysfunctional macrophage-like phenotype*. *Arterioscler Thromb Vasc Biol*, 2015. **35**(3): p. 535-46.
55. Alphonse, C.S. and R.N. Rodseth, *The endothelial glycocalyx: a review of the vascular barrier*. *Anaesthesia*, 2014. **69**(7): p. 777-84.

56. Hou, G., et al., *Type VIII collagen stimulates smooth muscle cell migration and matrix metalloproteinase synthesis after arterial injury*. *Am J Pathol*, 2000. **156**(2): p. 467-76.
57. Adiguzel, E., et al., *Migration and growth are attenuated in vascular smooth muscle cells with type VIII collagen-null alleles*. *Arterioscler Thromb Vasc Biol*, 2006. **26**(1): p. 56-61.
58. Wesley, R.B., 2nd, et al., *Extracellular matrix modulates macrophage functions characteristic to atheroma: collagen type I enhances acquisition of resident macrophage traits by human peripheral blood monocytes in vitro*. *Arterioscler Thromb Vasc Biol*, 1998. **18**(3): p. 432-40.
59. Chistiakov, D.A., I.A. Sobenin, and A.N. Orekhov, *Vascular extracellular matrix in atherosclerosis*. *Cardiol Rev*, 2013. **21**(6): p. 270-88.
60. Olsson, U., G. Ostergren-Lunden, and J. Moses, *Glycosaminoglycan-lipoprotein interaction*. *Glycoconj J*, 2001. **18**(10): p. 789-97.
61. Karangelis, D.E., et al., *Glycosaminoglycans as key molecules in atherosclerosis: the role of versican and hyaluronan*. *Curr Med Chem*, 2010. **17**(33): p. 4018-26.
62. Jiang, D., J. Liang, and P.W. Noble, *Hyaluronan as an immune regulator in human diseases*. *Physiol Rev*, 2011. **91**(1): p. 221-64.
63. Torronen, K., et al., *Tissue distribution and subcellular localization of hyaluronan synthase isoenzymes*. *Histochem Cell Biol*, 2014. **141**(1): p. 17-31.
64. Tien, J.Y. and A.P. Spicer, *Three vertebrate hyaluronan synthases are expressed during mouse development in distinct spatial and temporal patterns*. *Dev Dyn*, 2005. **233**(1): p. 130-41.
65. Bart, G., et al., *Fluorescence resonance energy transfer (FRET) and proximity ligation assays reveal functionally relevant homo- and heteromeric complexes among hyaluronan synthases HAS1, HAS2, and HAS3*. *J Biol Chem*, 2015. **290**(18): p. 11479-90.
66. Camenisch, T.D., et al., *Disruption of hyaluronan synthase-2 abrogates normal cardiac morphogenesis and hyaluronan-mediated transformation of epithelium to mesenchyme*. *J Clin Invest*, 2000. **106**(3): p. 349-60.
67. Csoka, A.B., G.I. Frost, and R. Stern, *The six hyaluronidase-like genes in the human and mouse genomes*. *Matrix Biol*, 2001. **20**(8): p. 499-508.
68. Laurent, T.C. and J.R. Fraser, *The properties and turnover of hyaluronan*. *Ciba Found Symp*, 1986. **124**: p. 9-29.
69. Vigetti, D., et al., *Hyaluronan synthesis is inhibited by adenosine monophosphate-activated protein kinase through the regulation of HAS2 activity in human aortic smooth muscle cells*. *J Biol Chem*, 2011. **286**(10): p. 7917-24.
70. Wang, Y., et al., *Hyaluronan synthase 2 protects skin fibroblasts against apoptosis induced by environmental stress*. *J Biol Chem*, 2014. **289**(46): p. 32253-65.
71. Misra, S., et al., *Interactions between hyaluronan and its receptors (CD44, RHAMM) regulate the activities of inflammation and cancer*. *Frontiers in Immunology*, 2015. **6**(201).
72. Lesley, J., et al., *Hyaluronan binding function of CD44 is transiently activated on T cells during an in vivo immune response*. *J Exp Med*, 1994. **180**(1): p. 383-7.
73. DeGrendele, H.C., et al., *CD44 activation and associated primary adhesion is inducible via T cell receptor stimulation*. *J Immunol*, 1997. **159**(6): p. 2549-53.

74. Maeshima, N., et al., *Hyaluronan binding identifies the most proliferative activated and memory T cells*. Eur J Immunol, 2011. **41**(4): p. 1108-19.
75. Hodge-Dufour, J., et al., *Induction of IL-12 and chemokines by hyaluronan requires adhesion-dependent priming of resident but not elicited macrophages*. J Immunol, 1997. **159**(5): p. 2492-500.
76. Scheibner, K.A., et al., *Hyaluronan fragments act as an endogenous danger signal by engaging TLR2*. Journal of Immunology, 2006. **177**(2): p. 1272-1281.
77. McKee, C.M., et al., *Hyaluronan (HA) fragments induce chemokine gene expression in alveolar macrophages. The role of HA size and CD44*. J Clin Invest, 1996. **98**(10): p. 2403-13.
78. Termeer, C.C., et al., *Oligosaccharides of hyaluronan are potent activators of dendritic cells*. J Immunol, 2000. **165**(4): p. 1863-70.
79. Termeer, C., et al., *Oligosaccharides of Hyaluronan activate dendritic cells via toll-like receptor 4*. J Exp Med, 2002. **195**(1): p. 99-111.
80. DeGrendele, H.C., et al., *CD44 and its ligand hyaluronate mediate rolling under physiologic flow: a novel lymphocyte-endothelial cell primary adhesion pathway*. J Exp Med, 1996. **183**(3): p. 1119-30.
81. Bollyky, P.L., et al., *Th1 cytokines promote T-cell binding to antigen-presenting cells via enhanced hyaluronan production and accumulation at the immune synapse*. Cell Mol Immunol, 2010. **7**(3): p. 211-20.
82. Evanko, S.P., et al., *Proteoglycan distribution in lesions of atherosclerosis depends on lesion severity, structural characteristics, and the proximity of platelet-derived growth factor and transforming growth factor-beta*. Am J Pathol, 1998. **152**(2): p. 533-46.
83. Kolodgie, F.D., et al., *Differential accumulation of proteoglycans and hyaluronan in culprit lesions: insights into plaque erosion*. Arterioscler Thromb Vasc Biol, 2002. **22**(10): p. 1642-8.
84. Srinivasan, S.R., et al., *Lipoprotein-hyaluronate associations in human aorta fibrous plaque lesions*. Atherosclerosis, 1980. **36**(1): p. 25-37.
85. Sakr, S.W., et al., *Hyaluronan accumulation is elevated in cultures of low density lipoprotein receptor-deficient cells and is altered by manipulation of cell cholesterol content*. J Biol Chem, 2008. **283**(52): p. 36195-204.
86. Chai, S., et al., *Overexpression of hyaluronan in the tunica media promotes the development of atherosclerosis*. Circ Res, 2005. **96**(5): p. 583-91.
87. Papakonstantinou, E., et al., *The differential distribution of hyaluronic acid in the layers of human atheromatic aortas is associated with vascular smooth muscle cell proliferation and migration*. Atherosclerosis, 1998. **138**(1): p. 79-89.
88. Vigetti, D., et al., *The effects of 4-methylumbelliferone on hyaluronan synthesis, MMP2 activity, proliferation, and motility of human aortic smooth muscle cells*. Glycobiology, 2009. **19**(5): p. 537-46.
89. Wilkinson, T.S., et al., *Overexpression of hyaluronan synthases alters vascular smooth muscle cell phenotype and promotes monocyte adhesion*. J Cell Physiol, 2006. **206**(2): p. 378-85.
90. Tabata, T., et al., *Low molecular weight hyaluronan increases the Uptaking of oxidized LDL into monocytes*. Endocr J, 2007. **54**(5): p. 685-93.
91. Cuff, C.A., et al., *The adhesion receptor CD44 promotes atherosclerosis by mediating inflammatory cell recruitment and vascular cell activation*. J Clin Invest, 2001. **108**(7): p. 1031-40.
92. Braun, M., et al., *Cellular adhesion molecules on vascular smooth muscle cells*. Cardiovasc Res, 1999. **41**(2): p. 395-401.

93. Zhao, L., et al., *CD44 expressed on both bone marrow-derived and non-bone marrow-derived cells promotes atherogenesis in ApoE-deficient mice*. *Arterioscler Thromb Vasc Biol*, 2008. **28**(7): p. 1283-9.
94. Nagy, N., et al., *Inhibition of hyaluronan synthesis accelerates murine atherosclerosis: novel insights into the role of hyaluronan synthesis*. *Circulation*, 2010. **122**(22): p. 2313-22.
95. Kiene, L.S., et al., *Deletion of Hyaluronan Synthase 3 Inhibits Neointimal Hyperplasia in Mice*. *Arterioscler Thromb Vasc Biol*, 2016. **36**(2): p. e9-16.
96. Madaan, A., et al., *A stepwise procedure for isolation of murine bone marrow and generation of dendritic cells*. *Journal of Biological Methods*, 2014. **1**(1).
97. Breslin, W.L., et al., *Mouse blood monocytes: standardizing their identification and analysis using CD115*. *J Immunol Methods*, 2013. **390**(1-2): p. 1-8.
98. Van den Broeck, W., A. Derore, and P. Simoens, *Anatomy and nomenclature of murine lymph nodes: Descriptive study and nomenclatory standardization in BALB/cAnNCrl mice*. *J Immunol Methods*, 2006. **312**(1-2): p. 12-9.
99. Butcher, M.J., et al., *Flow cytometry analysis of immune cells within murine aortas*. *J Vis Exp*, 2011(53).
100. Menotti, A., et al., *Short and long term association of a single serum cholesterol measurement in middle-aged men in prediction of fatal coronary and other cardiovascular events: a cross-cultural comparison through Europe*. *Eur J Epidemiol*, 2005. **20**(7): p. 597-604.
101. Menotti, A., et al., *Forty-year mortality from cardiovascular diseases and all causes of death in the US Railroad cohort of the Seven Countries Study*. *Eur J Epidemiol*, 2004. **19**(5): p. 417-24.
102. Pekkanen, J., et al., *Short- and long-term association of serum cholesterol with mortality. The 25-year follow-up of the Finnish cohorts of the seven countries study*. *Am J Epidemiol*, 1992. **135**(11): p. 1251-8.
103. Gomez, D. and G.K. Owens, *Smooth muscle cell phenotypic switching in atherosclerosis*. *Cardiovasc Res*, 2012. **95**(2): p. 156-64.
104. Caplice, N.M., et al., *Smooth muscle cells in human coronary atherosclerosis can originate from cells administered at marrow transplantation*. *Proc Natl Acad Sci U S A*, 2003. **100**(8): p. 4754-9.
105. Conway, D.E. and M.A. Schwartz, *Flow-dependent cellular mechanotransduction in atherosclerosis*. *J Cell Sci*, 2013. **126**(Pt 22): p. 5101-9.
106. Lever, M.J., *The role of haemodynamic forces in the localization of atherosclerotic lesions*. *Vascular Medicine Review*, 1994. **5**: p. 347-362.
107. Rosenfeld, M.E., et al., *Advanced atherosclerotic lesions in the innominate artery of the ApoE knockout mouse*. *Arterioscler Thromb Vasc Biol*, 2000. **20**(12): p. 2587-92.
108. VanderLaan, P.A., C.A. Reardon, and G.S. Getz, *Site specificity of atherosclerosis: site-selective responses to atherosclerotic modulators*. *Arterioscler Thromb Vasc Biol*, 2004. **24**(1): p. 12-22.
109. Gupta, S., et al., *IFN-gamma potentiates atherosclerosis in ApoE knock-out mice*. *J Clin Invest*, 1997. **99**(11): p. 2752-61.
110. Tedgui, A. and Z. Mallat, *Cytokines in atherosclerosis: pathogenic and regulatory pathways*. *Physiol Rev*, 2006. **86**(2): p. 515-81.
111. Klingenberg, R., et al., *Depletion of FOXP3+ regulatory T cells promotes hypercholesterolemia and atherosclerosis*. *J Clin Invest*, 2013. **123**(3): p. 1323-34.

112. Taleb, S., A. Tedgui, and Z. Mallat, *IL-17 and Th17 cells in atherosclerosis: subtle and contextual roles*. *Arterioscler Thromb Vasc Biol*, 2015. **35**(2): p. 258-64.
113. Mallat, Z., et al., *The role of adaptive T cell immunity in atherosclerosis*. *J Lipid Res*, 2009. **50 Suppl**: p. S364-9.
114. Ley, K., *The second touch hypothesis: T cell activation, homing and polarization*. *F1000Res*, 2014. **3**: p. 37.
115. Ng, Y.H. and G. Chalasani, *Role of secondary lymphoid tissues in primary and memory T-cell responses to a transplanted organ*. *Transplant Rev (Orlando)*, 2010. **24**(1): p. 32-41.
116. Gao, Y.J., et al., *Modulation of vascular function by perivascular adipose tissue: the role of endothelium and hydrogen peroxide*. *Br J Pharmacol*, 2007. **151**(3): p. 323-31.
117. Chatterjee, T.K., et al., *Proinflammatory phenotype of perivascular adipocytes: influence of high-fat feeding*. *Circ Res*, 2009. **104**(4): p. 541-9.
118. Britton, K.A., et al., *Prevalence, distribution, and risk factor correlates of high thoracic periaortic fat in the Framingham Heart Study*. *J Am Heart Assoc*, 2012. **1**(6): p. e004200.
119. Mummert, M.E., et al., *Synthesis and surface expression of hyaluronan by dendritic cells and its potential role in antigen presentation*. *J Immunol*, 2002. **169**(8): p. 4322-31.
120. Hochrein, H., et al., *Differential production of IL-12, IFN-alpha, and IFN-gamma by mouse dendritic cell subsets*. *J Immunol*, 2001. **166**(9): p. 5448-55.
121. Heufler, C., et al., *Interleukin-12 is produced by dendritic cells and mediates T helper 1 development as well as interferon-gamma production by T helper 1 cells*. *Eur J Immunol*, 1996. **26**(3): p. 659-68.
122. Larsen, C.P., et al., *Functional expression of the costimulatory molecule, B7/BB1, on murine dendritic cell populations*. *J Exp Med*, 1992. **176**(4): p. 1215-20.
123. Cella, M., et al., *Inflammatory stimuli induce accumulation of MHC class II complexes on dendritic cells*. *Nature*, 1997. **388**(6644): p. 782-7.
124. Jiang, D., J. Liang, and P.W. Noble, *Hyaluronan in tissue injury and repair*. *Annu Rev Cell Dev Biol*, 2007. **23**: p. 435-61.
125. Majesky, M.W., *Developmental basis of vascular smooth muscle diversity*. *Arterioscler Thromb Vasc Biol*, 2007. **27**(6): p. 1248-58.
126. Topouzis, S. and M.W. Majesky, *Smooth muscle lineage diversity in the chick embryo. Two types of aortic smooth muscle cell differ in growth and receptor-mediated transcriptional responses to transforming growth factor-beta*. *Dev Biol*, 1996. **178**(2): p. 430-45.
127. Meran, S., et al., *Hyaluronan facilitates transforming growth factor-beta1-mediated fibroblast proliferation*. *J Biol Chem*, 2008. **283**(10): p. 6530-45.
128. Gomez, D., et al., *Detection of histone modifications at specific gene loci in single cells in histological sections*. *Nat Methods*, 2013. **10**(2): p. 171-7.
129. Bennett, M.R., S. Sinha, and G.K. Owens, *Vascular Smooth Muscle Cells in Atherosclerosis*. *Circ Res*, 2016. **118**(4): p. 692-702.
130. Goueffic, Y., et al., *Hyaluronan induces vascular smooth muscle cell migration through RHAMM-mediated PI3K-dependent Rac activation*. *Cardiovasc Res*, 2006. **72**(2): p. 339-48.
131. Vigetti, D., et al., *Hyaluronan-CD44-ERK1/2 regulate human aortic smooth muscle cell motility during aging*. *J Biol Chem*, 2008. **283**(7): p. 4448-58.

132. Rabausch, B., S. Twarock, and J.W. Fischer, *Abstract 733: Regulation and Function of Hyaluronic Acid Synthase-3 in Human Vascular Smooth Muscle Cells*. *Circulation*, 2007. **116**(Suppl 16).
133. Viola, M., et al., *Oxidized low density lipoprotein (LDL) affects hyaluronan synthesis in human aortic smooth muscle cells*. *J Biol Chem*, 2013. **288**(41): p. 29595-603.
134. van den Boom, M., et al., *Differential regulation of hyaluronic acid synthase isoforms in human saphenous vein smooth muscle cells: possible implications for vein graft stenosis*. *Circ Res*, 2006. **98**(1): p. 36-44.
135. Stewart, C.R., et al., *CD36 ligands promote sterile inflammation through assembly of a Toll-like receptor 4 and 6 heterodimer*. *Nat Immunol*, 2010. **11**(2): p. 155-61.
136. Bhaskar, V., et al., *Monoclonal antibodies targeting IL-1 beta reduce biomarkers of atherosclerosis in vitro and inhibit atherosclerotic plaque formation in Apolipoprotein E-deficient mice*. *Atherosclerosis*, 2011. **216**(2): p. 313-20.
137. Kirii, H., et al., *Lack of interleukin-1beta decreases the severity of atherosclerosis in ApoE-deficient mice*. *Arterioscler Thromb Vasc Biol*, 2003. **23**(4): p. 656-60.
138. Chi, H., et al., *Interleukin-1 receptor signaling mediates atherosclerosis associated with bacterial exposure and/or a high-fat diet in a murine apolipoprotein E heterozygote model: pharmacotherapeutic implications*. *Circulation*, 2004. **110**(12): p. 1678-85.
139. Kleemann, R., S. Zadelaar, and T. Kooistra, *Cytokines and atherosclerosis: a comprehensive review of studies in mice*. *Cardiovasc Res*, 2008. **79**(3): p. 360-76.
140. Vigetti, D., et al., *Proinflammatory cytokines induce hyaluronan synthesis and monocyte adhesion in human endothelial cells through hyaluronan synthase 2 (HAS2) and the nuclear factor-kappaB (NF-kappaB) pathway*. *J Biol Chem*, 2010. **285**(32): p. 24639-45.
141. Mohamadzadeh, M., et al., *Proinflammatory stimuli regulate endothelial hyaluronan expression and CD44/HA-dependent primary adhesion*. *J Clin Invest*, 1998. **101**(1): p. 97-108.
142. Swirski, F.K., *Monocyte recruitment and macrophage proliferation in atherosclerosis*. *Kardiol Pol*, 2014. **72**(4): p. 311-4.
143. Rayahin, J.E., et al., *High and low molecular weight hyaluronic acid differentially influence macrophage activation*. *ACS Biomater Sci Eng*, 2015. **1**(7): p. 481-493.
144. Leitinger, N. and I.G. Schulman, *Phenotypic polarization of macrophages in atherosclerosis*. *Arterioscler Thromb Vasc Biol*, 2013. **33**(6): p. 1120-6.
145. Chinetti-Gbaguidi, G., S. Colin, and B. Staels, *Macrophage subsets in atherosclerosis*. *Nat Rev Cardiol*, 2015. **12**(1): p. 10-7.
146. McKee, C.M., et al., *Hyaluronan fragments induce nitric-oxide synthase in murine macrophages through a nuclear factor kappaB-dependent mechanism*. *J Biol Chem*, 1997. **272**(12): p. 8013-8.
147. Krausgruber, T., et al., *IRF5 promotes inflammatory macrophage polarization and TH1-TH17 responses*. *Nat Immunol*, 2011. **12**(3): p. 231-8.
148. Yu, X.L., et al., *Overexpression of IL-12 reverses the phenotype and function of M2 macrophages to M1 macrophages*. *International Journal of Clinical and Experimental Pathology*, 2016. **9**(9): p. 8963-8972.

149. Szasz, T., G.F. Bomfim, and R.C. Webb, *The influence of perivascular adipose tissue on vascular homeostasis*. Vasc Health Risk Manag, 2013. **9**: p. 105-16.
150. Verhagen, S.N. and F.L. Visseren, *Perivascular adipose tissue as a cause of atherosclerosis*. Atherosclerosis, 2011. **214**(1): p. 3-10.
151. Campbell, K.A., et al., *Lymphocytes and the adventitial immune response in atherosclerosis*. Circ Res, 2012. **110**(6): p. 889-900.
152. Wrobel, T., et al., *LYVE-1 expression on high endothelial venules (HEVs) of lymph nodes*. Lymphology, 2005. **38**(3): p. 107-10.
153. Mahaffey, C.L. and M.E. Mummert, *Hyaluronan synthesis is required for IL-2-mediated T cell proliferation*. J Immunol, 2007. **179**(12): p. 8191-9.
154. Kim, H.P., J. Imbert, and W.J. Leonard, *Both integrated and differential regulation of components of the IL-2/IL-2 receptor system*. Cytokine Growth Factor Rev, 2006. **17**(5): p. 349-66.
155. Hughes-Fulford, M., et al., *Early immune response and regulation of IL-2 receptor subunits*. Cell Signal, 2005. **17**(9): p. 1111-24.
156. Summers deLuca, L. and J.L. Gommerman, *Fine-tuning of dendritic cell biology by the TNF superfamily*. Nat Rev Immunol, 2012. **12**(5): p. 339-51.
157. Hsieh, C.S., et al., *Development of TH1 CD4+ T cells through IL-12 produced by Listeria-induced macrophages*. Science, 1993. **260**(5107): p. 547-9.
158. Macatonia, S.E., et al., *Dendritic cells produce IL-12 and direct the development of Th1 cells from naive CD4+ T cells*. J Immunol, 1995. **154**(10): p. 5071-9.
159. Henry, C.J., et al., *IL-12 produced by dendritic cells augments CD8+ T cell activation through the production of the chemokines CCL1 and CCL17*. J Immunol, 2008. **181**(12): p. 8576-84.
160. Babasola, O., et al., *Chemically modified N-acylated hyaluronan fragments modulate proinflammatory cytokine production by stimulated human macrophages*. J Biol Chem, 2014. **289**(36): p. 24779-91.
161. Hauer, A.D., et al., *Blockade of interleukin-12 function by protein vaccination attenuates atherosclerosis*. Circulation, 2005. **112**(7): p. 1054-62.
162. Swanson, B.J., et al., *RANTES production by memory phenotype T cells is controlled by a posttranscriptional, TCR-dependent process*. Immunity, 2002. **17**(5): p. 605-15.
163. Li, J., et al., *CCR5+T-bet+FoxP3+ Effector CD4 T Cells Drive Atherosclerosis*. Circ Res, 2016. **118**(10): p. 1540-52.
164. Veillard, N.R., et al., *Antagonism of RANTES receptors reduces atherosclerotic plaque formation in mice*. Circ Res, 2004. **94**(2): p. 253-61.
165. Aiello, R.J., et al., *Monocyte chemoattractant protein-1 accelerates atherosclerosis in apolipoprotein E-deficient mice*. Arterioscler Thromb Vasc Biol, 1999. **19**(6): p. 1518-25.
166. Taub, D.D., et al., *Monocyte chemotactic protein-1 (MCP-1), -2, and -3 are chemotactic for human T lymphocytes*. J Clin Invest, 1995. **95**(3): p. 1370-6.
167. Huffnagle, G.B., et al., *The role of monocyte chemotactic protein-1 (MCP-1) in the recruitment of monocytes and CD4+ T cells during a pulmonary Cryptococcus neoformans infection*. J Immunol, 1995. **155**(10): p. 4790-7.
168. Gu, L., et al., *Control of TH2 polarization by the chemokine monocyte chemoattractant protein-1*. Nature, 2000. **404**(6776): p. 407-11.
169. Zadelaar, S., et al., *Mouse models for atherosclerosis and pharmaceutical modifiers*. Arterioscler Thromb Vasc Biol, 2007. **27**(8): p. 1706-21.

170. Getz, G.S. and C.A. Reardon, *Animal models of atherosclerosis*. *Arterioscler Thromb Vasc Biol*, 2012. **32**(5): p. 1104-15.
171. Bentzon, J.F. and E. Falk, *Atherosclerotic lesions in mouse and man: is it the same disease?* *Curr Opin Lipidol*, 2010. **21**(5): p. 434-40.

Appendix

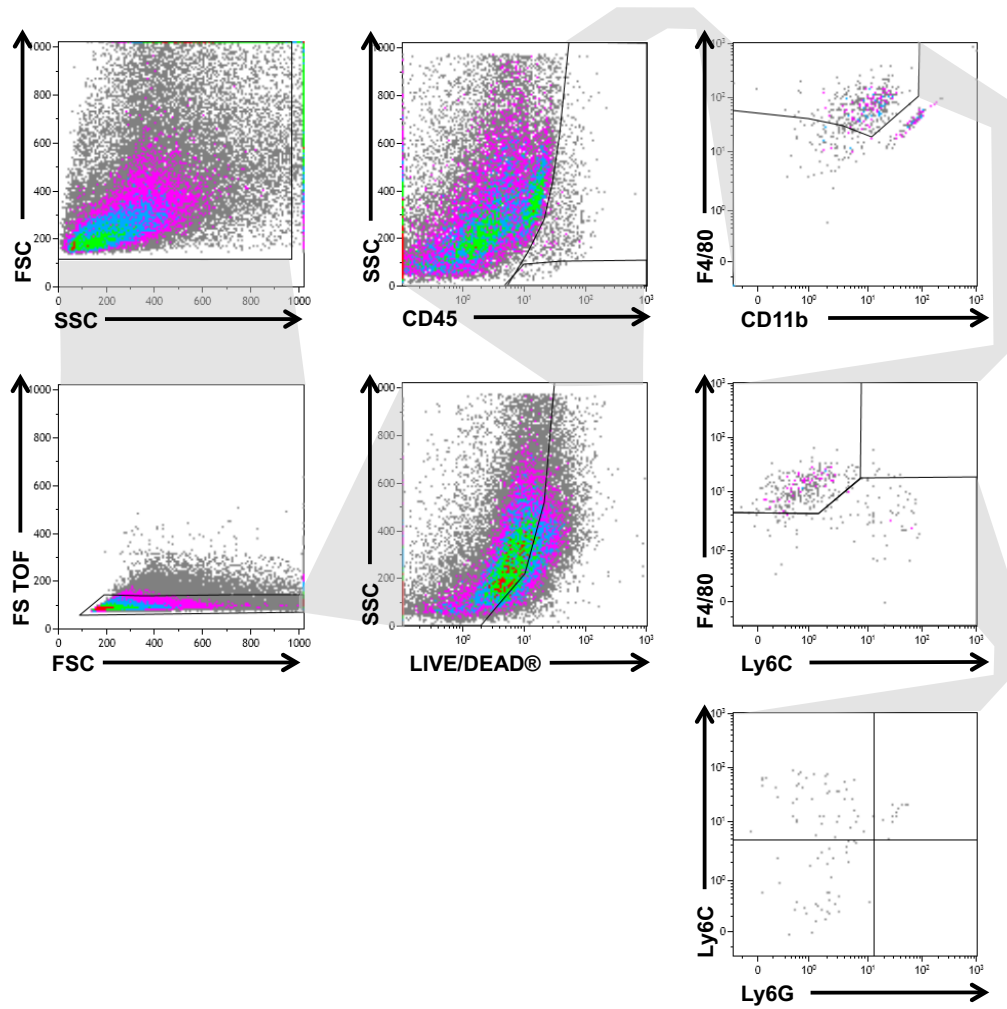


Figure 27: Gating strategy for the detection of monocytes, macrophages, and dendritic cells in the aortic wall after 4 weeks of WD feeding.

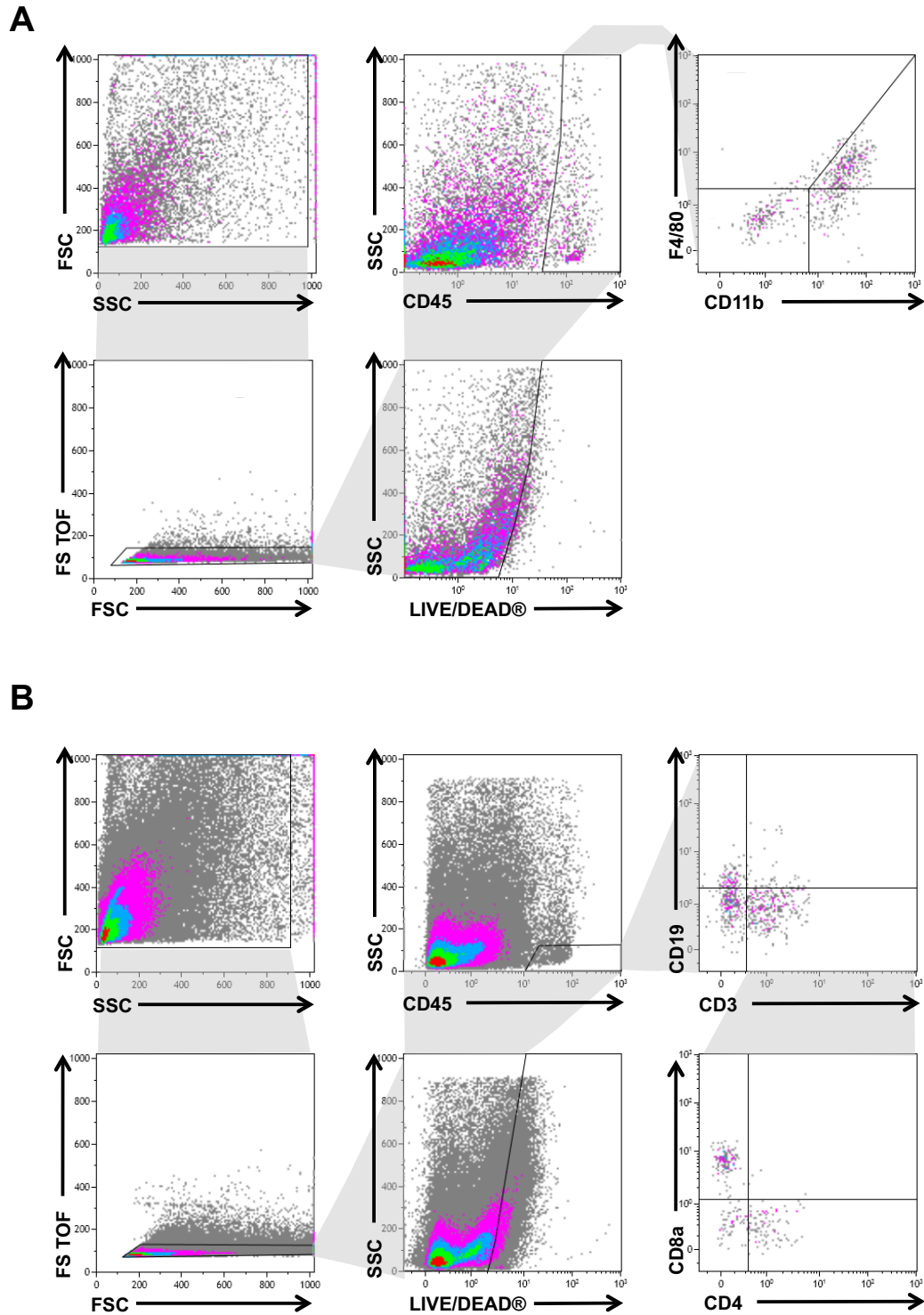


Figure 28: Gating scheme for the flow cytometric analyses of immune cells in the aorta and PVAT after 15 weeks of WD feeding.

(A) Scheme for the determination of $CD11b^+F4/80^+$ macrophages. **(B)** Gating for the analyses of $CD19^+$ B cells, $CD3^+$ T cells, as well as the $CD4^+$ and $CD8a^+$ T cell subsets.

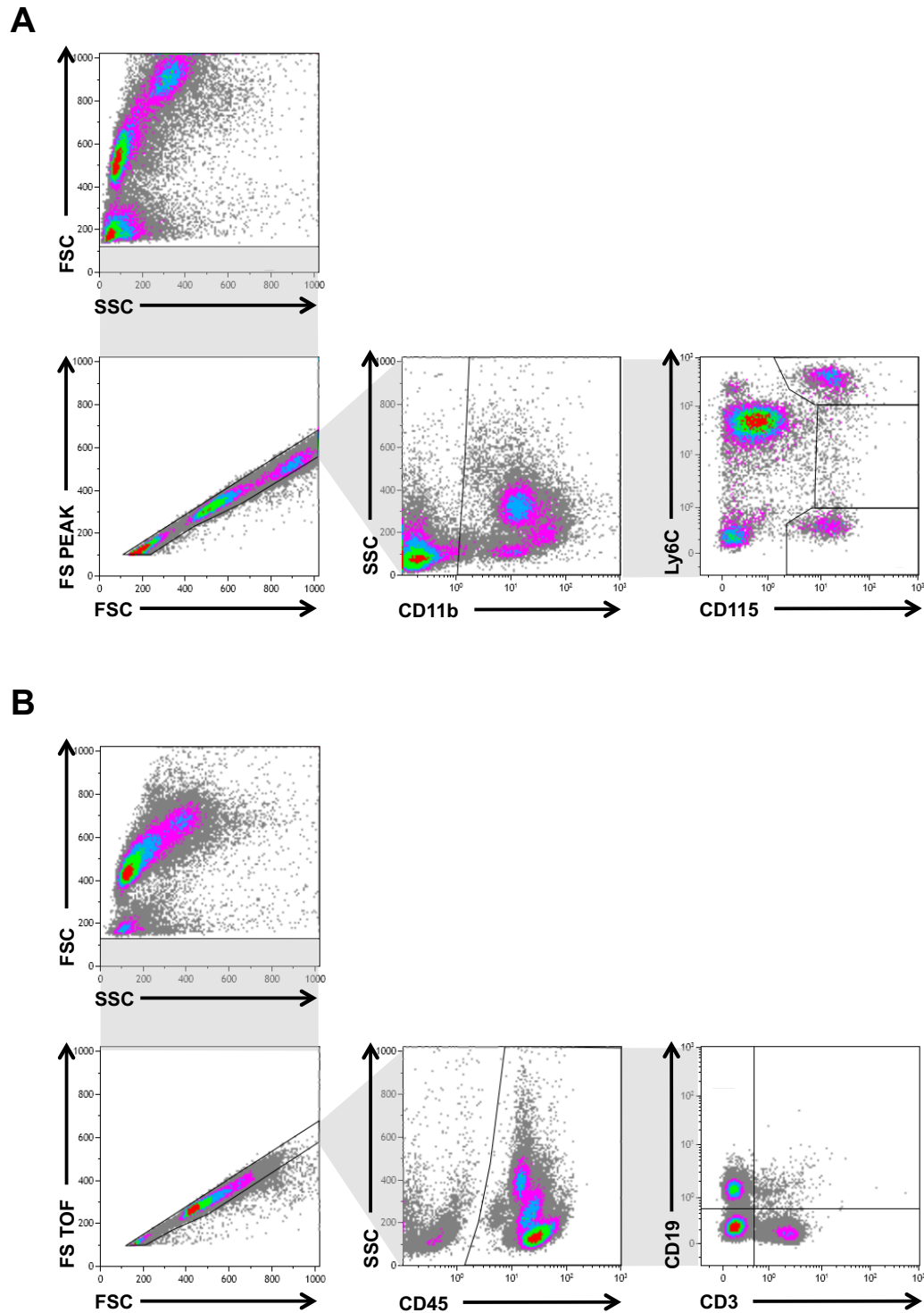


Figure 29: Diagram for the analyses of circulating monocytes, B cells, and T cells.

Flow cytometric determination of circulating monocytes is depicted in (A) and the gating strategy for CD19⁺ and CD3⁺ lymphocytes is shown in (B).

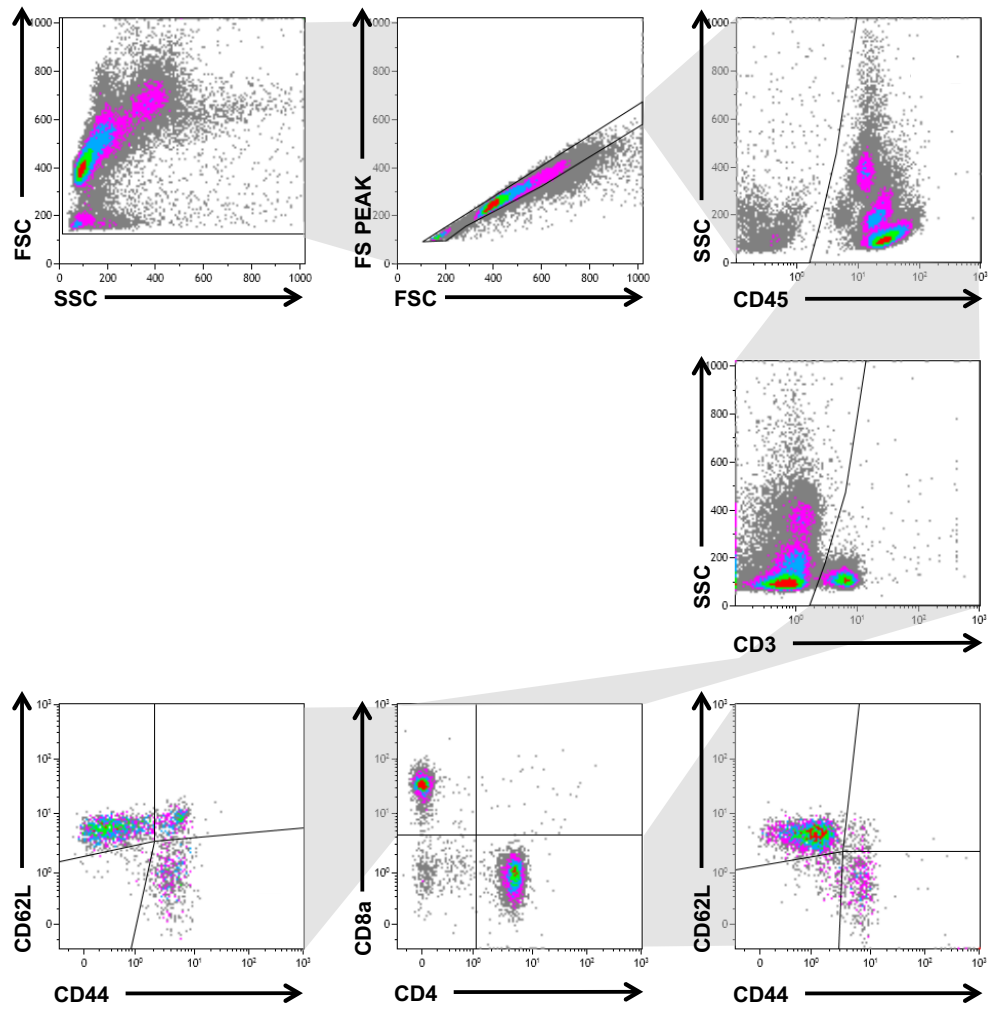


Figure 30: Representative gating for the determination of CD62L⁺CD44⁻ naïve, CD62L⁻CD44⁺ effector, and CD62L⁺CD44⁺ memory T cells in the blood.

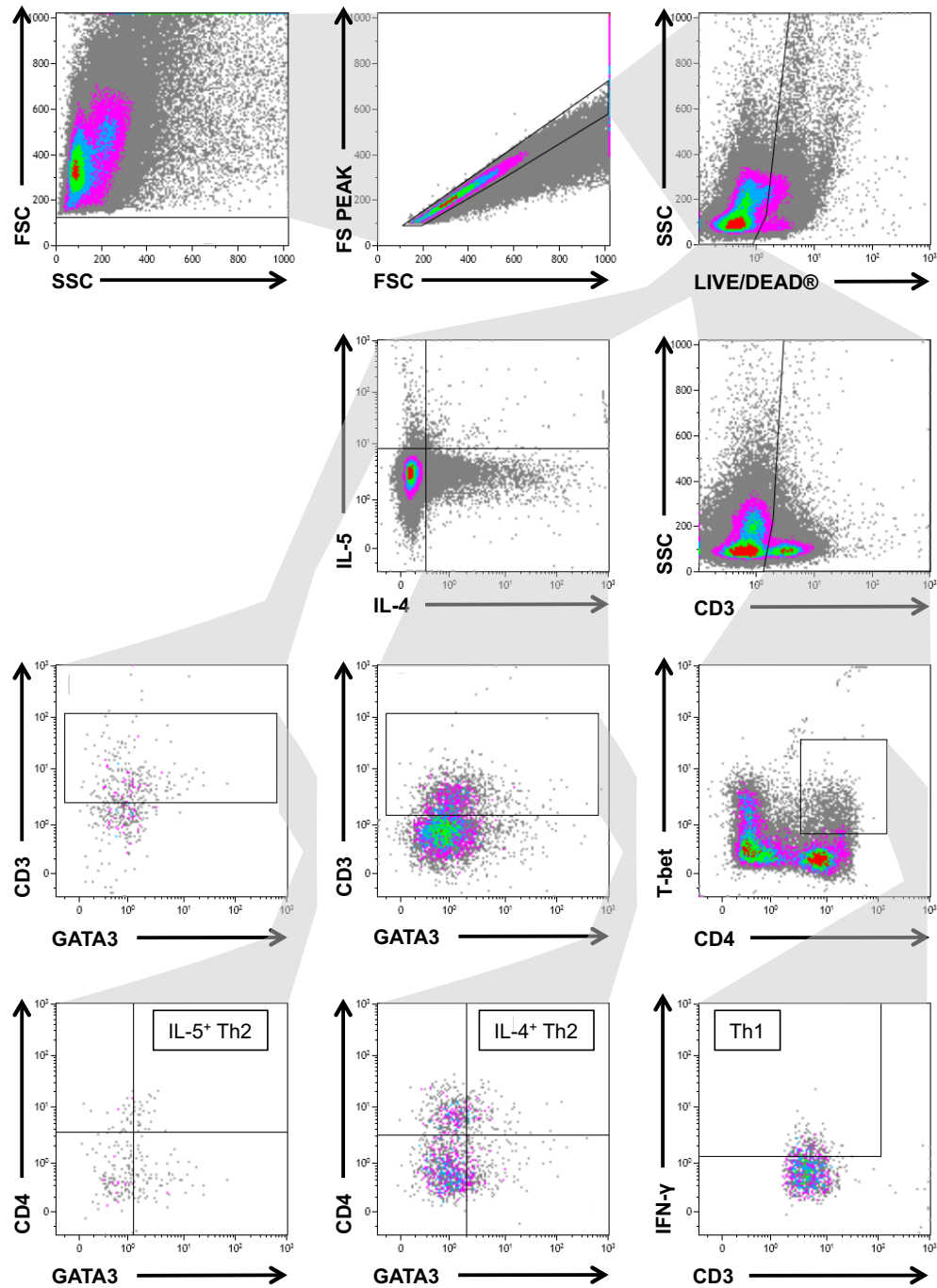


Figure 31: Scheme for the flow cytometric analysis of circulating Th1 and Th2 lymphocytes.

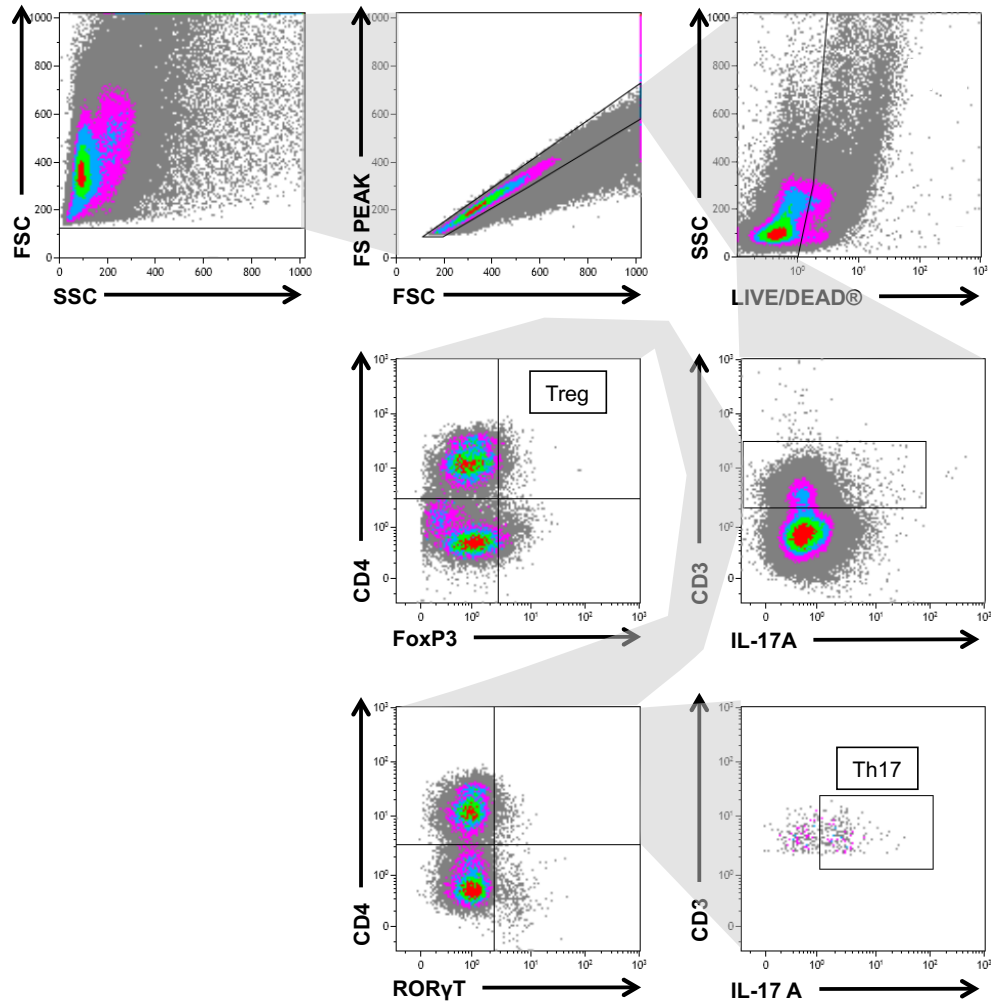


Figure 32: Gating strategy for the analysis of circulating Th17 and Treg cells.

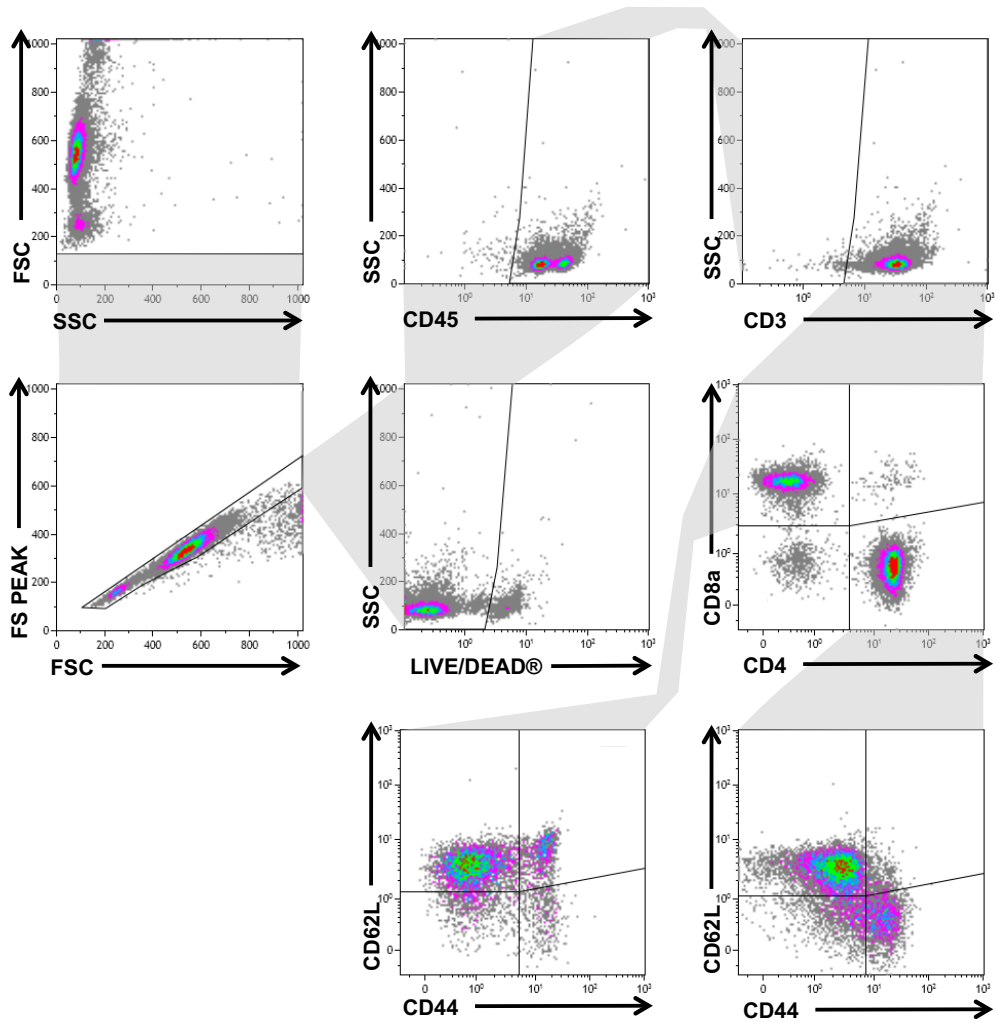


Figure 33: Diagram for the gating of naïve, effector, and memory T cells in axillary lymph nodes, spleen, and *in vitro* experiments.

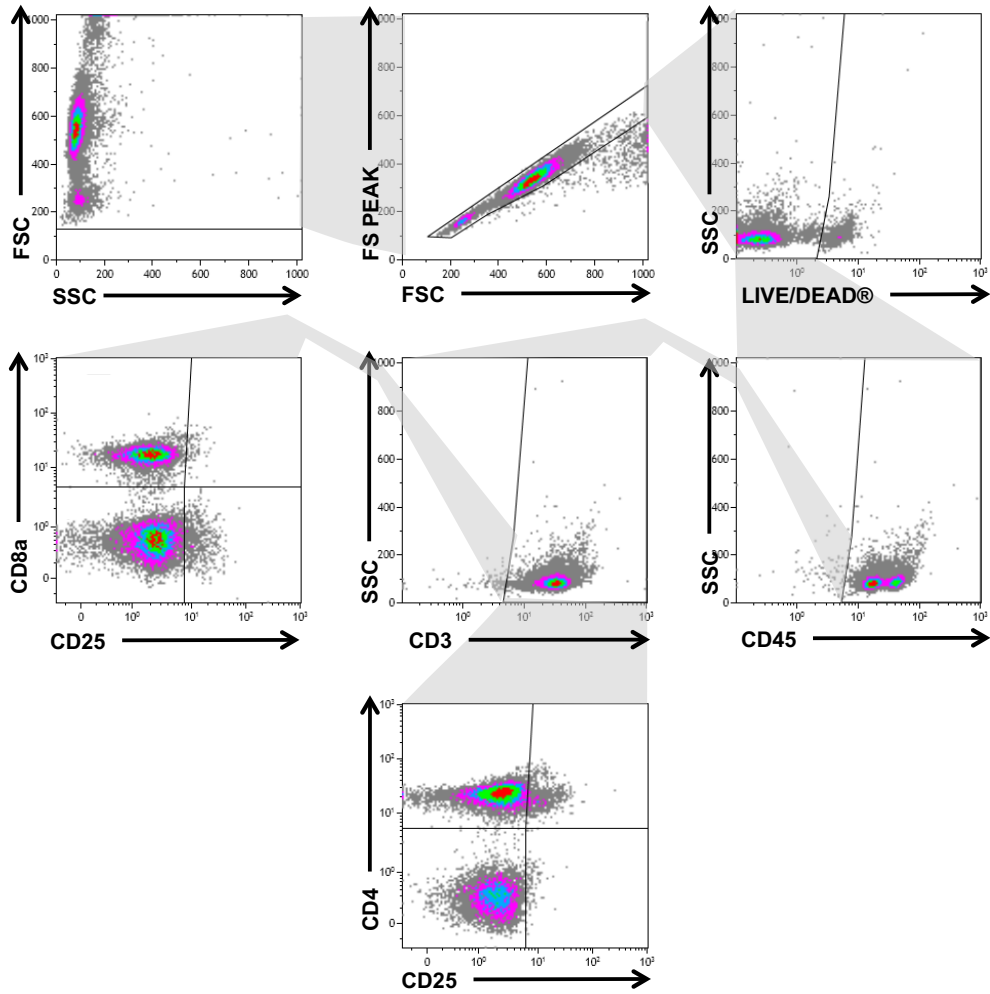


Figure 34: Scheme for the gating of CD25-expressing T cells after stimulation with anti-CD3/-CD28 beads *in vitro*.

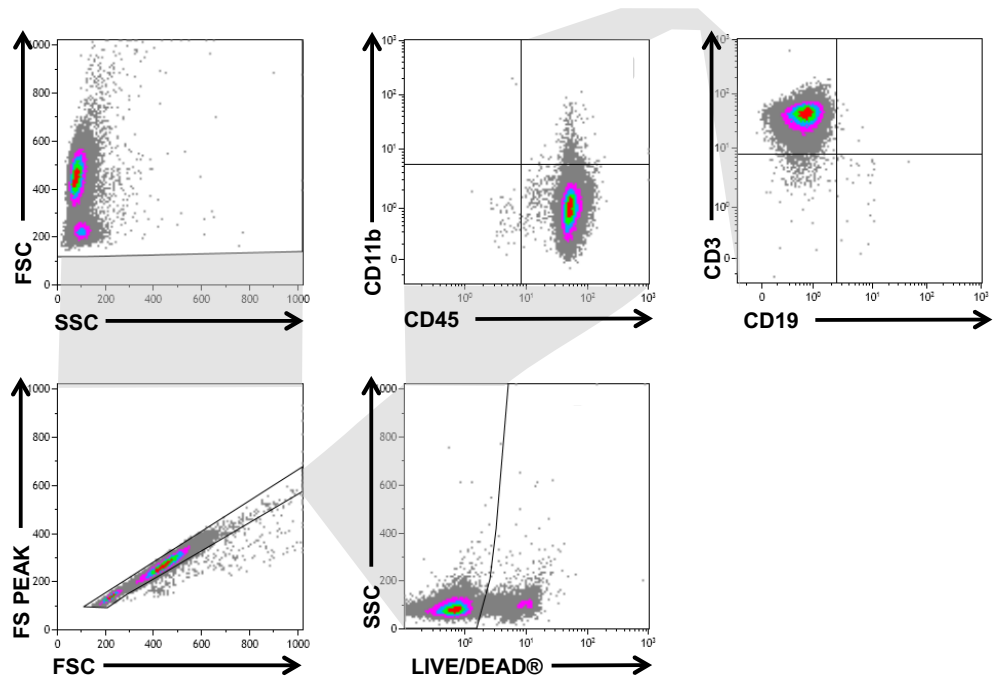


Figure 35: Gating strategy for the determination of T cell purity after T cell isolation.

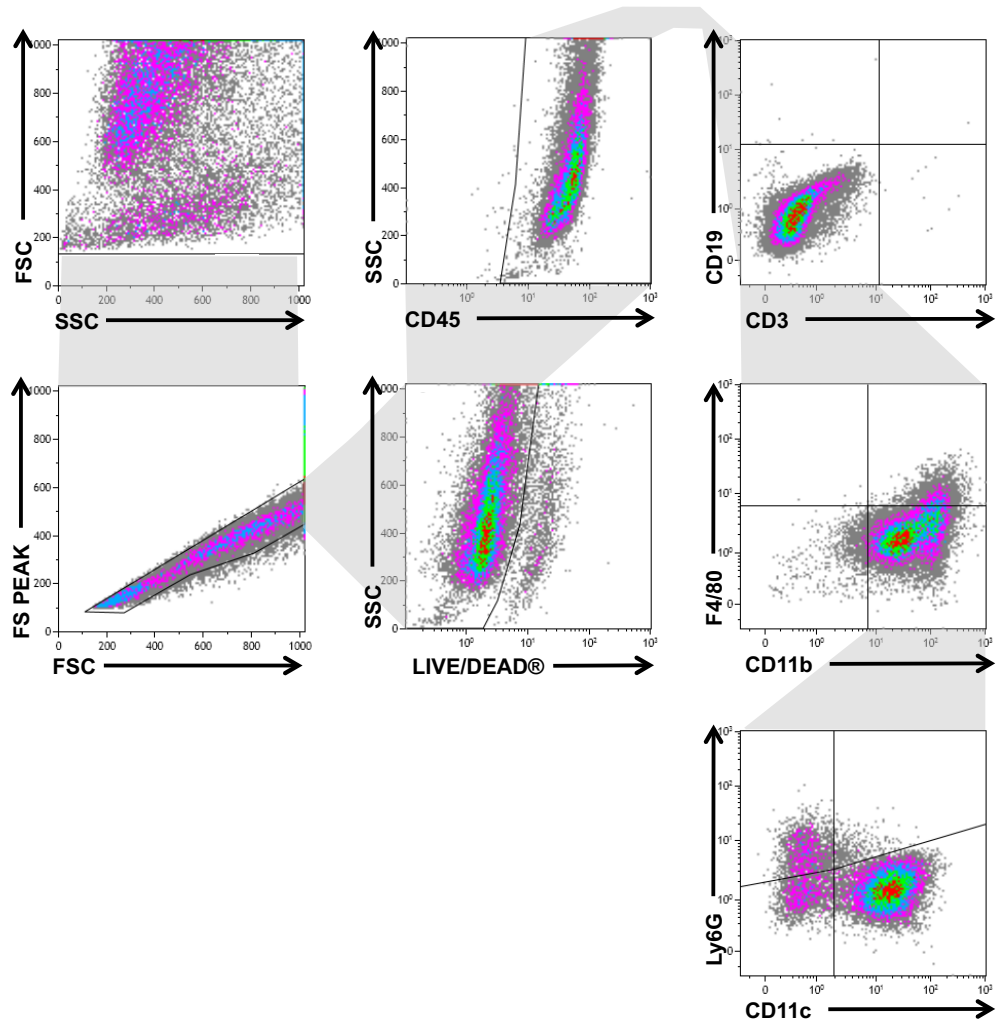


Figure 36: Representative gating to analyze the purity of the BM-DC culture on day 8 of cultivation.

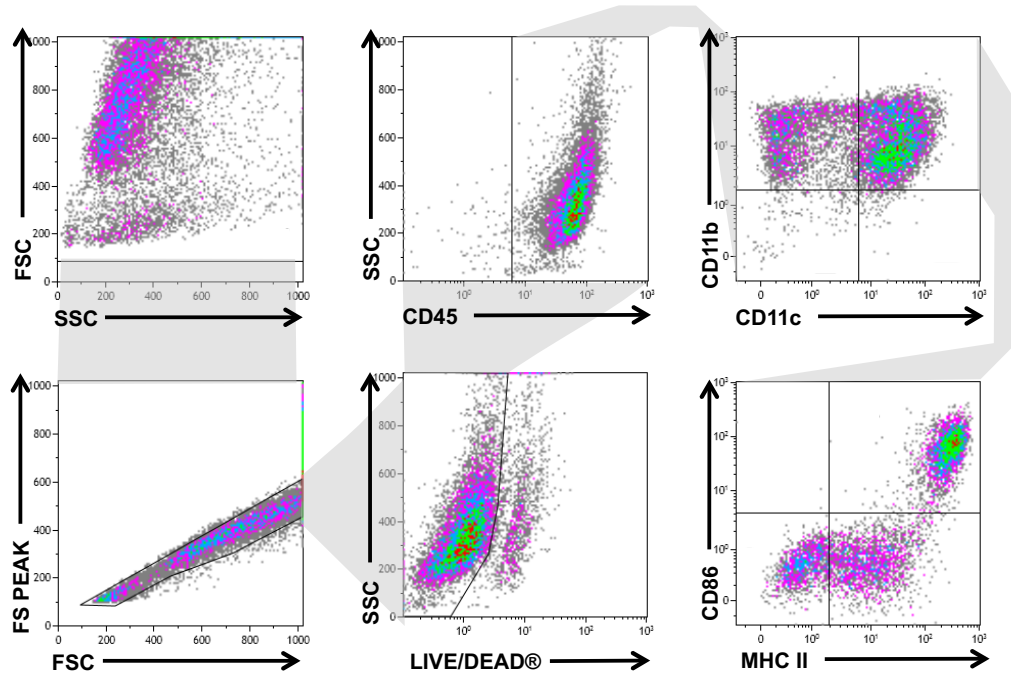


Figure 37: Scheme for the flow cytometric analysis of the activation status of BM-DCs after LPS stimulation *in vitro*.

Publications

- Grandoch M, Feldmann K, Göthert JR, Dick LS, **Homann S**, Klatt C, Bayer JK, Waldheim JN, Rabausch B, Nagy N, Oberhuber A, Deenen R, Köhrer K, Lehr S, Homey B, Pfeffer K, Fischer JW. *Deficiency in lymphotoxin beta receptor protects from atherosclerosis in apoE-deficient mice*. *Circ Res*, 2015. **116**(8).
- Kiene LS, **Homann S**, Suvorava T, Rabausch B, Müller J, Kojda G, Kretschmer I, Twarock S, Dai G, Deenen R, Hartwig S, Lehr S, Köhrer K, Savani RC, Grandoch M, Fischer JW. *Deletion of Hyaluronan Synthase 3 Inhibits Neointimal Hyperplasia in Mice*. *Atheroscler Thromb Vasc Biol*, 2016. **36**(2).
- Grandoch M, Melchior-Becker A, Kohlmorgen C, Feldmann K, Gowert N, Müller J, **Homann S**, Kiene LS, Zeng-Brouwers J, Schmitz F, Nagy N, Polzin A, Skroblin P, Yin X, Elvers M, Mayr M, Schaefer L, Tannock L, Fischer JW. *Loss of Biglycan Enhances Thrombin Generation in Apolipoprotein E-Deficient Mice: Implications for Inflammation and Atherosclerosis*. *Arterioscler Thromb Vasc Biol*, 2016. **36**(5).

Congress participation

Perspectives in Vascular Biology 2016 – Frankfurt am Main, Germany

Talk as one of six finalists in “Young Investigator Award” Session
Title: **Genetic deletion of *Hyaluronan synthase 3* in *Apolipoprotein E* deficient mice protects from atherosclerosis.**

Abstracts

Dick LS, **Homann S**, Müller J, Rabausch B, Grandoch M, Fischer JW. *Genetic deletion of hyaluronan-synthase 3 is protective in vascular lesion formation.* Naunyn-Schmiedeberg's Arch Pharmacol, 2015; 388(Suppl.1):S533.

Dick LS, **Homann S**, Müller J, Grandoch M, Fischer JW. *Vascular lesion formation is attenuated by genetic deletion of hyaluronan-synthase 3.* Arteriosclerosis, Thrombosis, and Vascular Biology, May 2015, Volume 35, Issue Suppl 1, A554.

Dick LS, **Homann S**, Müller J, Grandoch M, Fischer JW. *Hyaluronan-synthase 3 deletion attenuates vascular lesion formation.* Book of Abstracts, 10th International Conference on Hyaluronan, June 2015, Florence.

Homann S, Kiene LS, Hartwig S, Lehr S, Grandoch M, Fischer JW. *Genetic deletion of Hyaluronan synthase 3 in Apolipoprotein E deficient mice protects from atherosclerosis.* Joint International Meeting Perspectives in Vascular Biology, September 2016, Frankfurt.

Curriculum vitae

Person

Name Susanne Friederike Homann

Date of birth 02. Dezember 1989

Place of birth Filderstadt

Family status Single

Nationality German

Doctoral studies

03/2014 – 06/2017 Heinrich-Heine-Universität Düsseldorf
 Doctoral studies to reach Dr. rer. nat. at the Institute for Pharmacology and Clinical Pharmacology in Cooperation with the Cardiovascular Research Center at University of Virginia, Charlottesville, USA
 Supervisor: Director of Institute Prof. Dr. Jens W. Fischer
 Thesis:
 Study on the role of hyaluronan synthase 3 in the pathogenesis of atherosclerosis

11/2016 – 03/2017 Research stay in the laboratory of Gary Owens, Ph.D., Division of Molecular Physiology and Biological Physics, University of Virginia, Charlottesville, USA

University

10/2011 - 08/2013 Universität Würzburg
 Biomedicine, Graduation 08/2013: Master of Science (1.2)
 Thesis:
 Regulation of ERK1/2 signaling by subcellular localization - ERK dimerization as a potential target in cardiac hypertrophy

10/2008 - 07/2011 Universität Würzburg
 Biomedicine, Graduation 07/2011: Bachelor of Science (1.4)
 Thesis:
 Analysis of the ERK1/2 Localisation - Generation of tools for the evaluation of the impact of ERK localisation on its phosphorylation

School

1999 - 2008 Gymnasium Neckartenzlingen, Graduation: A level (1.0)

Acknowledgement

First of all, I would like to express my highest gratitude to my supervisor Prof. Dr. Jens W. Fischer for the opportunity to write my doctoral thesis in his research group as a member of the international research training group (IRTG) 1902. His guidance allowed me to grow as a scientist.

My special thanks and appreciation goes to Prof. Dr. Maria Grandoch, who not only aided me with the professional support but also encouraged me whenever needed. Her patience and leniency at any time of day has helped me to refocus and adjust and has therefore played a vital role these past years.

Furthermore, I would particularly like to thank Gary Owens, Ph.D., who offered me the chance to collaborate with his laboratory at UVa, Charlottesville. His approach on challenges arising has truly inspired me. His and his wife's hospitality during my initial visit in 2015 and during Christmas 2016 will happily be remembered.

Lena Kiene laid the foundation to this project by ascertaining the initial results this project relies upon. Her inputs and support require special thanks.

Without the untiring perseverance and relentless energy Yanina Podsvyadek, Kathrin Feldmann, and Kerstin Freidel spent on my project during my time abroad this thesis would not have been the same. Besides that I want to thank all three of you for your patience whether for hours discussing about gating strategies or teaching me new methods. Especially, Yanina has become a beloved friend without whom the long nights in the laboratory would not have been the same. I am immensely grateful.

Being abroad can be a great challenge as most of your every day life changes at once. Thank you Alexandra Newman for making it simple and for all your help getting my project started.

The IRTG 1902 helped me to enhance my professional and personal skills by offering a broad range of courses, trainings, and general guidance. I would like to show my gratitude to Prof. Dr. Axel Gödecke for leading the IRTG 1902 and Dr. Sandra Berger for more than once helping me with any matter at hand.

Scientific research cannot be done without those organizing all office related matters and the technical assistants with their professional experience. I therefore like to thank Erika Lohmann and Karin Montag as well as Petra Rompel, Irmhild Rüter, Annika Zimmermann, Beate Weyrauther, and Martina Hübel.

Thanks to all my colleges both in Düsseldorf and in Charlottesville who could not be named here. You all created an amazing work environment.

Last but not least, I would like to wholeheartedly thank my boyfriend Julian Henning Heitmann, my family, his family, and my friends for all their patience, sympathy, encouragement, and support. I could not have done any of this without you!

Eidesstattliche Erklärung

Ich versichere an Eides Statt, dass die Dissertation von mir selbständig und ohne unzulässige fremde Hilfe unter Beachtung der „Grundsätze zur Sicherung guter wissenschaftlicher Praxis an der Heinrich-Heine-Universität Düsseldorf“ erstellt worden ist.

Ich versichere, dass dies mein erster Promotionsversuch ist und ich diese Arbeit nur an der Mathematisch-Naturwissenschaftlichen Fakultät der Heinrich-Heine-Universität Düsseldorf vorgelegt habe.

Düsseldorf, den

Susanne Homann